

Diss. ETH No. 22261

Novel Polymer-Brush Based Coatings for Regulating Bioadhesion

A dissertation submitted to
ETH ZURICH

for the degree of
Doctor of Sciences

presented by
ÂNGELA SERRANO
MSc of Chemistry, Instituto Superior Técnico, Portugal
born on February 25th, 1983
citizen of Portugal

accepted on the recommendation of
Prof. Dr. Nicholas D. Spencer, examiner
Prof. Dr. Jan Genzer, co-examiner
Dr. Stefan Zürcher, co-examiner
Dr. Samuele Tosatti, co-examiner

2014

To my everlasting 'Xtrudes' Maria

Abstract

Biofouling is a phenomenon that can be explained as the undesirable accumulation of biological materials on submerged surfaces. It can be comprised of proteins, cells, bacteria or even bigger microorganisms such as algae, and consequently results in a negative effect on the performance of the system considered. Biofouling of ships' hulls increases drag, leading to speed reduction and additional fuel consumption, formation of bacterial film on medical devices increases infection risks and in food processing biofouling can affect the quality of the product as well as its safe consumption.

Considering the broad spectrum of fields and applications affected by biofouling, plenty of research has already been made in order to better understand and thus control the interfacial processes involved. The vast majority focuses on surface-modification strategies, as this allows modifying and manipulating a material's physicochemical properties. Among the various surface-treatment possibilities, the application of a coating is a simple and straightforward method to add new functionalities and properties to a base material. Surface functionalization by polymeric thin films has already been used in a wide number of demanding areas, such as those mentioned above.

The work presented in this thesis forms part of a European project that aimed at a better understanding of the processes involved in marine biofouling. To that end two major studies were performed within this work. The goals were to 1) develop a surface-modifying testing platform that would allow for a parallel comparison between the nonfouling efficiency of several hydrophilic uncharged polymers; and 2) investigate the effect that the nature of surface binding has on the performance of a nonfouling polymeric coating.

Regarding the first study, we successfully managed to use a common polymeric monolayer containing photochemical groups to attach several hydrophilic uncharged polymers with nonfouling abilities. Upon activation by UV irradiation of the

photochemical group, a radical species is formed, enabling the formation of a covalent bond to the organic compounds in closest proximity, which in this case consisted of a spin-coated nonfouling polymer. The latter included the well-known poly(ethylene glycol) (PEG), poly(2-ethyl-2-oxazoline) (PEOXA), low and high-molecular-weight poly(vinyl pyrrolidone) (PVP), poly(vinyl alcohol) (PVA) and dextran. After characterizing the modified surfaces with techniques such as variable-angle spectroscopic ellipsometry, X-ray photoelectron spectroscopy and contact-angle measurements, they were exposed to several fouling assays that included immersion in a complex protein solution (followed by characterization *via* ellipsometry and quartz crystal microbalance with dissipation), as well as adhesion studies using marine bacteria (*Cobetia marina* and *Marinobacter hydrocarbonoclasticus*) and zoospores of the green alga *Ulva linza*. The resulting data were used to draw conclusions on structure-property relationships. It was found that chemical resistance towards marine fouling can be achieved using the described immobilization method, but is highly dependent on the species tested. Our findings showed that low-molecular-weight PVP (55 kDa)-coated surfaces display consistent resistance towards all tested solutions and organisms and hence this polymer could be considered as a potential material for marine-nonfouling applications.

In the second approach, to be able to study the effect that surface binding has on a coating's performance, a polymeric backbone that can easily be postmodified was used to build a matrix consisting of several analogous polymers. An active-ester-containing backbone was successfully synthesized via RAFT and characterized by means of elemental analysis, nuclear magnetic resonance (^1H , ^{19}F and ^1H - ^1H COSY), Fourier-transform infrared spectroscopy and gel-permeation chromatography. Its facile postmodification allowed for the construction of a polymeric library whose elements were designed to have PEG brushes grafted at the same density as a nonfouling function and a variable combination of both electrostatic and covalent surface binding groups. The nature of the covalent binding was taken into account based on the model surfaces used: silicon and titanium oxide. To this end, silane chemistry was used for targeting the former substrate and catechol and phosphonate for the latter one. For electrostatic interactions, positively charged amines were used to bind to the negatively charged substrates. Following nuclear magnetic resonance characterization of the analogous polymers, their adsorption onto the model surfaces was investigated via

ellipsometry. The predicted results based on the binding chemistry, were all obtained and later tested, using the same surface-sensitive techniques: for stability, by using a low and high ionic strength medium, and for protein resistance, by exposing the modified surfaces to a complex protein solution. The most promising combinations were further exposed to acidic and surfactant-containing solutions and their real-time adsorption, stability and protein resistance were monitored via quartz crystal microbalance with dissipation. Data indicate that the combination of electrostatic and covalent binding groups suitable for the two substrates allows for the creation of a coating that is extremely stable under very harsh conditions, and that afterwards still preserves its nonfouling function due to the retention of a brush-type conformation.

Zusammenfassung

Unter "Biofouling" versteht man allgemein eine unerwünschte Ansammlung von biologischen Materialien auf einer in Flüssigkeit getauchten Oberfläche. Diese Ansammlung kann aus Proteinen, Zellen, Bakterien oder sogar grösseren Mikroorganismen wie Algen bestehen und sich negativ auf das Verhalten eines Systems auswirken. "Biofouling" an Schiffsrümpfen erhöht den Strömungswiderstand, was zu langsamerer Fahrt und zusätzlichem Treibstoffverbrauch führt, die Bildung von Bakterienfilmen auf medizinischen Geräten erhöht die Infektionsrisiken und in der Lebensmittelverarbeitung kann "Biofouling" die Qualität des Produktes sowie dessen sicheren Verzehr beeinflussen.

In Anbetracht des breiten Spektrums von Anwendungen und Gebieten, die von "Biofouling" betroffen sind, wurde bereits viel Forschung in das Verständnis und die Kontrolle der involvierten Grenzflächenprozesse investiert. Überwiegend konzentrierte sich die Forschung auf Strategien zur Modifizierung der Oberflächen, da die physikalisch-chemischen Eigenschaften eines Materials so relativ einfach verändert werden können. Unter den verschiedenen Oberflächenbehandlungsmöglichkeiten ist das Aufbringen einer Beschichtung eine einfache und direkte Methode, um einem Basismaterial neue Funktionen und Eigenschaften zu verleihen. Eine solche Funktionalisierung der Oberfläche mit dünnen Polymerfilmen wird bereits in verschiedensten Anwendungsgebieten eingesetzt, so zum Beispiel auch in den oben erwähnten.

Die hier präsentierte Arbeit ist Teil eines europäischen Projekts, welches sich mit den Prozessen des marinen "Biofouling" befasst hat. Zu diesem Zweck wurden im Rahmen dieser Arbeit zwei große Studien durchgeführt. Die Ziele waren 1. eine Testplattform für verschiedene Oberflächenmodifizierungen zu entwickeln, mit welcher das "Biofouling" von mehreren hydrophilen, ungeladenen Polymeren parallel miteinander verglichen werden kann; und 2. zu untersuchen, welche Wirkung die Art der

Bindung zwischen Polymerbeschichtung und Oberfläche auf die effiziente Verhinderung von "Biofouling" hat.

In der ersten Studie wurden mehrere hydrophile Polymere, welche bekanntermassen "Biofouling" verhindern, auf einer mit photochemischen Gruppen versetzten Polymerschicht verankert. Wenn diese photochemische Gruppe durch UV-Bestrahlung aktiviert wird, bildet sich ein Radikal, welches mit der nächstgelegenen organischen Verbindung, in diesem Fall dem durch Spin-Coating aufgetragenen Polymerfilm, eine kovalente Bindung eingeht. Verankert wurden Polyethylenglykol (PEG), Poly(2-ethyl-2-oxazolin) (PEOXA), Polyvinylpyrrolidon (PVP) mit niedrigem und hohem Molekulargewicht, Polyvinylalkohol (PVA) und Dextran. Nach der Charakterisierung mit Hilfe von Ellipsometrie, Röntgenstrahl-Photoelektronenspektroskopie und Kontaktwinkel-Messungen, wurden diese modifizierten Oberflächen verschiedenen Tests zur Untersuchung der "Biofouling"-Eigenschaften unterzogen. Zum einen wurden sie in eine komplexe Proteinlösung eingetaucht (gefolgt durch Charakterisierung mit Hilfe von Ellipsometrie und Quarzkristall-Mikrowaage mit Dissipation), zum anderen wurden mit ihnen Haftstudien mit Meeresbakterien (*Cobetia marina* und *Marinobacter hydrocarbonoclasticus*) und Zoosporen der Grünalge *Ulva linza* durchgeführt. Aus diesen Daten wurden Rückschlüsse auf die Beziehung zwischen Struktur und Eigenschaft gezogen. Mit der oben beschriebenen Methode konnten Beschichtungen gefunden werden, die marinem "Biofouling" widerstehen. Der Grad der Beständigkeit hing stark vom untersuchten Polymer ab. Unsere Ergebnisse zeigen, dass Oberflächen, welche mit PVP mit niedrigem Molekulargewicht (55 kDa) beschichtet wurden, allen getesteten Lösungen und Organismen gegenüber eine gleichbleibende Resistenz aufzeigen. Damit könnte dieses Polymer für den Einsatz im Bereich des marinen "Biofouling" in Betracht gezogen werden.

Um den Einfluss der Bindungskräfte auf das Verhalten der Beschichtung zu untersuchen, wurde auf Basis einer einfach modifizierbaren polymeren Hauptkette eine Matrix von mehreren Polymeren erstellt. Die mit einer aktiven Ester-Gruppe versehene Hauptkette wurde erfolgreich über RAFT hergestellt und mit Hilfe von Elementaranalyse, NMR-Spektroskopie (^1H , ^{19}F und ^1H - ^1H COSY), Fourier-Transformations-Infrarot-Spektroskopie und Gel-Permeations-Chromatographie

charakterisiert. Daraus wurde eine Polymer-Bibliothek aufgebaut, deren Elemente jeweils gleich dichte PEG-Bürsten und eine variable Kombination von elektrostatischen und kovalenten Bindungsgruppen enthielten. Durch die Verwendung von zwei Modelloberflächen, Silizium und Titanoxid, konnte auch die Art der kovalenten Bindung berücksichtigt werden. Zu diesem Zweck wurden für das Silizium-Substrat Silane, für das Titanoxid-Substrat Catechole und Phosphonate verwendet. Die elektrostatische Wechselwirkung wurde mit Hilfe von positiv geladenen Amin-Gruppen untersucht. Nach der Charakterisierung durch NMR-Spektroskopie wurden die Polymere auf den Modelloberflächen adsorbiert. Mittels der oben erwähnten oberflächenempfindlichen Techniken wurde die Stabilität der Beschichtung gegenüber eines Mediums mit niedriger, respektive hoher Ionenstärke getestet. Die Proteinresistenz wurde bestimmt, indem die modifizierten Oberflächen einer komplexen Proteinlösung ausgesetzt wurden. Die vielversprechendsten Polymere wurden sauren und Tensid-haltigen Lösungen ausgesetzt, ausserdem wurde von diesen Polymeren die Adsorptionskinetik, Stabilität und Proteinresistenz in-Situ mit Hilfe von Quarzkristall-Mikrowaage bestätigt. Die auf Basis der Bindungschemie vorhergesagten Ergebnisse wurden bestätigt. Ausserdem zeigen die Daten, dass durch die Kombination von elektrostatischen und kovalenten Bindungsgruppen auf beiden Substraten eine Beschichtung hergestellt werden kann, welche sehr aggressiven Bedingungen widersteht, und welche durch die Aufrechterhaltung der bürstenartigen Konformation der Seitenketten, "Biofouling" effizient verhindert.

Table of Contents

Abstract	v
Zusammenfassung	viii
Table of Contents	xi
1 General Introduction	2
1.1 Biofouling on man-made surfaces	2
1.2 Scope of the thesis	8
2 Theoretical Background	16
2.1 Polymers at surfaces	16
2.1.1 General introduction.....	16
2.1.2 Polymers in solution.....	17
2.1.3 Polymers on a surface	18
2.1.4 Importance of conformation	20
2.1.5 Nonfouling behaviour through polymer brushes	22
2.2 Adhesion strategies	23
2.2.1 Polyelectrolytes	24
2.2.2 Self-assembly.....	25
2.2.3 Photochemical linkage	30
2.2.4 Multifunctional surface active polymers	32
3 Nonfouling Response of Hydrophilic Uncharged Polymers	36
3.1 Introduction	36
3.2 Experimental.....	37
3.2.1 Substrates	37

Table of Contents

3.2.2	Chemicals	38
3.2.3	Buffers.....	39
3.2.4	Synthesis of PAAm- <i>g</i> -PFPA (Poly(allylamine) <i>grafted</i> perfluorophenylazide)	40
3.2.5	Surface modification.....	40
3.2.6	Surface characterization	41
3.2.7	Biofouling assays	41
3.3	Results.....	44
3.3.1	Surface characterization	44
3.3.2	Short-term stability of coatings.....	50
3.3.3	Biofouling assessment	51
3.4	Discussion	56
3.4.1	Study of novel, multiply-tethered polymer coatings.....	56
3.4.2	Influence of polymer chemistry and proposed architecture on fouling response	60
3.5	Conclusions	63
4	Multimodal Binding of a Nonfouling Polymer	66
4.1	Introduction	66
4.2	Experimental.....	68
4.2.1	Substrates	68
4.2.2	Chemicals	68
4.2.3	Buffers.....	70
4.2.4	Synthesis of pentafluorophenyl acrylate monomer	70
4.2.5	Synthesis of poly(pentafluorophenyl acrylate) - PPFPAc.....	71
4.2.6	Matrix generation and postmodification reactions.....	72
4.2.7	Surface Modification.....	77
4.2.8	Surface Characterization.....	77
4.2.9	Stability assays	78
4.2.10	Protein adsorption assays.....	79

4.3	Results.....	79
4.3.1	Pentafluorophenyl acrylate monomer characterization.....	79
4.3.2	Poly(pentafluorophenyl acrylate) (PFPAc) characterization.....	82
4.3.3	Postmodification matrix.....	90
4.3.4	Surface modification.....	98
4.4	Discussion.....	115
4.4.1	Synthetic approach for developing a combinatorial polymeric matrix.....	116
4.4.2	Adsorption parameters.....	118
4.4.3	Influence of surface binding on stability and protein resistance response.....	120
4.5	Conclusions.....	124
5	Conclusions and Outlook.....	128
	Appendix.....	136
	Bibliography.....	159
	List of Abbreviations.....	179
	Acknowledgements.....	185
	Curriculum Vitae.....	189

Chapter 1

General Introduction

1 General Introduction

1.1 Biofouling on man-made surfaces

Biofouling can be defined as the attachment of unwanted biomass to surfaces allowing a biofilm comprised of fouling microorganisms to develop. This broad description fits various scenarios that range from biomedical devices and implants, biosensors or drug delivery systems^{1,2} to water purification equipment,³ marine equipment (ship hulls, fishing nets or any underwater structure)^{4,5} to packaging in the food industry.^{6,7} In the medicinal field, where biofouling often just refers to biofilm formation, the adverse effects of this process can lead to serious health risks such as microbial contamination, infection, implant rejection or biosensor malfunction.⁸ In both the industrial and marine fields, where biofilm formation is followed by the attachment of micro- to macroscale organisms (see Figure 1.1) or even deposition of inorganic material,⁹ the impact of biofouling translates directly into considerable financial losses and negative environmental impact. Issues such as pipe blockage, corrosion, decreased membrane flow or heat-exchanger efficiency and water contamination are often induced by biofouling.¹⁰

In order to better understand how to circumvent these issues, collaborations between academia and industry are quite often established with the aim of forming interdisciplinary research networks. This thesis is part of a larger research project involving several academic and industrial partners called *Seacoat*. The project aims were to gain a deeper understanding of the interfacial processes involved in marine biofouling.

The importance of minimizing biofouling become obvious when considering the surface of a ship's hull. There, biofouling results in an increase in drag, which increases fuel consumption and engine stress,¹¹ causes corrosion¹² and necessitates more frequent dry-docking cleaning operations, which can lead to the discharge of toxic

chemicals into the ocean. For these reasons it is not surprising that nowadays nonfouling properties are among of the most important considerations when studying the adsorption of ultrathin polymer films.

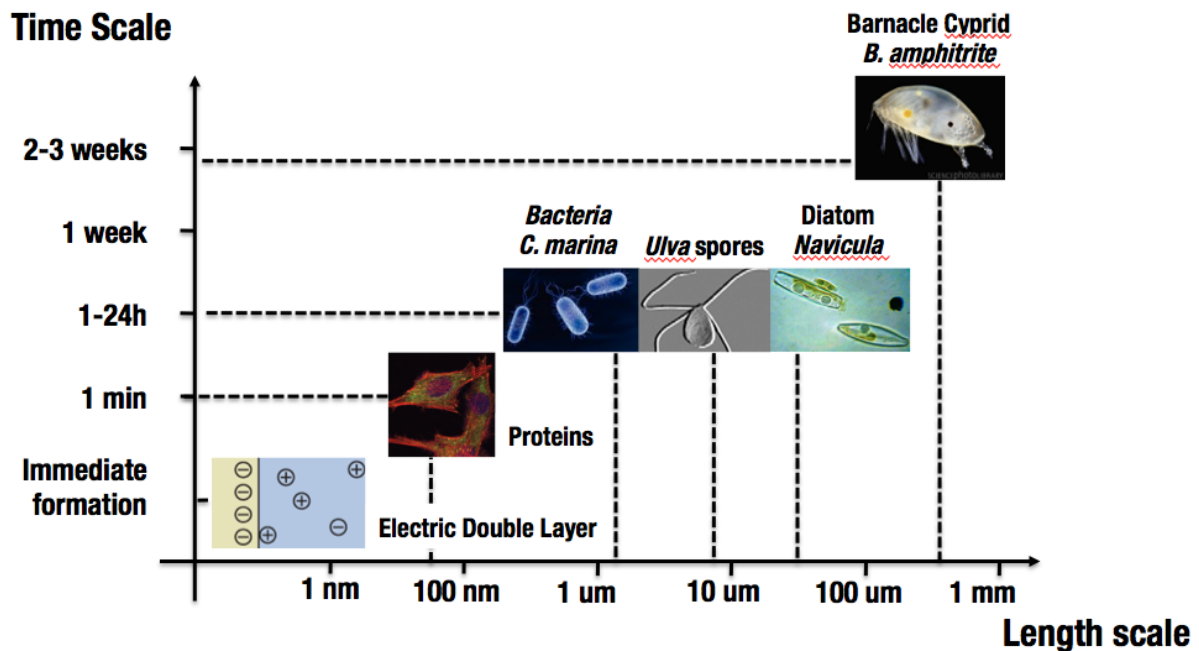


Figure 1.1 Time and length scales for marine biofouling processes after immersion of a sample into seawater.

Biofouling is a complex, four-stage process¹³ that starts immediately after immersion of a clean surface in a water-based environment. It depends on several physical, chemical and biological factors¹⁴ and begins with the non-specific adsorption of macromolecules, such as proteins, polysaccharides and humic substances that are present in trace amounts in water.¹⁵ When the proper conditions of nutrient availability, pH and humidity are present after this conditioning, a biofilm is created in a second stage, as fouling microorganisms such as bacteria start to be attracted to the surface due to factors like Brownian motion, sedimentation and hydrodynamic forces.¹⁶ They reversibly adsorb onto these surfaces due to van der Waals forces, electrostatic, and hydrophobic interactions.¹⁷ Upon secreting an adhesive matrix designated as EPS (extracellular polymeric substances), mainly composed of polysaccharides, proteoglycans, proteins, glycans, lipids and DNA,¹⁸ they begin the colonization process

by adhering irreversibly to the surface and to one another. The third stage includes the attachment and development of a complex, multicellular community of macrofoulers, and in the last step, larger invertebrates settle and grow. With increasing biodiversity of the biofilm, the number of species attracted to it will be larger, as the already present ones can indicate settlement suitability.¹⁹

Since biofouling and its prevention have been addressed for centuries, beginning with problems concerning ships' hulls,²⁰ several strategies have been developed to approach the subject. In addition to mere simplification of the process of mechanical removal of the formed deposits, the older and traditionally more effective methods have been focused on biocides, and thus many of the coatings contained large quantities of copper or tin-based compounds.²¹ Since copper has become costly and is associated to issues related to corrosion,²² and tin has been recognized as being toxic and is thus banned from commercial use,²³ a universal motivation to develop a generation of non-toxic, biocidal-free, non-adhesive surface structures or coatings^{24,25} is currently driving both market and research activities.

When thinking about designing nonfouling surfaces there are three major mechanisms and principles to be considered:

- physical – considering some organisms are known to use physical methods to deter biofouling (e.g. shark skin and lotus leaves),²⁶ this approach has inspired some biomimetic approaches through modifications in surface topography and hydrophobic properties.²⁷⁻²⁹ The motivation to artificially modify surface geometry as a nonfouling strategy arises from the fact that certain marine organisms, e.g. sharks, show characteristic topographies on their skin that render them resistant against adhesion from the fouling community. Studies have been made where the effect of different shapes on biofouling was investigated, the scales (nano to macro) of the structures were varied or mixed, and the influence of combining nonfouling chemistry was evaluated. A more detailed description of this topic can be found in the work of Myan and co-workers.³⁰ Regarding the hydrophobic modification of surfaces, or rather changes in wettability, the rationale that supports this approach is in trying to minimize contact with the medium (water) where the fouling community can be found. This is achieved either by creating a super hydrophobic surface that will immediately repel any

water droplets due to surface energy and topography (not relevant for immersed structures), or by creating an air film between solid and water. Nevertheless other physical methods such as electrolysis, radiation and vibration have proven to exhibit specific nonfouling effects towards certain species, although difficulties in their practical application have limited the success of these technologies⁴. For more details on the topic, further reading is advised;³¹

- biological – in this approach, enzymes embedded in a polymeric matrix have been considered. The non-fouling reaction is dependent on the enzyme-specific activity, e.g. degradation of the adhesives secreted during the biofilm formation, disintegration of the conditioning film's matrix, generation of biocides or disruption of the cell development of foulers.^{32,33} Unfortunately, enzymatic activity can be easily compromised by changes in pH, temperature or ionic strength, which narrows the industrial applicability of the strategy considerably.

- chemical – surface modification is by far the most exploited field in trying to understand and prevent biofouling, although it has already become very clear that the problem requires an overall interdisciplinary approach. Since it is an extremely broad topic, it was decided to focus this introduction on homogeneous 2D structures based on tethered polymers on surfaces for conditioning biofouling, as opposed to 3D systems (e.g. nanoparticles).³⁴

There are three general approaches currently under study: fouling-degrading polymers, which incorporate enzymes or quaternary ammonium compounds,³⁵ fouling-release polymers, which aim for low modulus and/or low surface energy in order to decrease adhesion strength of the fouling organisms,^{36,37} and fouling-resistant polymers. The present work is concerned with the last of these strategies.

The most promising nonfouling ability in coatings has been achieved through the use of either uncharged hydrophilic or zwitterionic polymers,²⁴ as both have the necessary criteria to resist the first step in biofouling, which is the nonspecific adsorption of proteins. This implies the existence of polar functional groups and hydrogen-bond acceptor groups, absence of net charge and hydrogen-bond donor groups.^{38,39} Another common feature of this type of coating is the strongly bound hydration layer that is generated at the surface. This occurs due to hydrogen bonding with water molecules for the hydrophilic materials or electrostatic interactions for the

zwitterionic ones,⁴⁰ creating both a physical and an energetic barrier to protein adsorption.⁴¹ Since a high degree of hydration implies an ordered array of water molecules, this will increase the enthalpic penalty necessary to remove them and allow for proteins to adhere.

When trying to predict a polymer film's surface hydration, there are an underlying number of factors that firstly need to be taken into account, as their interconnection and dependence on chemistry makes generalization difficult. Such factors are: chain length (or thickness), surface density and chain conformation.

The most studied model for hydrophilic polymers is, by far, poly (ethylene glycol) (PEG) deposited in form of polymeric films or as oligo(ethylene glycol) (OEG) in self-assembled monolayers.⁴²⁻⁴⁸ For the former case it was observed that the longer the chain length, i.e. molecular weight, the better the protein resistance, provided the grafting density is high enough for the polymer to acquire the right conformation (brush-like) that allows for the formation of a complete steric barrier at the surface.⁴⁷ Nonfouling, ultradense PEG-based polymer films can be achieved by reducing their hydrodynamic volume during adsorption via temperature and increase of salt concentration—cloud-point grafting method.⁴⁹ Although PEG will lose much of its hydration capabilities at this stage, as the water amount available is now reduced, it will still retain protein resistance if found in a brush or mushroom-like conformation.^{49,50} Equivalent conformation dependence was even observed in SAMs containing a three ethylene glycol (EG) unit,⁵¹ where a helical rather than a trans conformation provides better protein resistance by allowing more water molecules to penetrate into the SAM. The reason why only a few EG units are enough to provide nonfouling characteristics in SAMs as opposed to the trend observed for PEG, is related to the different proposed mechanisms. For short-chain SAMs it is surface hydration that plays the key role, but for polymeric films it is steric repulsion. This effect is caused by the existence of large excluded-volume effects and high conformational entropies of the long, tethered PEG chains, which upon approach of a protein will create an energetically unfavorable compression of the polymer segments.^{52,53}

Among the best hydrophilic polymers, which include polysaccharides, poly(ethylene glycol) (PEG) clearly assumes an advantageous position as it is capable

of reducing the adsorption of various proteins (fibrinogen, myoglobin, albumin or full blood serum) but also the settlement (attachment) of foulers such as zoospores of the marine alga *Ulva linza* and diatoms (unicellular slime-forming algae);^{42,54-56} polymeric coatings incorporating PEGylated moieties are equally beneficial towards preventing fouling.⁵⁷⁻⁵⁹ Nevertheless, other polymers have stimulated equal interest in order to overcome certain limitations of PEG, such as its degradation under oxidative conditions.⁶⁰ Examples include poly(2-ethyl-2-oxazoline) (PEOXA) which has been studied as a liposomal surface modifier for drug-delivery vesicles with an efficiency similar to PEG⁶¹ but also shows resistance to bovine serum albumin (BSA) adsorption;⁶² poly(vinyl pyrrolidone) (PVP) decreases fouling by lysozyme, BSA and fibrinogen;⁶³⁻⁶⁵ poly(vinyl alcohol) (PVA) was found to be effective in reducing the adhesion of the diatom *Amphora coffeaeformis* independently of the shear rate to which the surfaces were subjected⁶⁶ and as a gel has been shown to reduce barnacle attachment;^{67,68} and dextran has shown the ability to reduce adsorption of human-serum proteins.⁶⁹

Regarding zwitterionic polymer films, which contain both negative and positively charged groups in each repeating unit but with an overall net charge of zero, although there is no equivalent well-established model system like PEG, the overall guidelines for protein resistance have been verified.⁷⁰⁻⁷² Additional key features are the surface charge balance, which should be as homogeneous as possible providing a negative to positive charge ratio of 1:1, and minimized dipole via close packing density.⁴⁰ What makes these materials so appealing as alternatives to PEG-based films is the fact that the hydration layer binds more strongly, as it is formed not only by hydrogen bonding, but also by the ionic solvation of the charged groups by water molecules.⁷³ They also constitute a biomimetic approach to nonfouling as similar structures are to be found in red blood cells⁷⁴ and they do not face the same oxidative degradation issues as those related to PEG.⁶⁰

Zwitterionic polymers often contain a quaternary ammonium as the cationic group and various anionic groups (see Figure 1.2). Some examples are sulfobetaine, which has proved to be resistant to fibrinogen adsorption,⁷⁵ reduces attachment of the diatom *Amphora coffeaeformis* and the settlement of cyprid larvae of the barnacle

Amphibalanus Amphitrite;⁷⁶ carboxybetaine has shown low fouling from blood plasma⁷⁷ and resistance to fibronectin adsorption;⁷⁸ and phosphorylcholine, which presents low adsorption of lysozyme, fibrinogen and BSA^{70,79} and low cell adhesion.^{80,81}

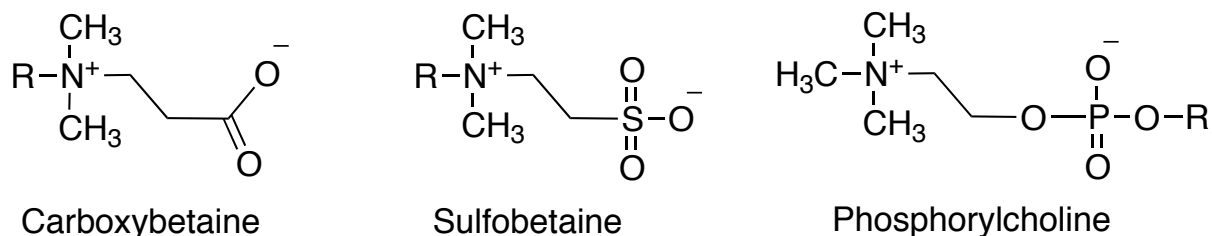


Figure 1.2 Chemical structures of some zwitterionic structures used in nonfouling coatings.

Within this thesis, to compare the efficiency of nonfouling coatings, we have put the focus on different, hydrophilic, uncharged polymers.

1.2 Scope of the thesis

Taking into account the complexity of the biofouling process, the work presented in this thesis never aimed at trying to find a solution for the problem, but rather the aim was to develop methodologies that can facilitate its understanding. Although an awareness of the multidisciplinary core of this problem was taken into account, the interpretation of the results obtained focused on physicochemical understanding.

Considering the current trends to approach biofouling, surface-tethered polymers were used in novel ways throughout this work. There is an extensive available literature based on similar approaches that shows underlying support for the use of this chemistry. Reasons include their versatility in chemical architecture, varied synthesis methods with different advantages and drawbacks that can fit tailored scenarios, easy postmodification manipulation and ability to produce uniform surfaces characterized by high thermal and chemical stability.

The overall aim of this work was to understand and improve the efficiency of nonfouling coatings. There are two approaches addressed: to develop a platform that would allow a reliable comparison between the activity of different well-known nonfouling chemistries (Chapter 3) and investigate the influence of a coating's adhesion strength in its overall protein resistance ability (Chapter 4). Both these two issues were studied using different postmodification methodologies, which consist in modifying the chain side functions of an already-synthesized polymer, in order to facilitate its specific architecture and consequent application. Although the establishment and advances of controlled polymerization techniques already allow for the manufacture of a variety of polymeric structures under mild conditions, there can still be incompatibilities between chemical functionalities or with the reaction conditions, giving rise to the importance of postmodification.^{82,83}

In the first approach, to be able to develop the above-mentioned comparative platform, a primer layer containing reactive chemical entities known as azides⁸⁴ was used to pre-functionalize a surface, followed by the deposition and subsequent individual immobilization of nonfouling polymers with brush-like conformations. Azides are known to possess the ability to decompose into nitrenes upon thermal or photo activation.^{85,86} Nitrenes are highly reactive, short-lifetime chemical species that undergo various reactions such as cycloaddition, rearrangements or, most importantly for this work, insertion reactions.⁸⁷ Aryl azides have been widely used due to their high stability and, when halogenated, preferential formation of the required singlet nitrene intermediate that preferentially inserts, unspecifically, into for example C-H and N-H bonds,⁸⁸ rather than the alternative reactions of hydrogen abstraction or ring expansion taking place. The existence of this latter conformation would pose a problem, since it mainly reacts with nucleophiles such as amines, substantially decreasing the yield of products resulting from C-H insertion.⁸⁹ Examples of applications of this approach are: crosslinking,⁹⁰ photolabeling,⁸⁹ photolithography⁸⁶ and surface modification.⁹¹

Our approach was accomplished by means of a monolayer that possesses a cationic polymeric backbone and pendant azide groups (Figure 1.3). The backbone allows an electrostatic interaction to be formed with a negatively charged substrate and

the nitrenes, formed from the azides following photo activation, readily form covalent bonds with any organic matter in their close proximity, generating multi-tethered polymer brushes that are monomolecular in thickness.

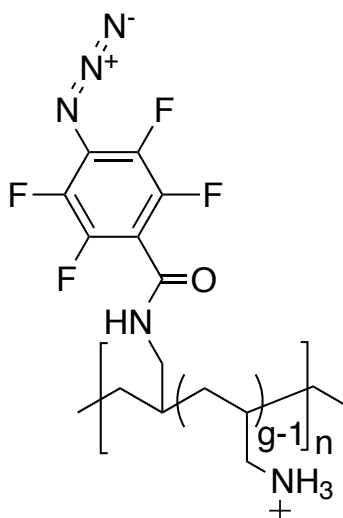


Figure 1.3 Chemical structure of Poly(allylamine)-*grafted*-perfluorophenylazide (PAAm-*g*-PFPA).

Following the aim of this work, hydrophilic uncharged polymers were attached, i.e. PEG, PVA, PEOXA, PVP and dextran (Figure 1.4) onto a surface using the same modification procedure, to study if parameters exist that determine the overall capacity to resist specifically marine fouling on different length and time scales.

The modified surfaces were then characterized by means of variable-angle spectroscopic ellipsometry (VASE), X-ray photoelectron spectroscopy (XPS), dynamic water contact angle (dCA) and quartz-crystal microbalance with dissipation (QCM-D). Further comparative biological studies were performed by exposure of the coated samples to a complex protein solution (full human serum), so that nonspecific protein adsorption could be evaluated, two marine bacteria (*Cobetia marina* and *Marinobacter hydrocarbonoclasticus*) and zoospores of the marine alga *Ulva linza*. Spores of *U. linza* are motile pyriform cells, 7-8 μm length, which must locate and settle (permanently adhere) on a surface in order to complete the life cycle.⁹² Spores respond to a variety of surface-associated cues and have been extensively used in comparative assays of the

antifouling performance of experimental coatings.³⁵ The approach adopted in the research reported here allowed the newly developed surface-functionalization protocol to be validated and performance evaluated against a selection of well-known fouling organisms.

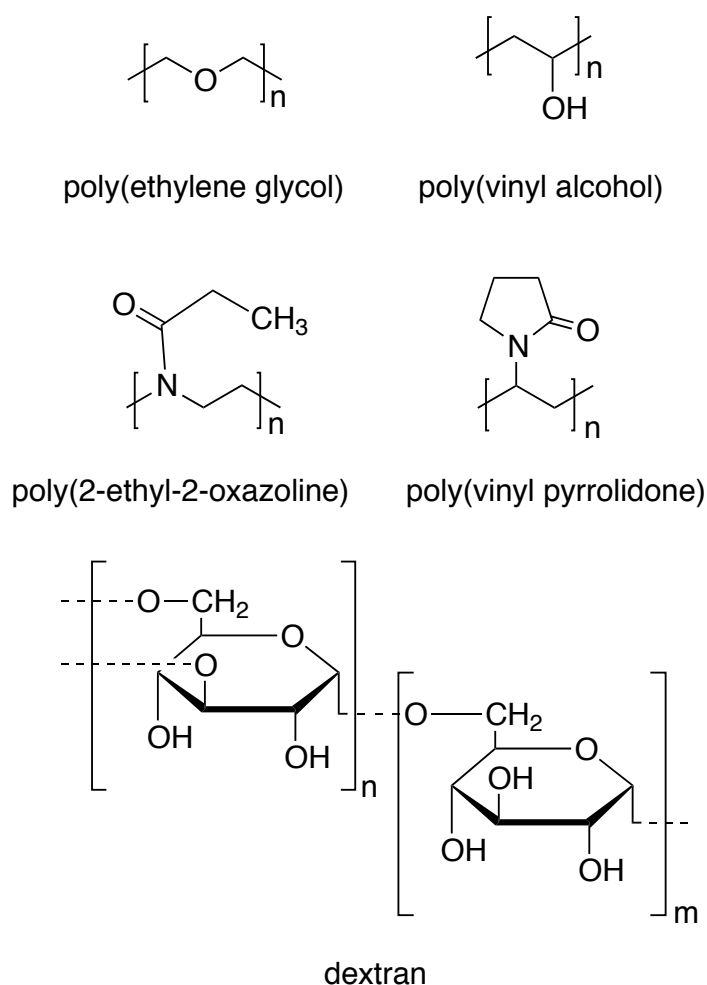


Figure 1.4 Chemical structures of the hydrophilic uncharged polymers used.

In the second approach, a multimodal backbone was used, onto which functional groups of interest could be readily grafted, providing an ideal *test bench* for our synthetic studies regarding surface adhesion. In order to be able to tailor the strength of a polymer's adhesion onto a surface or to allow the introduction of specific functionalities, the versatile postmodification approach is particularly of great interest to both industrial and academic fields considering the physicochemical possibilities it can

entail. This method used for the engineering of functional polymers can be achieved through a variety of reactions that include the above-mentioned azide chemistry, the modification of active esters or other chemical groups such as anhydrides or oxazolones, through the use of Michael type or radical thiol addition reactions, Diels-Alder cycloadditions or click chemistry, just to name a few.

For this work section, an active-ester-containing polymer was used to provide the ability to create a wide library of postmodified polymers due to the possibility of introducing various chemical functionalities, provided they are amine terminated. This feature therefore can enable the facile synthesis of well-defined polymer brush architectures.

The key polymeric backbone, synthesized based on a pentafluorophenyl acrylate monomer by means of the controlled reversible addition-fragmentation chain transfer (RAFT) polymerization technique (Figure 1.5).

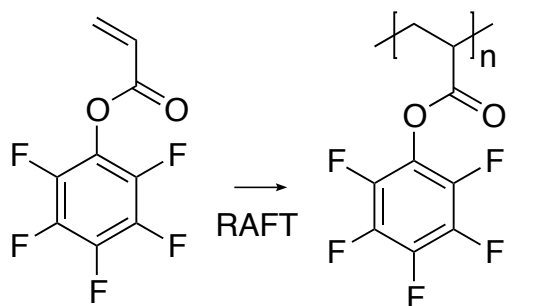


Figure 1.5 Polymerization of poly(pentafluorophenyl acrylate) – PPFPAc.

The resulting polymer has been post-modified with a fixed grafting ratio of a nonfouling function (mPEG-NH₂), in order to test for protein resistance, and a varying combination of functional groups that can provide a strong affinity to model substrates. The latter groups include amine, silane, catechol and phosphonate in different combinations, which enables substrate binding and its influence on protein adsorption to be efficiently investigated (Figure 1.6). This study was complemented by the synthesis of control polymers having the non-binding ethanolamine instead of the binding groups.

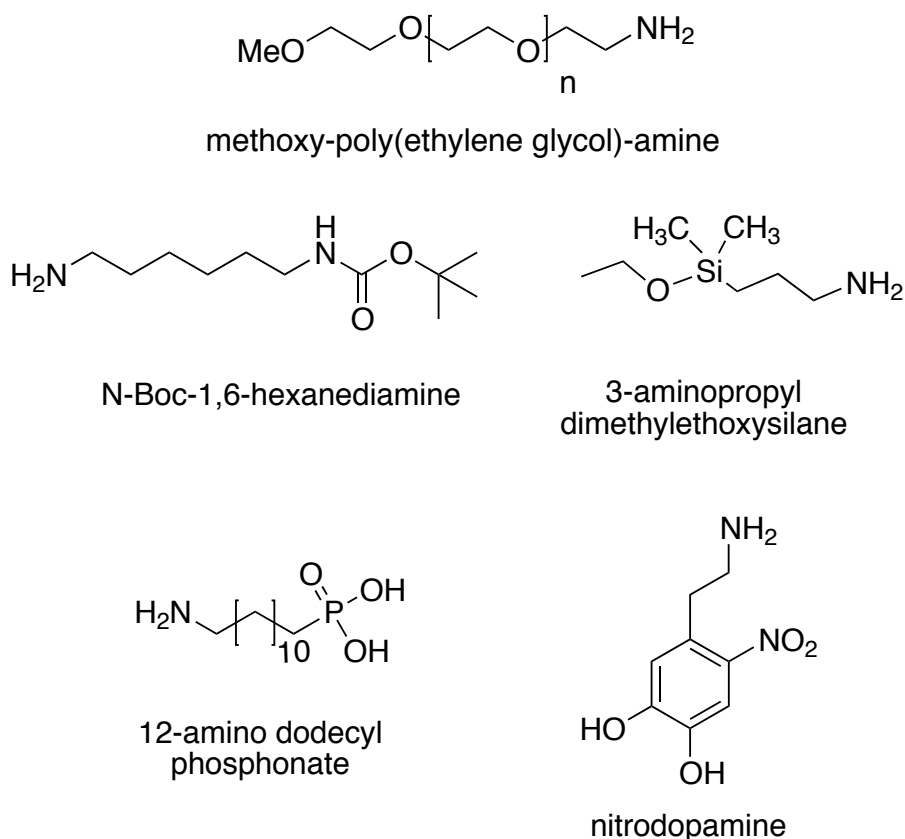


Figure 1.6 Chemical structures of the surface binding moieties used.

Bulk characterization of the synthesized polymers includes gel-permeation chromatography (GPC), nuclear magnetic resonance (¹H, ¹⁹F and ¹H-¹H COSY), Fourier transform infrared spectroscopy (FT-IR) and elemental analysis (EA). The surface-related techniques such as variable-angle spectroscopic ellipsometry (VASE), X-ray photoelectron spectroscopy (XPS) and quartz-crystal microbalance with dissipation (QCM-D) were also applied to characterize the polymer's performance towards non-specific protein uptake (full human serum).

Chapter 2

Theoretical Background

2 Theoretical Background

The content of this chapter will provide an insight towards this thesis motivation and work. Basic concepts will be explained and a general context along with a relevant state of the art will be given.

2.1 Polymers at surfaces

2.1.1 General introduction

Monolayers or multilayers of ultrathin polymeric films (up to 100 nm thick) tethered to a solid substrate have proven to be applicable to a wide range of technologies, whether just as adlayers, or stratified and/or patterned films. Examples of fields where these are often applied are the manufacture of protective and functional coatings⁹³, nonfouling (bio)surfaces,⁹⁴ medical implants,⁹⁵ molecular electronics,⁹⁶ sensors,^{97,98} microfluidics,⁹⁹ solar cells,¹⁰⁰ corrosion inhibition,¹⁰¹ lubrication and friction modification,¹⁰² etc.

Besides the interest from the industrial sector, ultrathin films are also highly studied in academia, as it is known that adsorbed polymers at the nano-scale often present strong deviations from their bulk properties, such as glass-transition temperature, diffusivity, crystallization behaviour or wettability, among others.¹⁰³ This phenomenon occurs when the thickness of the film (h) is comparable to the dimension of the polymer, which is given by its radius of gyration R_g in a given solvent or ambient. At this scale the energetic contributions of the interfacial layers start affecting the polymer's behaviour, either dynamically or structurally.¹⁰⁴ It is believed that the confinement between the substrate (solid-polymer) and the free (air/liquid-polymer) interface is primarily responsible for such changes in the properties of the polymer.

Therefore it is mandatory to first comprehend the essential concepts inherent to polymers when in solution and when on a surface.

2.1.2 Polymers in solution

The behaviour of an ideal neutral polymer chain in a diluted bulk solution, where interactions between different polymer chains can be neglected, were historically described with a random-walk model that leads to a stage of maximum conformational entropy, all steps in any direction having equal probability to be occupied by a monomer unit of equivalent size. This would lead the polymer chains to adopt a random-coil conformation and would allow for its simple statistical behavioural analysis.¹⁰⁵ Nevertheless the influence of parameters such as chain rigidity (created by bond and rotation angles) and excluded-volume effects caused by both polymer-polymer and polymer-solvent interactions would be neglected. The self-avoiding walk (SAW) theory was then proposed altering the scaling dependence of the radius of gyration of the chain, R_g , defined as the average distance between the centre of mass of a polymer coil to any other existing point in it.¹⁰⁶

$$\text{Ideal Chain} \quad R_g \approx N^{1/2} \quad (1)$$

$$\text{Real Chain} \quad R_g \approx N^{3/5} \quad (2)$$

where N is the number of segments/monomers along a polymer chain

In this case, the much stiffer polymer chains have a decreased number of conformational states available, as segments cannot overlap and the degree of expansion of the chain ends up being dictated by the solvent quality, given by the Flory-Huggins interaction parameter χ .^{107,108} In the case where polymers are in a thermodynamically good solvent ($\chi < 0.5$), the polymer segments are surrounded by a maximum number of solvent molecules, leading to a repulsion effect between segments and forcing the polymer chain to adopt a long and flexible conformation with low

monomer density (excluded volume effect). In a bad solvent ($\chi > 0.5$), the chain segments will contract in order to minimize contact with the solvent molecules and adopt a conformation as close to a high-density random coil as possible. As the properties of the latter will depend on temperature, there is yet another case when the attractive and repulsive forces cancel each other leading the chain to behave ideally. It happens at a θ temperature and χ is equal to 0.5. The Flory-Huggins theory can also be used for multicomponent systems (e.g. polymer/polymer/solvent) and predict (im)miscibilities but it can also be used to study inhomogeneous multicomponent systems of polymers with arbitrary architectures in arbitrary geometries. However these are not the cases found in our work. Further reading on this subject can be found elsewhere.¹⁰⁹

2.1.3 Polymers on a surface

The behaviour of a polymer once successfully linked to a surface depends intrinsically on the adsorption conditions. When thinking about polymer adsorption on a surface, the concept of Flory-Huggins interaction parameter mentioned in the previous section can be considered a good starting point to describe the new situation: if $\chi < \chi_{\text{surf}}$ (χ now refers to polymer-solvent, polymer-surface and solvent-surface interaction energy, while χ_{surf} gives the polymer-surface interaction energy), the polymer will not adsorb, while if $\chi > \chi_{\text{surf}}$ the polymer will adsorb spontaneously and the adopted conformation will depend on the equilibrium found between the conformational entropy loss as it binds to the surface, and the enthalpic gain of the surface-polymer contact.¹¹⁰ It was suggested that upon initial adsorption, polymers can adopt three types of conformation depending on the coverage and molecular weight: if both are high they will most likely adopt a tail (non adsorbed polymer) or loop (no contact with surface) shape, while at low coverage and molecular weight, and in case of a strong polymer-surface interaction energy, a train will be formed (see Figure 2.1).¹¹¹

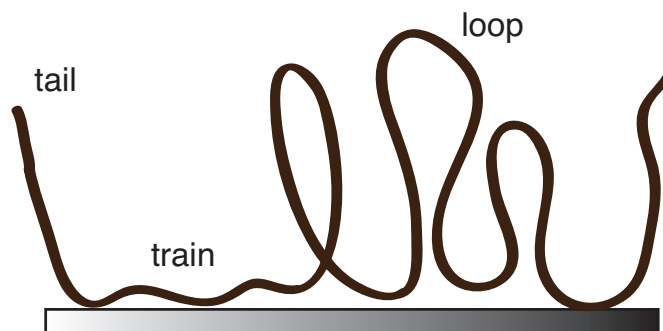


Figure 2.1 Representation of an adsorbed polymer adopting train-tail-loop type of conformation.

For end-tethered polymers, the polymer–surface interaction energy also influences the final adsorbed conformation: if the interaction is zero, the surface is considered inert and, depending on the solvent quality, the chains will either be found in a globular (bad solvent) or coil (good solvent) shape as they are found in bulk, but if the interaction energy is below zero then the polymer is attracted to the surface and it can adopt a pancake type of conformation¹¹² provided the grafting density (σ) is low enough (see Figure 2.2).

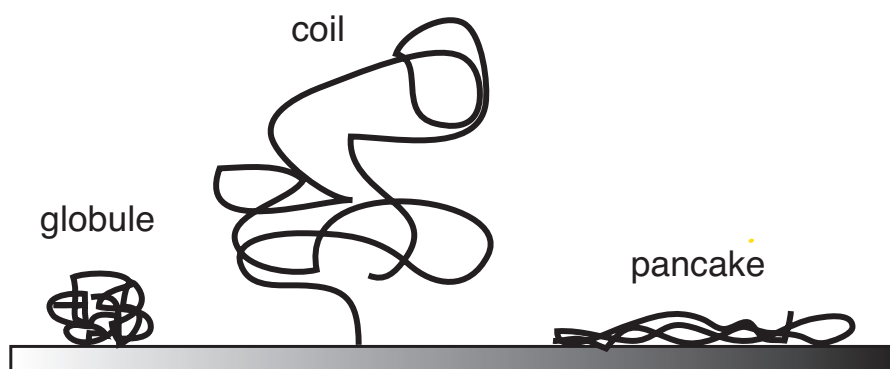


Figure 2.2 Possible conformations for single-tethered polymers: globule (non-adsorbing, bad solvent), coil (non-adsorbing, good solvent) and pancake (adsorbing) at low grafting densities.

Another conformational scenario is possible for high grafting densities of end-tethered polymers. If the chains are found to be in a good solvent and the distance between anchoring sites (L) is larger than twice the size of the chain coil ($L \gg 2R_g$) they

will adopt a 'mushroom-type' of conformation as they are distant enough to prevent any possible repulsive interactions between neighboring chains, much like the coil conformation presented before. As soon as the distance between anchoring sites starts decreasing and the interchain repulsion starts to become significant, the chains begin stretching normally to the surface plane to minimize this effect and end up adopting a 'brush-type' conformation when $L < 2R_g$ is finally reached (see Figure 2.3). The amount of stretching (or height of the film) achieved depends on an equilibrium found between the repulsive forces and the elastic free energy of the chains, which is caused by the significant conformational loss.¹¹³

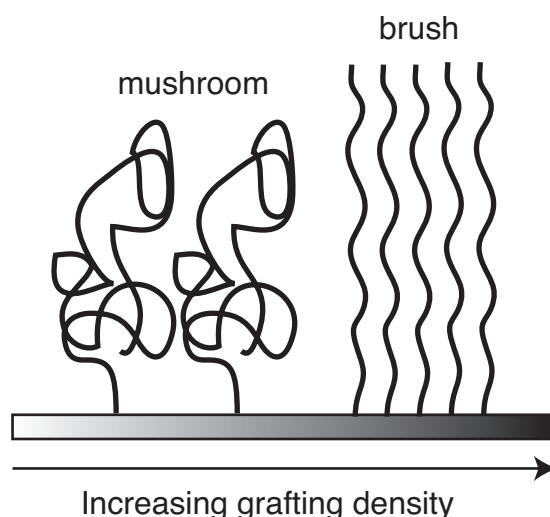


Figure 2.3 Possible conformations for single-tethered polymers in good solvent with increasing grafting densities: mushroom and brush, respectively.

2.1.4 Importance of conformation

In recent years, the polymer-brush regime has been widely studied and used in functional ultrathin films due to its unique physicochemical properties. As mentioned previously, this regime is known to result from high surface chain density of grafted polymers, when in the presence of a good solvent¹¹⁴ and in order for a polymer to reach this conformation, the distance between anchoring sites has to be smaller than twice the radius of gyration of free polymer chains ($L < 2R_g$).¹¹³ Nevertheless they can still be

distinguished between two types of categories according to their grafting density (σ), which is defined in equation (3).

$$\sigma = \frac{h \times \rho \times N_A}{M_n} \quad (3)$$

where h is the brush thickness, ρ is the bulk density of the brush composition, N_A is Avogadro's number and M_n is the number average molecular weight.

In semi-dilute systems, the chains will still overlap when in a good solvent although they possess low volume fraction, but their behaviour (thickness, interactions, segment density profiles, etc) can be easily predicted by scaling models. In concentrated systems, the grafting density of the polymer chains is considerably higher and interchain interactions start playing a role such that behavioural properties can no longer be predicted according to the established models.¹¹⁵ The initial difficulties in understanding their properties rely much on the limitations of the synthesis methods available to obtain dense grafted polymer chains. Although a general model is still yet to be proposed, great improvements have already been made in this specific field with the appearance of surface-initiated living radical polymerization techniques.¹¹⁶ For instance, it was discovered that the increased rigidity of the film by increasing grafting density may be due to a permanent end-monomer tension, which can be relevant to applications where end-functionalization is key,¹¹⁵ e.g. biosensing.¹¹⁷

Coatings comprising these systems, semi-dilute and concentrated brush regimes, can be prepared with two different methods: 'grafting to' and 'grafting from'. In the former, end-functionalized polymer chains are end-tethered to a solid substrate containing functional groups. These can be obtained via chemical reaction or, in case of side-chain adsorption, multiple tethering is observed, yielding a film with flat conformation. The formation of such coatings by adsorption is limited by the diffusion kinetics of free chains attempting to attach to an increasingly crowded and sterically hindered surface. Thus this approach normally results in a lower grafting density (semi-dilute brush system). One complication to bear in mind is the possible competition between other functionalities present in the polymer to the anchoring moieties often

found when trying to adsorb alkoxysilanes containing amines to a SiO₂ substrate. However, within this grafting method there is an approach that allows overcoming the repulsive forces that limit higher surface densities designated as 'cloud point grafting'. In this strategy, adsorption conditions, namely temperature and/or ionic strength, are increased provided the polymer demonstrates an inverse solubility-temperature relation. These conditions lead to the loss of coordinated water molecules to the polymer chains causing a partial collapse of the latter and allowing for a closer packing to be reached upon adsorption. The principle was initially developed in the early 1960s¹¹⁸ for PEG systems in complex solvent mixtures but it was not until early 2000s that it was applied to surface grafting.⁵⁰

The 'grafting-from' method, in which chains are grown from the substrate by surface-initiated polymerization techniques (e.g. atom-transfer radical polymerization (ATRP), nitroxide-mediated polymerization (NMP), reversible addition-fragmentation chain-transfer polymerization (RAFT)),^{116,119} a higher grafting density as well as control over thickness is reached (concentrated brush regime) since the small monomer units more easily access the growing end of the chain. Challenges with this approach are to be found in potentially long reaction times, the complexity and control of the reaction due to oxygen sensitivity, and solution-versus-surface polymerization.

Polymer brushes are found to be extraordinarily responsive to the environment surrounding them, including changes in solvent quality,^{120,121} temperature,¹²² pH¹²³ or salt concentrations.¹²⁴ This makes polymer-brush-based coatings highly interesting in a wide range of applications such as biomaterials, as they can be easily tailored and triggered so as to enhance the desired function.

2.1.5 Nonfouling behaviour through polymer brushes

Preventing the nonspecific adsorption of proteins, cells or other microorganisms is of great importance for being able to control the process of biofouling on solid substrates. For the reasons presented at the end of the previous section, polymer brushes are highly explored entities used to understand the interfacial processes

involved in this phenomenon. They allow studying the influence of several design parameters depending on the targeted application.

As stated in section 1.1, both hydrophilic and zwitterionic polymers are known for their excellent performance in deterring biofouling at the nanoscale, but this is not solely dependent on chemistry itself. For instance, studies based on the nonfouling model molecule poly(l-lysine)-*graft*-poly(ethylene glycol) (PLL-*g*-PEG),^{44,125} suggest that surface density is an exploitable parameter, as ultradense brushes have enhanced nonfouling behaviour,⁴⁹ most presumably due to a surface increase of ethylene glycol (EG) units per area. Chain length of the polyelectrolyte backbone can also affect the resistance of PLL-*g*-PEG, as conformational issues may arise upon adsorption, leading to an overall lack of effectiveness of PEG.¹²⁶ As for the influence of chain length of the nonfouling polymer, it has been observed that an optimal value does exist but it is highly dependent on the entities tested for¹²⁷ and chemistry used.¹²⁸ Charge is yet another possible feature to study. It was found that a neutral net charge of the polymer, whether it is charged (e.g. case of zwitterionic polymers) or uncharged, acquire the best resistance to protein adsorption (see section 1.1). Also the effect of chemical patterning can be investigated via polymer brushes, most often to manipulate cell behaviour.^{129,130} Among the most famous approaches are the initiator substrate patterning via lithographic or contact printing techniques prior to functionalization via a surface-initiated polymerization (SIP),¹³¹ creation of binary polymer systems based on successive SIPs^{132,133} and preparation of polymeric gradients by varying their grafting density to the surface photochemically¹³⁴ or by creating initiator monolayer gradients, the latter being used for polymerization via SIP techniques.¹³⁵ Studies on the effect of chemical patterning have indeed shown both reduced protein uptake, *Ulva* spores settlement and cell adsorption depending on the structures containing nonfouling polymers,^{134,136} provided the length scale of the patterns is smaller than the tested organism (or the part of it that is responsible for surface exploration).¹³⁷

2.2 Adhesion strategies

Overall, there are two main ways according to which a polymer can adsorb onto a surface: this can be due to chemisorption or physisorption. The first one implies the

formation of a chemical bond between the polymer and the surface and is often irreversible, e.g. covalent, while the latter is based on weaker interactions such as van der Waals, hydrogen or electrostatic bonding. The difference between these two types of adsorption is not only the difference in bonding strength, but also that the adsorption kinetics of the two classes of interaction is quite different. Physisorption is considerably faster, as there is no covalent bond to be formed there is no activation barrier to overcome,¹³⁸ and, according to the DLVO theory, can be dominated either at short distances via van der Waals or at longer distances via electrostatic forces. Indeed, it is well known that the use of weak-binding, long-range interactions enables good surface spatial organization of the molecules containing ionisable groups due to intramolecular charge repulsion, as will be discussed in the polyelectrolyte adsorption section. In particular, due to the stretched conformation of the polymers in solution, one could hypothesize that upon adsorption, the train conformation will be favoured.

2.2.1 Polyelectrolytes

Polyelectrolytes can be described as homopolymers carrying ionisable groups on each monomer and as they are found in solution (water) there will be a charge associated to them, enhancing the role of electrostatic interactions. This can lead to a stretching of the chain in solution to minimize intramolecular repulsion, although salt addition to the solution will cause charge screening which can affect the conformation and hence influence the adsorption behaviour.¹³⁹ Another parameter that equally participates in the adsorption process is charge density along the polyelectrolyte and the surface. The following scenarios may take place on oppositely charged surfaces:

- when both charge density at the surface and the salt concentration are low, the polyelectrolytes will adsorb to a low extent and adopt a mostly train conformation; by increasing salt concentration, the adsorption will be promoted as the repulsion between charged segments will be screened and the solvent quality may also decrease, provided the surface charge is still residual – *screening-enhanced adsorption*;
- if the surface has a high charge density and again low salt concentration, the polyelectrolyte will adopt that of a tail-train conformation as an equilibrium is found between the strong interaction with the surface and repulsion between monomers.

Increasing salt concentration, the screening that will dominate will be that of polyelectrolyte-surface and a reduced adsorption effect will be observed – *screening-reduced adsorption*.¹⁴⁰

- multilayers can also be obtained by alternating adsorption between a cationic and an anionic polyelectrolyte as the last adsorption will determine the net charge of the ‘surface’ and promote interaction with an oppositely charged polymer.

Polyelectrolyte adsorption is often found to be irreversible when in stable conditions, with the few exceptions found in cases of low molecular weight and/or low charge density.¹⁴¹

2.2.2 Self-assembly

For the formation of monolayers on a surface there are two possible techniques to be considered. One is the Langmuir-Blodgett (LB) technique and the other is the self-assembled monolayer (SAM) method. The LB concept involves the fabrication of an amphiphilic monolayer at the air/liquid interface that is then transferred onto a surface by simple immersion of the latter in the liquid. This occurs as a consequence of the high surface pressure (caused by reducing the surface area of the monolayer through the introduction of a lateral barrier system) that guarantees cohesion and homogeneity of the monolayer when transferred to the substrate.¹⁴² Successive dipping of the latter can also lead to the formation of multilayers but the thermal and mechanical stability of these can be compromised in cases where low-molecular-weight compounds are used. Due to the stronger intra- and intermolecular forces, the use of polymeric monolayers can circumvent this limitation.¹⁴³ This ultrathin film technique has been frequently applied to molecular electronics.¹⁴⁴

Self-assembled monolayers are a result of a spontaneous process that implies a structural reorganization of a disordered system due to its physicochemical interactions that act as driving forces of an anchoring group towards a support or surface, which hence form a stable and organized film. The affinity is often driven by covalent bonds, as is the case of silanes on silica,¹⁴⁵ ionic interaction, found between alumina and carboxylic acids,¹⁴⁶ or by a combination of covalent and charge-transfer complex

interactions, such as is the case for alkanethiols on noble metals.¹⁴⁷ Films obtained by this technique are characterized by a high thermal, mechanical and chemical stability, as they can achieve high packing densities.¹⁴⁸ The versatility in tailoring both head and tail groups make this technique widely used in a variety of fields of study, such as microelectronics,¹⁴⁹ electroanalytical chemistry,¹⁵⁰ tribology,¹⁵¹ biotechnology,¹⁵² among others.¹⁵³ Despite the name of the process, multilayer formation is also possible by reacting the end-groups of the first monolayer with the correspondent reactive functionality present in another already deposited layer. This process can sequentially be repeated but may be compromised by steric hindrance or low reactivity.¹⁵⁴ For multilayer systems, the layer-by-layer (LbL) method, initially developed in the early 90s,¹⁵⁵ is often used. It can be applied to any charged species or more specifically, and within the scope of this introduction, to polyelectrolytes. As indicated, it is mainly ruled by electrostatic interactions but can involve other forces, such as hydrogen bonding or hydrophobic interactions.¹⁵⁶ Initially, a monolayer of a charged polyelectrolyte in a solution is deposited onto an oppositely charged surface (typically negative). The consequent charge neutralization or charge reversal¹⁵⁷ of the support will guarantee that when the latter is subsequently exposed to a second solution of another, oppositely charged polyelectrolyte, this will lead to the adsorption of a second layer. Accompanied by yet another charge reversal, the support now re-establishes its initial charge sign. This strategy allows for the continuous formation of a multilayer system with a high degree of control over thickness and layering sequence.¹⁵⁸

Since the strategy of the work presented in this thesis relies solely on self-assembled monolayers, further information will be exclusively related to this subject. Details regarding the other techniques mentioned in this section can be found elsewhere.¹⁵⁹

Self-assembled monolayers can be achieved by two different elements: either polymeric structures or smaller, amphiphilic molecules often containing long aliphatic chains with a polar head group which binds to the substrate, and another that presents a surface functionality of choice. However, in both cases, the adsorption success of a self-assembled monolayer system depends on the affinity between substrate and the chemical functionalities present in the adsorbate. The existence of a bond of a covalent nature between the two contributors guarantees enhanced stability to the monolayer,

allowing it to be manipulated without compromising its chemical stability. Our work will be mainly focused on two types of substrate: silicon oxide (Si/SiO₂) and titanium oxide (TiO₂) (reasons described in section A.2 of the Appendix). For this reason, the chemistries we explore in this section are suitable for self-assembly on these two substrates.

Silanes on Si/SiO₂

Self-assembly of silanes on SiO₂, or other hydroxylated surfaces, is, beside alkanethiols on gold substrates, the most studied self-assembly system. The most common structures used for silane attachment can be found in Figure 2.4.

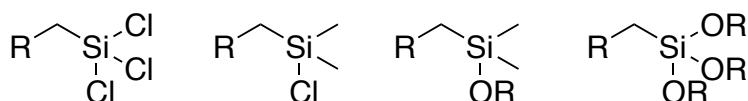


Figure 2.4 Structures of the most used organosilanes for self-assembly on SiO₂ surfaces, where R stands for an alkyl chain.

For covalent binding to be assured on silicon oxide, both chlorosilanes and alkoxy silanes are often diluted in a water-alcohol system in order to guarantee hydrolysis of the -Si-Cl/-Si-OR bond to form -Si-OH, and later on -Si-O-Si- (siloxane) bonds to the surface. However, condensation reactions make this a not so straightforward process. Considering that the silanols present in the adsorbate will react with the silanols present on the surface, it is favoured that these will form siloxane bonds between each other instead of with the surface. These selfcondensation reactions lead to the formation of dimeric or oligomeric structures, instead of a monolayer on the surface. Therefore the kinetics between hydrolysis and condensation reactions must be considered, which depend on factors such as the organic component of the silane and several reaction conditions (medium, amount of water, temperature, pH, etc).¹⁶⁰ Chlorosilanes are known to be more reactive than alkoxy silanes but extremely dependent on the presence of water yielding polymerized structures quite

easily. Under ambient conditions, like temperature and humidity, alkoxy silanes are associated to a higher stability and are easier to manipulate.¹⁶¹ Their tendency towards hydrolysis and condensation reactions depending on their substituents for trialkoxy silanes is shown in Figure 2.5.

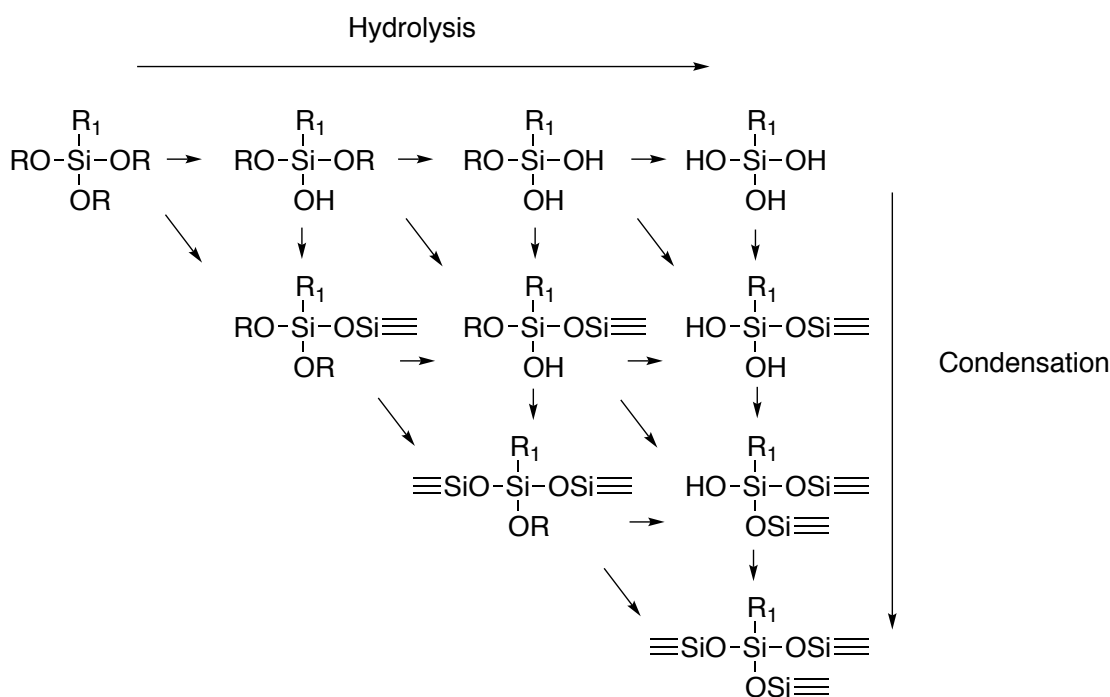


Figure 2.5 Hydrolysis and condensation reactivity in alkoxy silanes.¹⁶²

Catechols on TiO₂

Since one of its derivatives, 3,4-dihydroxy-L-phenylalanine (DOPA), was found in the composition of adhesives secreted by mussels¹⁶³, catechols (see structure in Figure 2.6) have drawn a lot of interest as biomimetic approach to graft polymers onto substrates.¹⁶⁴ They are known to bind strongly to metal ions via formation of a bidentate charge-transfer complex,¹⁶⁵ for instance in the anacat¹⁶⁶ or mimosine form,¹⁶⁷ but also bind coordinatively to a wide range of metal oxides, including TiO₂.^{168,169} However, catechols are known to undergo oxidation at pH>7, forming o-quinones, which can limit its adsorption and allow for crosslinking reactions to take place.¹⁷⁰ The cause of this is related to the high oxidation potential of the deprotonated phenol, leading to the formation of a highly reactive radical species. Introduction of electron-withdrawing

groups to the catechol ring (e.g. $-\text{NO}_2$) have made it possible to obtain catechols that are stable even under high-pH conditions.¹⁷¹⁻¹⁷³

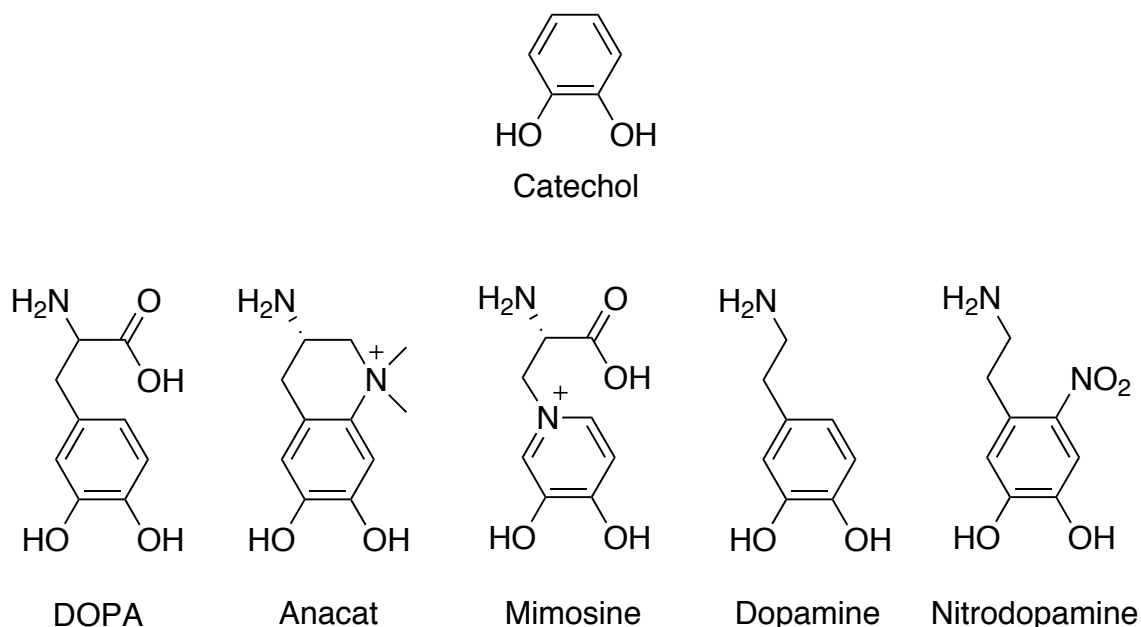


Figure 2.6 Structures of catechol and its derivatives used as anchoring groups.¹⁷¹

The binding of catechols to TiO_2 has been subject of extensive research using various methods and four possibilities have been suggested.¹⁷⁴⁻¹⁷⁹

- molecular adsorption –the hydroxyl groups bind via hydrogen bonding to the -Ti-OH layer formed on the surface, resulting in a non-covalent and weak bond;
- dissociative/coordinative adsorption – the hydroxyl groups of the catechol dissociate and the residual oxygen binds directly to titanium, causing the removal of the surfaces' hydroxyl groups by way of water molecules. There are three possible scenarios for this type of binding: either only one oxygen of the catechol participates in the (monodentate) binding, while the other may further increase stabilization via hydrogen bonding; or both oxygens participate in the stronger (bidentate) binding either in the same titanium atom (chelate) or in different ones (bridging). However It has been shown that in this type of adsorption on TiO_2 surfaces only the monodentate and bidentate bridging occur as the chelate scenario would demand a titanium cation with seven coordination numbers which is more rare to find in first series transition metals.¹⁷⁹

Phosph(on)ates on TiO₂

Phosph(on)ates (see Figure 2.7) are a chemical group also used for the production of well-ordered self-assembled monolayers on different substrates like TiO₂, ZrO₂, Al₂O₃ and Nb₂O₅, among other metal oxides.^{180,181} Much like catechols, they can hydrogen bond to the hydroxyls present on the substrate but also coordinatively through the oxygens present in their structures in a mono-, bi- (bridging or chelate form) or even tridentate fashion to titanium. The latter, however, is limited by length as the three oxygens need to bind to three different cations spaced further apart between each other than the O-O distance found in phosph(on)ates.

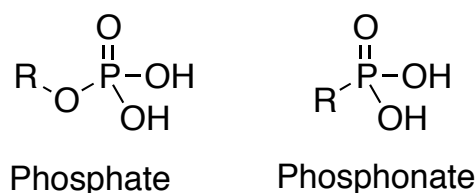


Figure 2.7 Structures of phosphates and phosphonates.

Bonding of this chemistry on SiO₂ surfaces is also possible but it is highly susceptible to hydrolysis, resulting in an unstable bond.¹⁸²

2.2.3 Photochemical linkage

Photoactive groups are characterized by their decomposition into a reactive species upon absorption of radiation energy. These reactive species, mainly in the form of radicals or diradicals, have been mainly used as initiators for polymerization reactions. However there has been a growing interest in applying this strategy to alter, degrade or activate, either synthetic or natural polymers, as it can be quite versatile. Insertion of photoactive groups in polymer structures has allowed creating a range of polymeric materials that can effortlessly interact with their environment upon light stimulus. One of the most famous uses of photochemical linkage is to achieve polymer crosslinking often as a postpolymerization process by ultraviolet (UV) curing. Upon light absorption and consequent breaking of the covalent bonds of the photoactive groups

present in a polymer, the resulting radicals will recombine with other radicals, intra or intermolecularly, leading to the formation of a direct and indiscriminate crosslinking.

Examples of photoactive groups used for these purposes are often pendant azides,¹⁸³ phenyl azides,^{134,184,185} benzophenones,¹⁸⁶ xanthenes¹⁸⁷ or phthalimide^{188,189} (see Figure 2.8).

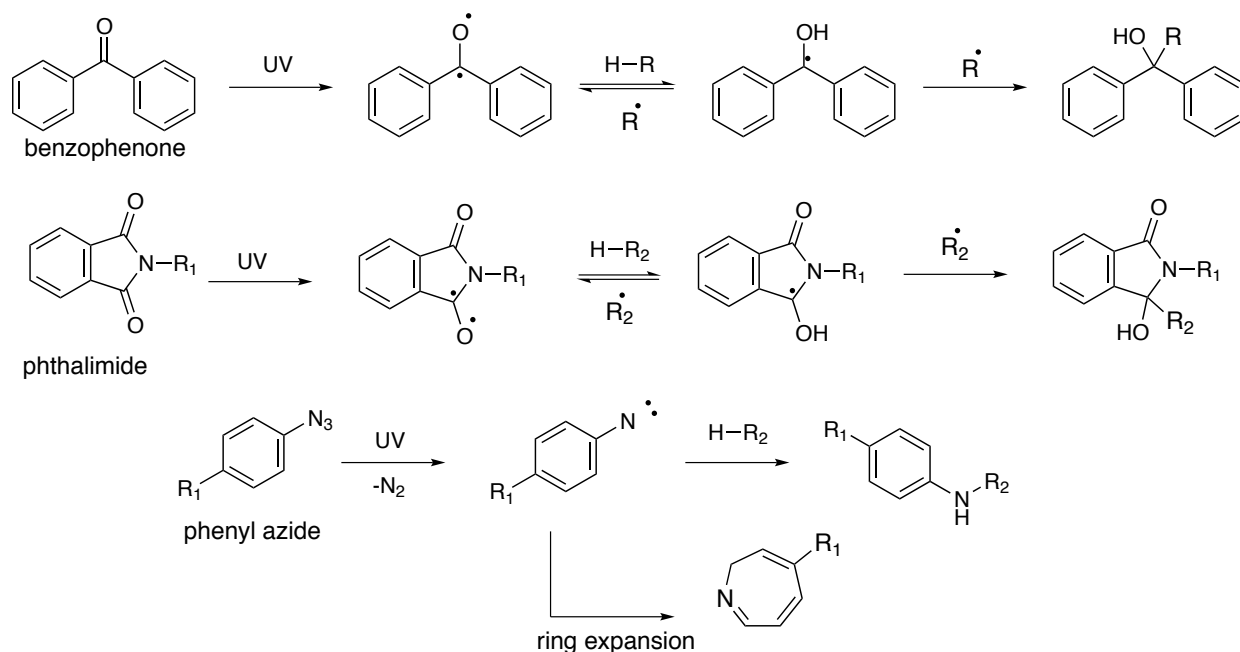


Figure 2.8 Photomechanisms for benzophenone, phthalimide and phenyl azide.

The mechanisms believed to be involved in the photoreactions of benzophenone, xanthone, and phthalimide are based on hydrogen abstraction from a C-H bond by the excited photoinitiator species. A recombination will then take place between the two new radicals. Both systems present are versatile, well studied, only require a low energetic UV wavelength (300nm for benzophenone and 350nm for phthalimide) and proceed with good yields.¹⁹⁰ However they also possess some drawbacks as benzophenones are known to crystallize easily^{191,192} and phthalimides undergo several side reactions, photorearrangements and ring-enlargements.¹⁹³

Azides, and also diazo compounds, use a different mechanism as they react via C-H, N-H and C-C insertion reactions upon the formation of nitrenes and carbenes, respectively.¹⁹⁴ Although carbenes possess higher reactivity than nitrenes, as the latter

differentiates more between primary to tertiary C-H bonds, aryl azides are by far the most popular approach for crosslinking as they possess increased stability, are less prone to rearrangements and synthesis of diazo compounds is less straightforward.^{87,195,196} Ring expansion due to deactivation of the nitrene singlet (higher energy, lower life time) is still possible in aryl azides but has been circumvented by the use of fluorine or chlorine atoms on the ring to increase stability.^{89,197} Besides crosslinking, these latter perfluorophenylazide photoactive groups have been successfully used in a variety of areas, as already stated in section 1.2.

2.2.4 Multifunctional surface active polymers

Combining multiple functionalities with different surface-binding affinities in different ratios in a polymer is yet another strategy towards the study of their influence in a particular polymeric system's stability. Although in theory this approach sounds promising, the synthetic issues that can arise (e.g. solubility incompatibilities between different chemistries or polymerization conditions) can limit its use. Nonetheless, there were some successful works that used this approach.

In her thesis,¹⁹⁸ Saxer studied the influence of electrostatic and coordinative binding on the stability of a nonfouling polymeric coating by postmodifying poly(L-lysine)-*graft*-poly(ethylene glycol) (PLL-*g*-PEG) with variable amounts of catechol (3,4-dihydroxyphenyl acetic acid – DHPAA - at different grafting ratios) and testing the effect of several adsorption parameters, such as incubation time, ionic strength and temperature, on its adsorption. Several substrates were used (SiO₂, TiO₂ and gold) and the effectiveness of the adsorption measured through non-specific fibrinogen interactions. Besides successfully postmodifying PLL-*g*-PEG into PLL-*g*-(DHPAA; PEG), she verified that high temperatures promoted assembly due to increase of chain mobility, crosslinking between catechols and near-cloud-point grafting conditions were achieved. Ionic strength, due to the electrostatic participation of the lysine monomers, compromised adsorption on TiO₂ but that effect was not so pronounced on SiO₂. As for adsorption kinetics, all postmodified polymers reached maximum surface coverage within 30 min. She also observed that on TiO₂ a wide range of densities of catechols on the backbone induced stability and protein resistance even at high salt conditions while

on SiO₂ and gold surfaces that range was substantially smaller and did not resist protein uptake exposure to a high-ionic-strength medium. Overall, these results showed the importance of a non-electrostatic based component towards achieving a polymeric self-assembled monolayer with a high stability, correct conformation and hence protein resistance.

The thesis work of Dr. Vincent Zoulalian, comprised of synthesizing a polymeric matrix where methacrylates containing either alkylphosphonates (C₁₁ or C₃), butyl groups (as spacers) or PEG were polymerized in different combinations and ratios in order to evaluate which provide the more stable self-assembled monolayers and PEG-grafted polyelectrolytes on TiO₂. Besides the successful synthesis of the elements included in this extensive matrix, he observed that the best polymer structure was achieved when longer alkylphosphonates were used, spacers were in a ratio of 8:1 to the former and PEG was in a 1:1 relation also with the former. As this combination presents multiple attachments to the substrate and PEG is grafted at a sufficient density to be found in a brush regime, results showed its high short-term stability against acidic, alkaline and salt solutions but also its excellent protein resistance against serum proteins when compared to the bare substrate.¹⁹⁹

Inspired by the previous work, Dr. Christoph Mayer synthesized PEG-poly(alkylphosphonates) using different backbones (poly(maleic anhydride-alt-1-octadecene) and poly(isobutylene-alt-maleic anhydride)) and different backfillers (butylamine, ethanolamine and 1,6-hexanediamine). Grafting ratios were also a studied parameter and adsorption was performed on TiO₂ surfaces in order to study stability and protein-resistance performance. Results showed that adsorption kinetics were slowed down due to micelle formation, but XPS data confirmed both chemical composition of the synthesized polymers and phosphonate binding to the surface of the adsorbed layers. Increasing phosphonate binding moieties and PEG surface density of the adlayer resulted in better nonfouling abilities and resistance to cell adhesion. Furthermore, long-term stability was also verified at different pHs with increasing phosphonate content to polymeric coating.²⁰⁰

All these examples emphasize not only the versatility of possible studies when using multifunctional surface active polymers but also the importance of a non-

electrostatic binding to enhance their stability. Based on the success and results obtained by these approaches we decided to apply a similar one with the work presented in Chapter 4. Although we also studied the effect of anchors with different binding natures to a substrate - electrostatic vs non-electrostatic – we went a step further. Within the latter type of binding we simultaneously inserted several chemical functionalities that are known to bind, either covalently or coordinatively, to different substrates. The aim was not only to develop a simple synthetic procedure that could allow tailoring a polymeric coating according to different functional needs but also to create one polymeric coating that could bind simultaneously to several substrates.

Chapter 3

Nonfouling Response of Hydrophilic Uncharged Polymers

*The data presented here can be found in the published paper: Serrano, Á.; Sterner, O.; Mieszkin, S.; Zürcher, S.; Tosatti, S.; Callow, M. E.; Callow, J. A.; Spencer, N. D. Nonfouling Response of Hydrophilic Uncharged Polymers. Adv. Funct. Mater. **2013**, 23, 5706–5718.²⁰¹ This work was accomplished by myself, with the exception of the *Ulva linza* assays, which were performed by Olof Sterner. All the assays involving biological entities were performed under the supervision of Dr. Sophie Mieszkin from the group of Prof. James Callow and Dr Maureen Callow of School of Biosciences in the University of Birmingham. Drs Zürcher and Tosatti and Prof. Spencer were involved in supervision, manuscript preparation, and scientific discussions.*

3 Nonfouling Response of Hydrophilic Uncharged Polymers

3.1 Introduction

The main goal of the work presented in this chapter was to compare and evaluate the marine fouling resistance of different hydrophilic uncharged polymers for the reasons already stated in Chapter 1.

In order to simplify the deposition procedure, and instead of synthesizing a surface-active version of the polymer of interest either by grafting-to or grafting-from techniques, the use of a common grafting platform has been considered (see section 1.2).

Many studies have been performed in order to assess the fouling resistance of different polymeric systems, but due to a lack of experimental similarities, a direct comparison of the different polymers is hardly possible between the different investigations.

By pre-functionalizing SiO_2 surfaces with an azide-terminated adhesion monolayer (PAAm-*g*-PFPA), which allows the formation of a covalent bond with any organic matter while electrostatically binding to metal oxide, a platform for the direct comparison of a variety of different polymers is provided. A selected series of hydrophilic uncharged polymers, such as PEG, PVP, PVA or dextran, was used to functionalize the surfaces, which were then characterized with techniques such as X-ray photoelectron spectroscopy (XPS), dynamic contact-angle measurements (dCA) and variable-angle spectroscopic ellipsometry (VASE). The *in situ*, real-time adsorption of proteins was monitored with quartz crystal microbalance with dissipation (QCM-D) measurements. Furthermore, the coated samples were exposed to marine-fouling

entities such as marine bacteria and algae (*U. linza*), to observe the adhesiveness of the coatings towards these organisms.

3.2 Experimental

3.2.1 Substrates

Wafers

All SiO_x wafers were purchased from Powatech, GmbH (Switzerland). Two sizes were used: 10mm x 9mm and 76mm x 26mm, the latter being solely used for biological assessment assays.

All wafers were cleaned according to the following protocol: sonication for 2x15min in toluene, 2x15min in 2-propanol, drying under a stream of N₂ and exposure to O₂ plasma in a Diener Electronic Nano instrument (Germany) for 2 min. This last step would only be performed immediately prior to functionalization.

QCM-D sensors

AT-cut polished crystals with a fundamental resonance of 5 MHz and SiO₂ (50nm) coated were used and obtained by LOT-Oriel AG (Switzerland). Before functionalization, sensors were sonicated for 15 min in toluene, 15 min in 2-propanol, dried under a stream of N₂, and exposed to UV/Ozone in a UV Clean Model 135500 for 30 min (Boekel Industries, Inc., USA). Prior to functionalization the sensors were exposed to O₂ plasma for 2 min. For surface regeneration, before repeating the above-mentioned cleaning procedure, the sensors were immersed overnight in 2% (v/v) SDS solution.

Well plates

Both storage and incubation of the 10mm x 9mm wafers and QCM-D sensors were done in BD Falcon cell culture plates (6 and 48-well).

3.2.2 Chemicals

All chemicals herein listed were used as received unless stated otherwise.

Solvents

Ethanol ($\geq 99.9\%$), toluene ($\geq 99.9\%$), 2-propanol ($\geq 99.8\%$) were obtained from Merck (Switzerland). Ultrapure water (purified with a water-treatment apparatus from Millipore, $\geq 18.2 \text{ M}\Omega \text{ cm}^{-1}$ resistivity, total organic content $\leq 5 \text{ ppb}$) was used throughout the experiments.

Salts

Potassium carbonate (K_2CO_3 , $\geq 99\%$), sodium chloride (NaCl , $\geq 99.5\%$), sodium sulphate (Na_2SO_4 , $\geq 99\%$), and potassium chloride (KCl , $\geq 99.5\%$) were acquired from Merck (Switzerland). Calcium chloride dihydrate ($\text{CaCl}_2 \cdot 2\text{H}_2\text{O}$, $\geq 99.5\%$), and magnesium chloride hexahydrate ($\text{MgCl}_2 \cdot 6\text{H}_2\text{O}$, $\geq 99\%$) were provided by Sigma-Aldrich.

Polymers

The following materials were purchased from Sigma-Aldrich (Switzerland): poly(allylamine hydrochloride) ($\text{PAAm} \cdot \text{HCl}$, average $M_w = 15\,000 \text{ g mol}^{-1}$), poly(ethylene glycol) (PEG, average $M_n = 20\,000 \text{ g mol}^{-1}$), poly(2-ethyl-2-oxazoline) (PEOXA, average $M_w = 50\,000 \text{ g mol}^{-1}$), poly(vinyl alcohol) (PVA, average $M_w = 27\,000 \text{ g mol}^{-1}$) and poly(vinyl pyrrolidone) (PVP, average $M_w = 55\,000$ and $1\,300\,000 \text{ g mol}^{-1}$). Dextran T2000 ($M_w = 2\,000\,000 \text{ g mol}^{-1}$) was purchased from Pharmacosmos (Denmark).

^1H NMR was performed for the polymers as received with a Bruker 300 MHz spectrometer, in order to confirm purity of the reagents.

Protein solutions

Lyophilized human serum, Precinorm U, Roche Diagnostics (Switzerland) was dissolved in artificial seawater (ASW) with a final ionic strength of 0.7 M and used in the protein-adsorption assays.

Other used reagents

N-hydroxysuccinimide perfluorophenylazide was provided by SuSoS AG (Switzerland). 4-(2-hydroxyethyl)piperazine-1-ethane sulfonic acid (HEPES, $\geq 99\%$) was acquired from BDH Biochemical (Switzerland).

Protein solutions

Lyophilized human serum, Precinorm U, Roche Diagnostics (Switzerland) was dissolved in artificial seawater (ASW) with a final ionic strength of 0.7 M and used in the protein-adsorption assays.

3.2.3 Buffers

Ultrapure water MilliQ was used in all solutions herein described which were stored in the dark at 4°C.

- *HEPES* 1: 10 mM *N*-(2-hydroxyethyl)piperazine-*N'*-(2-ethanesulfonic acid) (HEPES) (Fluka) pH was adjusted to 7.4 with NaOH.
- *Artificial seawater (ASW)*: a) for all protein adsorption assays, ASW was freshly prepared according to the protocol described elsewhere²⁰² from a mixture of five individual salts, filtered with a 0.22 μm filter and pH adjusted to 8.2 with NaOH; b) for assays with bacteria and algae, ASW (Tropic Marin®) was freshly prepared according to manufacturer's instructions, filtered with a 0.22 μm filter and pH adjusted to 8.2 with NaOH.

3.2.4 Synthesis of PAAm-*g*-PFPA (Poly(allylamine) *grafted* perfluorophenylazide)

PAAm-*g*-PFPA was synthesized according to the protocol developed by SuSoS AG (Dübendorf, Switzerland).²⁰³ In brief, poly(allylamine hydrochloride) (6.33 mg, 6.8×10^{-3} mM monomer) and excess potassium carbonate (15.82 mg, 0.11 mM) were dissolved in water (1.3 mL) and boiled for a short period of time. After cooling down to room temperature, a solution of *N*-hydroxysuccinimide-perfluorophenylazide (NHS-PFPA) (5.62 mg, 1.7×10^{-2} mM) dissolved in ethanol (1.3 mL) was slowly added. The resulting solution was stirred overnight in the dark and the stock solution was then diluted to 100 mL with a 3:2 (m/v) ethanol/HEPES I mixture, yielding a polymer concentration of 0.1 mg/mL.

3.2.5 Surface modification

Unless stated otherwise, samples were coated according to the protocol described in this section. The cleaned substrates were dipped in a 0.1 mg/mL PAAm-*g*(4)-PFPA solution for 30 min and subsequently rinsed twice with a solution of 3:2 (v/v) ethanol/HEPES I, once with ultrapure water and again dried under a stream of N₂. The wafer surface was completely covered with the polymer solution and spin coating was carried out according the parameters described in Table 3.1.

Table 3.1 Polymer solution details and corresponding spin-coating parameters.

Chemistry	Concentration (mg/mL)	Solvent	Spin-coating parameters
PEG 20 kDa	50	75% ultrapure water 25% 2-propanol (v/v)	2000 rpm for 40s 4000 rpm for 10s
PVA 27 kDa	50		
PEOXA 50 kDa	50		
PVP 55 kDa	50	Ethanol	
PVP 1300 kDa	25	Ethanol	4000 rpm for 40s
Dextran 2000 kDa	25	ultrapure water	5000 rpm for 10s

Surfaces were then left in the dark at room temperature for at least 15 min until completely dry and then exposed to UV-C light (254 nm, Philips TUV 11W) for 2 min. Excess non-bound polymers were removed by overnight immersion in ultrapure water. Finally the surfaces were rinsed with fresh ultrapure water and dried under a stream of N₂. All functionalized surfaces were stored in the dark at room temperature until further use.

3.2.6 Surface characterization

The above-functionalized surfaces were characterized by VASE, dCA and XPS. Experimental details of these measurements can be found in section A.1 of the Appendix.

3.2.7 Biofouling assays

3.2.7.1 Protein adsorption

By Ellipsometry

Before exposure to the protein solution, the thicknesses of the samples were measured according to the procedure described in the surface-characterization section

using this same technique. Afterwards, they were immersed in ASW for 15 min and exposed to serum-ASW for 30 min. During incubation, samples were stored under ambient conditions without agitation. After exposure, these were rinsed with ASW and ultrapure water, dried under a stream of N₂ and analysed.

By Quartz Crystal Microbalance with Dissipation

The modified crystals were exposed to HEPES I under a flow of 50 µL/min at 25°C until a stable baseline was established. After this, the buffer was replaced with ASW under the same flow and temperature until a new baseline was obtained. Protein solution was then injected and incubation followed for at least 30 min with no flow, followed by sequential washing with ASW and HEPES I at the same flow rate as before. For both solvents, baselines were again obtained.

3.2.7.2 Marine bacteria

The ability to resist attachment of marine bacteria was investigated for all polymer coatings. For this assay, two well-known strains, commonly used in the field of marine fouling testing⁴⁸, were chosen: *Cobetia marina* (*C. marina*, ATCC 25374^T, DSMZ, Germany) and *Marinobacter hydrocarbonoclasticus* (*M. hydrocarbonoclasticus*, ATCC 25374^T, DSMZ, Germany). Prior to exposure to the bacterial suspension, all surfaces were pre-equilibrated in ASW for one hour and then treated according to the protocol of Pranzetti *et al.*²⁰⁴ Briefly, after bacteria reached a logarithmic growth phase, they were washed with ASW and centrifuged at 8000 rpm for 1 min, twice. This allows the removal of culture medium and secreted extracellular polymeric substances (EPS). Test surfaces (three replicates per test surface) placed in individual compartments of Quadriperm dishes (Greiner Bio-One Ltd) were then exposed to 10 mL of bacterial suspension with an OD₆₀₀=0.1 (4x10⁻⁷ cells/mL) for one hour, while agitating at 50 rpm on a plate shaker. After this, the bacterial suspension was replaced by 10 ml ASW and the dishes agitated for 1 min at the same rotational speed. In order to fix the bacteria, the surfaces were exposed to a solution of 2.5% (v/v) of glutaraldehyde in ASW for 20 min, washed in deionised water and then left to air-dry overnight. Before microscopic

observation, the surfaces were stained with SYTO 13 (Invitrogen Molecular Probes) at 5 μM and left in the dark for 10 min. Cells were visualized using a 40x objective attached to a Zeiss epifluorescence microscope (λ excitation and emission: 450/490 and 515/565 nm, respectively) connected to the imaging analysis system AxioVision Rel. 4.8.1. For each sample, 30 fields of view were counted for each of the three replicate test surfaces. Two independent experiments were conducted with similar results. One set of data is shown in the Results section.

3.2.7.3 Zoospores of *Ulva linza*

The assay quantifies the number of spores that settle (i.e. permanently attach) to the test surfaces. All surfaces were equilibrated in ASW for one hour prior to the start of the assay. The protocol for the collection of *U. linza*, the release of spores and the settlement assay was followed as described previously.²⁰⁵ In brief, a suspension of zoospores in ASW with an $\text{OD}_{660}=0.15$ (appr. 1×10^6 spores/mL) was prepared. 10 mL of this suspension were added to individual compartments of Quadriperm dishes, each containing a test surface (three replicates per test surface). The dishes were incubated in the dark for 45 min and then washed by passing each sample 10 times through a beaker of ASW to remove unsettled (motile) spores. Settled spores were fixed using 2.5% (v/v) glutaraldehyde for 20 min. The surfaces were sequentially washed with ASW, 1:1 (v/v) ASW/deionised water and deionised water. Finally, the test surfaces were allowed to air-dry and settled spores were counted by chlorophyll autofluorescence using epifluorescence microscopy (20x objective; λ excitation and emission: 546 and 590 nm, respectively) as previously described for the marine bacteria assays.

3.2.7.4 Statistical analysis

Using the software Minitab 15, data were checked for normality and most data conformed to normality assumptions. One-way ANOVA with pairwise Tukey comparison test was then used to determine differences between the eight test surfaces. Values

were considered significantly different from each other when p-value (p) < 0.05 . Means and standard deviations or standard errors of the mean are shown.

3.3 Results

3.3.1 Surface characterization

The adlayer thickness, the contact angle and the chemical composition of the different coatings, as well as the freshly cleaned substrate and a UV-activated adhesion promoter (PAAm-*g*-PFPA) film were measured by VASE, dCA and XPS, respectively and as mentioned in the Experimental section. For XPS, detail spectra for Si 2p, C 1s, O 1s, N 1s and F 1s were measured, to determine the apparent atomic composition of the deposited films. Peak modeling allowed the contributions from the silicon oxide and the elemental silicon to be discerned, and the oxygen contribution from the SiO₂ substrate to be calculated. Subtraction of this value allowed the atomic composition of the polymeric films to be calculated and compared with the theoretical composition of the pure polymer (see results in Table 3.2 and experimental parameters in Table 3.3). Peak modeling also enabled the C 1s to be deconvoluted into its various contributions. Their relative peak areas were compared to the theoretical carbon compositions of the analyzed films (see Table 3.4)

3.3.1.1 Si-wafer and adhesion promoter

The freshly cleaned substrate was characterized by a high surface energy (low contact angle) and the presence of elemental silicon, oxidized silicon as interfacial SiO and SiO₂, oxygen and a small residual carbon adventitious contamination. No other elements, specifically nitrogen or fluorine, were detected.

The successful deposition of the adhesion promoter (see Figure 1.3) onto Si-wafers could be confirmed by an increase in carbon, the presence of nitrogen and fluorine, and the subsequent decrease of silicon and oxygen as a consequence of a 1.8 ± 0.1 nm thick adlayer. Due to the presence of the PFPA groups, an increase in

advancing contact angle value of 43° with respect to bare silicon was also observed (Table 3.2).

Upon subtraction of the silicon and silicon oxide contributions, the polymeric film composition of the adhesion promoter differs from the theoretically calculated stoichiometry. From the F/N ratio, an effective grafting ratio of 9.0 for PAAm-*g*-PFPA can be calculated, where grafting ratio is defined as the number of allylamine monomer units divided by the number of PFPA units. The main deviation is an increased oxygen content (real composition of 20 ± 2 at.% and a theoretical composition of 2.0 at.%) that can be attributed to the deprotonated surface hydroxyl anions. These must be present for charge neutralization of the positively charged ammonium groups of the adhesion promoter.

3.3.1.2 Nonfouling polymeric adlayers

The deposition of non-fouling polymers was also confirmed by the same three techniques. Overall, an increase in film thickness and decrease in dCA (Table 3.2) was measured when compared to the adhesion-promoter layer. Dynamic water contact angles ranged from 19° to 46° (advancing) and $<10^\circ$ to 23° (receding). The decrease in advancing contact angle of the new layer, when compared to the adhesion promoter, is due to the hydrophilicity of the newly bound polymers. Also the relatively small hysteresis (between 14° and 24°) indicates a smoother and more homogeneous layer than for the adhesion promoter alone.

These changes in hydrophilicity throughout the various functionalization steps were accompanied by a sequential increase in dry thickness. PEOXA, PVA and PVP 55 are among the thinnest layers with values of 0.6 ± 0.3 , 0.9 ± 0.3 and 1.9 ± 0.3 nm, respectively, while dextran and PVP 1300 have layers of 7.1 ± 0.7 and 11.6 ± 0.9 nm, which is consistent with the trend in the molecular weight of the polymers.

Table 3.2 Surface characterization of the substrate (silicon with naturally grown SiO₂ layer), the adhesion promoter layer after activation, and the six investigated polymer films. The samples were characterized by dynamic water contact angle (dCA), the film thicknesses were determined by VASE and the apparent normalized atomic concentrations were measured by XPS. In the case of the polymer films, the compositions were determined by subtraction of the silicon and silicon oxide contributions. Calculated polymer compositions for comparison are given in brackets, for the adhesion promoter a grafting ratio of $g=9$, as calculated from the F/N ratio, was used. Changes in film thickness after immersion in artificial seawater (ASW) for 1 h at room temperature were measured by VASE as an indication of the coating stability under these conditions. Errors correspond to standard deviation (\pm SD) of at least three independent measurements, on different samples.

Chemistry	Surface characterization									Stabilization in ASW
	dCA		VASE	XPS						VASE
	Adv (°)	Rec (°)	Thickness (nm)		Si 2p	C 1s	O 1s	N 1s	F 1s	Thickness change after 1h immersion in ASW (nm)
SiO ₂	27 \pm 2	12 \pm 1	-	At. %	34.8 \pm 0.1	4.3 \pm 0.3	60.9 \pm 0.3	0.0 \pm 0.0	0.0 \pm 0.0	-
PAAm- <i>g</i> -PFPA*	70 \pm 1	19 \pm 1	1.8 \pm 0.1	At. %	25.3 \pm 0.2	24.5 \pm 0.6	43.4 \pm 0.7	4.9 \pm 0.3	1.9 \pm 0.1	$\Delta=0.2\pm0.2$
				Normalized at.% (overlayer)		63 \pm 1 (69.4)	20 \pm 2 (2.0)	12.5 \pm 0.6 (20.4)	5.0 \pm 0.2 (8.2)	
PVA 27 kDa	41 \pm 1	17 \pm 1	0.9 \pm 0.3	At. %	17.0 \pm 0.7	42.1 \pm 0.7	37.4 \pm 0.2	2.4 \pm 0.3	1.1 \pm 0.0	$\Delta=-0.4\pm0.3$
				Normalized at.% (overlayer)		67.8 \pm 0.8 (66.7)	26.5 \pm 1.0 (33.3)	3.9 \pm 0.5 (0.0)	1.8 \pm 0.0 (0.0)	
PEG 20 kDa	29 \pm 2	15 \pm 1	3.9 \pm 0.6	At. %	8.6 \pm 0.1	56.7 \pm 0.3	32.6 \pm 0.1	1.5 \pm 0.2	0.7 \pm 0.1	$\Delta=-2.2\pm0.4$
				Normalized at.% (overlayer)		70.6 \pm 0.4 (66.7)	26.7 \pm 0.2 (33.3)	1.8 \pm 0.2 (0.0)	0.8 \pm 0.2 (0.0)	
Dextran 2000 kDa	19 \pm 2	<10	7.1 \pm 0.7	At. %	2.6 \pm 0.2	55.8 \pm 0.3	41.6 \pm 0.2	0.0 \pm 0.0	0.0 \pm 0.0	$\Delta=-0.4\pm0.2$
				Normalized at.% (overlayer)		58.0 \pm 0.2 (54.5)	42.0 \pm 0.2 (45.5)	0.0 \pm 0.0 (0.0)	0.0 \pm 0.0 (0.0)	

Chemistry	Surface characterization									Stabilization in ASW
	dCA		VASE	XPS						VASE
	Adv (°)	Rec (°)	Thickness (nm)		Si 2p	C 1s	O 1s	N 1s	F 1s	Thickness change after 1h immersion in ASW (nm)
PEOXA 50 kDa	46±1	23±1	0.6±0.3	At. %	18.3±0.6	42.2±0.6	29.9±0.3	8.4±0.3	1.1±0.1	Δ=-0.1±0.2
				Normalized at.% (overlayer)		72.0±0.7 (71.4)	11.8±0.2 (14.3)	14.4±0.4 (14.3)	1.9±0.2 (0.0)	
PVP 55 kDa	35±2	14±1	1.9±0.3	At. %	8.5±0.6	63±1	17.9±0.7	9.9±0.1	0.6±0.2	Δ=-0.2±0.2
				Normalized at.% (overlayer)		78.5±0.4 (75.0)	8.5±0.3 (12.5)	12.3±0.0 (12.5)	0.7±0.2 (0.0)	
PVP 1300 kDa	35±1	12±3	11.6±0.9	At. %	0.8±0.1	76.6±0.3	10.7±0.2	11.9±0.3	0.0±0.0	Δ=-0.2±0.2
				Normalized at.% (overlayer)		77.9±0.4 (75.0)	9.9±0.2 (12.5)	12.1±0.2 (12.5)	0.0±0.0 (0.0)	

*activated and with a grafting ratio of 9

Table 3.3 XPS Binding energies and peak-deconvolution parameters. Data shown are average ± standard deviation.

Element	Assignment	BE	FWHM	Constraints	Line Shape	RSF
C 1s	C-C, C-H	285.0±0.0	1.4±0.2	none	GL(30)	1
	C-C=O	285.5±0.1	1.3±0.1	fwhm C1s aliphatic 1*area (C-F, C=O);	GL(30)	1
	C-N, C-O	286.4±0.4	1.4±0.2	fwhm C1s aliphatic	GL(30)	1
	C-F, C=O	287.9±0.2	1.4±0.1	fwhm C1s aliphatic	GL(30)	1
O 1s	(N)C=O	531.3±0.5	1.5±0.3	none	GL(50)	2.642
	SiO ₂ , C-OH, C-O-C	532.8±0.3	1.5±0.1	none	GL(50)	2.642
N 1s	N-H	399.7±0.2	1.6±0.2	none	GL(30)	1.721
	(O=C)-N	401.7±0.2	1.6±0.2	fwhm (N-H)	GL(30)	1.721
F 1s	C-F	688.0±0.1	1.8±0.2	none	GL(30)	3.672

Element	Assignment	BE	FWHM	Constraints	Line Shape	RSF
Si 2p	Si 2p _{3/2}	98.4±0.3	0.8±0.1	none	GL(30)	0.872
	Si 2p _{1/2}	99.1±0.3	0.8±0.1	fwhm (Si 2p _{3/2}); 0.5*area (Si 2p _{3/2}); BE= BE(Si 2p _{3/2})+0.7	GL(30)	0.436
	SiO 2p _{3/2}	100.3±0.3	1.4±0.2	none	GL(30)	0.872
	SiO 2p _{1/2}	101.0±0.3	1.4±0.2	fwhm (SiO 2p _{3/2}); 0.5*area (SiO 2p _{3/2}); BE= BE(SiO 2p _{3/2})+0.7	GL(30)	0.436
	SiO ₂ 2p _{3/2}	102.7±0.3	1.4±0.1	none	GL(30)	0.872
	SiO ₂ 2p _{1/2}	103.4±0.3	1.4±0.1	fwhm (SiO ₂ 2p _{3/2}); 0.5*area (SiO ₂ 2p _{3/2}); BE= BE(SiO ₂ 2p _{3/2})+0.7	GL(30)	0.436

BE: Binding energy

FWHM: Full width at half maximum

RSF: Relative sensitivity factor

Regarding chemical composition (Table 3.2), the deposited PVA can be clearly detected by an increase in the C-O component in the C 1s detail spectrum when compared to the adhesion promoter (Figure 3.1). Due to this thin deposited layer, nitrogen and fluorine are still detected, explaining the deviations from the calculated PVA stoichiometry. This fact is also verified in where an approximate contribution of 5% of all carbon content was due to the presence of groups such as C=O or C-F.

The thicker (3.9±0.6 nm) PEG coating behaved similarly to PVA, showing an overall increase of carbon, oxygen and a marked augmentation of the C-O peak due to the ether bond (Figure 3.1). The existence of other types of carbon (Table 3.4) as well as an overestimation of the film's stoichiometry (Table 3.2) is an indication that the adhesion-promoter layer is again contributing to the measured film composition.

In the case of dextran, the substrate signal is mostly masked by the 7.1±0.7 nm layer consisting of carbon and oxygen, which matches well to the theoretical composition. The bond between the polymer and the adhesion promoter is confirmed by data obtained from the C 1s peak deconvolution (see Table 3.4), where there is an increase in atomic percent from the C-OH and O-C-O/C=O, confirming the successful

attachment of this polysaccharide. The relatively high content of the latter peak, as observed in all chemistries described so far, can be attributed to the presence of the adhesion promoter.

In the case of PEOXA, when comparing the chemical composition with the adhesion promoter, one can observe a decrease of fluorine given by the presence of an overlayer and an increase of both nitrogen and C-N contributions in the carbon region, as expected from the chemical structure of this polymer. Attachment of both PVPs translated also into an increase in the nitrogen atomic percentage along with carbon. The normalized values are very close to the expected stoichiometry, where a fourth carbon peak attributed to the alpha carbon was found to be necessary to create a reasonable fit.

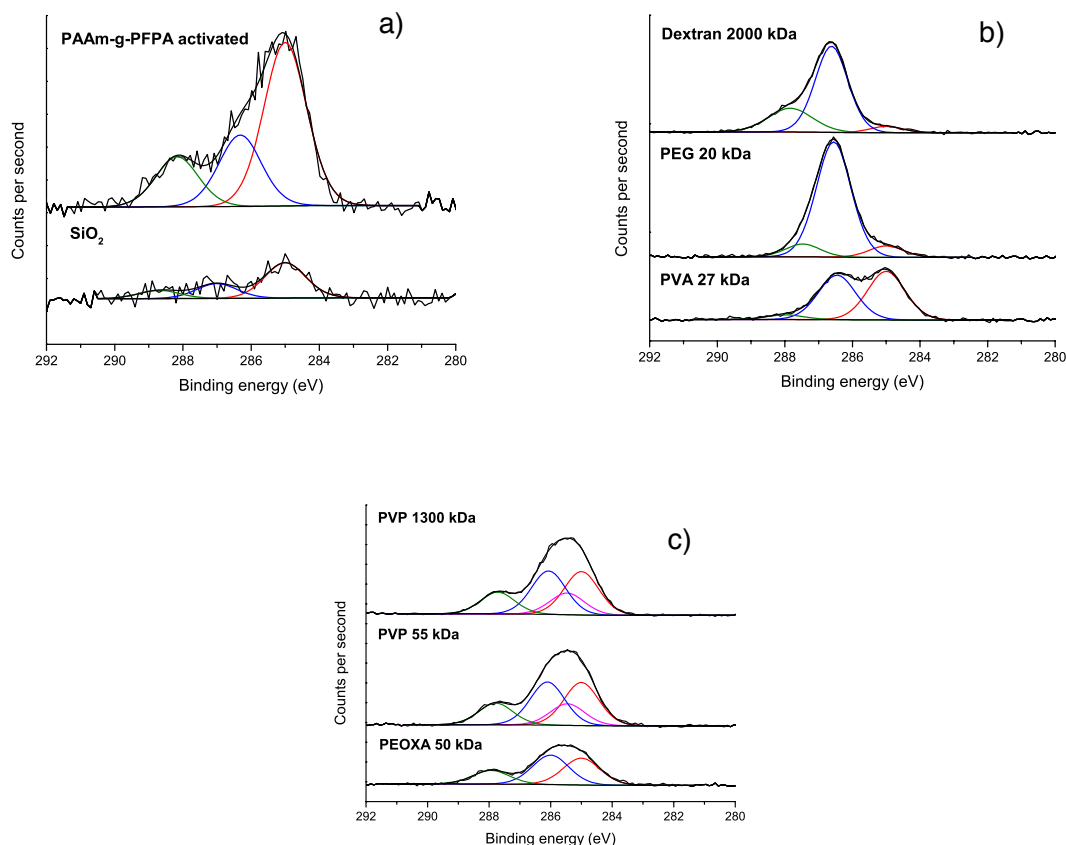


Figure 3.1 Detailed XPS spectra of the C1s region on the bare SiO₂ and various functionalized surfaces. Curve-fitted carbon component C-C, C-H in red; C-C=O in pink; C-N, C-O in blue and C-F, C=O in green (details in Table 3.3).

Table 3.4 Normalized C 1s content. The theoretical carbon compositions of the polymer films are given in parentheses, for comparison. Data shown are average \pm standard deviation.

Chemistry	Relative peak area (%)			
	C-C, C-H	C-C=O	C-O, C-N	O-C-O, C=O, C-F
SiO ₂	74 \pm 5	-	26 \pm 5	-
PAAm- <i>g</i> -PFPA	61 \pm 3 (52.9)	-	23 \pm 3 (32.4)	16.7 \pm 0.8 (26.3)
PVA 27 kDa	49.9 \pm 0.5 (50)	-	45.2 \pm 0.9 (50)	4.8 \pm 0.4 (0.0)
PEG 20 kDa	7 \pm 1 (0.0)	-	86 \pm 3 (100)	7 \pm 2 (0.0)
Dextran 2000 kDa	5.0 \pm 0.3 (0.0)	-	71 \pm 2 (83.3)	24 \pm 2 (16.7)
PEOXA 50 kDa	37 \pm 1 (40)	-	43.0 \pm 0.9 (40)	19.8 \pm 0.5 (20)
PVP 55 kDa	34 \pm 3 (33.3)	16.8 \pm 0.6 (16.7)	32 \pm 2 (33.3)	16.8 \pm 0.6 (16.7)
PVP 1300 kDa	31 \pm 3 (33.3)	16.6 \pm 0.2 (16.7)	36 \pm 3 (33.3)	16.6 \pm 0.2 (16.7)

3.3.2 Short-term stability of coatings

Table 3.2 gives the change in resulting adlayer thickness after short-term exposure (1h) to ASW. The data show how the exposure to ASW, a high-ionic-strength medium, caused an overall reduction of the thickness of the coatings. The less-affected chemistries with a decrease below 11.1% were the adhesion promoter, both PVPs and dextran. PVA and PEOXA suffered a reduction of thickness of the order of 44.4% and 16.7%, respectively, while PEG decreased in thickness by 56.4%. One possible reason for the reduction of PEG thickness is the formation of a hydrolytically unstable bond

upon nitrene insertion into C-H bonds of the PEG. However, with the exception of this last chemistry, all thickness variations are comparable to the standard deviation so that, with exception of PEG, no statistical relevance between fresh and exposed films could be determined. This suggests that the coatings are stable in the short term (1h) and that fouling events can be correlated to an interaction between species and coating material, rather than to an exposure of adhesive bare substrate due to coating loss. A control substrate (bare SiO₂) was simultaneously tested but, as expected, no changes in thickness were observed.

3.3.3 Biofouling assessment

The results for protein resistance, attachment of marine bacteria, *C. marina* and *M. hydrocarbonoclasticus*, and settlement (attachment) of spores of *U. linza* are all presented in Table 3.5. In order to allow for a direct comparison between all values, these have been normalized with respect to the positive control SiO₂ (100%) and are displayed in Figure 3.1.

Table 3.5 Results of all bioassays performed on test surfaces are shown (\pm 95% confidence interval, one-way ANOVA).

Chemistries	Human serum uptake ^{1,2}		Marine bacteria ^{1,3}		Spores of <i>U. linza</i> ^{1,4}
	VASE	QCM-D	<i>Cobetia marina</i>	<i>Marinobacter hydrocarbonoclasticus</i>	No. of settled spores per mm ²
	Thickness (nm)	Δm (ng cm ⁻²)	Attached bacteria per mm ²	Attached bacteria per mm ²	
SiO ₂	3.7 \pm 0.1 (a)	850 \pm 63 (a)	7606 \pm 809(a)	5320 \pm 442 (a)	595 \pm 96 (a)
PAAm- <i>g</i> -PFPA	1.9 \pm 0.1 (b)	381 \pm 70 (b)	11086 \pm 966(b)	12000 \pm 279 (b)	689 \pm 62 (a)
PVA 27 kDa	0.2 \pm 0.2 (c)	80 \pm 8 (c,e)	465 \pm 123(c,e)	3167 \pm 550 (c)	24 \pm 11 (b)
PEG 20 kDa	0.1 \pm 0.3 (c)	-45 \pm 26 (d)	90 \pm 57 (e)	182 \pm 38 (e)	365 \pm 102 (c)
Dextran 2000 kDa	0.2 \pm 0.1 (c)	65 \pm 12 (c,d,e)	215 \pm 53 (e)	9034 \pm 270 (f)	2 \pm 1 (b)

Chemistries	Human serum uptake ^{1,2}		Marine bacteria ^{1,3}		Spores of <i>U. linza</i> ^{1,4}
	VASE	QCM-D	<i>Cobetia marina</i>	<i>Marinobacter hydrocarbonoclasticus</i>	No. of settled spores per mm ²
	Thickness (nm)	Δm (ng cm ⁻²)	Attached bacteria per mm ²	Attached bacteria per mm ²	
PEOXA 50 kDa	0.3±0.1 (c)	333±53 (b)	1708±249 (c,d)	448±55 (e)	42±10 (b)
PVP 55 kDa	0.8±0.1 (d)	177±86 (e)	1601±364 (c,d)	340±57 (e)	82±10 (b)
PVP 1300 kDa	0.5±0.2 (c,d)	-12±10 (c,d)	2736±889 (d)	3131±302 (c)	39±5 (b)

^[1] Values followed by a different letter are significantly different to each other at $p < 0.05$ using one-way ANOVA with pairwise Tukey comparison test.

^[2] At least four samples for each test surface were used to calculate the means and errors.

^[3] Means obtained are based on 90 counts; 30 from each of three replicates per test surface.

^[4] Means obtained are based on 90 counts; 30 from each of three replicates per test surface. A second set of test surfaces was used to validate these results by obtaining the same trend in resistance (data not shown).

3.3.3.1 Protein adsorption

To evaluate protein resistance of the developed surfaces, a solution of human serum was used. While human serum may seem to be a surprising choice for testing surfaces for marine biofouling applications, it has the advantage of being well characterized, containing a wide range of proteins, and being readily available. Protein uptake, both on bare and functionalized surfaces, was studied using two different techniques: *ex-situ* ellipsometry and QCM-D. The first technique gives information regarding the dry thickness, or dry mass, and measurements were performed before and after protein exposure. It is characterized with a thickness resolution of 0.1-0.2 nm. The latter method, QCM-D, can provide information regarding polymer conformation, via associated water content and film thicknesses.^{206,207} It is highly sensitive to the absorbed mass, and allows *in situ* real-time monitoring. It has a mass sensitivity of about 5 ng/cm² and measures both changes in frequency and dissipation of the

oscillating system. Through the Sauerbrey equation (4), the frequency shift (Δf) can be related to the adsorbed mass per unit area (Δm).

$$\Delta m = -C \times \frac{\Delta f}{n} \quad (4)$$

Where C is the sensitivity constant of the quartz crystal with a value of 17.7 ng/(cm²•Hz) and n is the overtone number. This calculated acoustic mass comprises the mass associated with the adsorbed protein together with the water bound to those proteins (hydration via molecule entrapment and/or hydrodynamic coupling).

Ellipsometry results show that the protein uptake was maximal for the bare SiO₂ substrates, showing an increase in thickness of 3.7 nm, corresponding to a dry mass of 546.9 ng/cm², while with QCM-D it was measured as a hydrated uptake of 850 ng/cm². All other chemistries, including the more hydrophobic adhesion promoter, revealed a substantial decrease in the uptake, confirming the non-fouling nature of the studied polymers. The values for *ex-situ* analysis show that the best results were obtained for PEG, PVA and dextran, although there was no statistical difference from all the other nonfouling surfaces with the exception of PVP 55 kDa. The statistical similarity for PEG, PVA and dextran is not observed in the QCM studies, but PEG and the hydroxylated PVA and dextran still show extremely low uptake with *in-situ* measurements, validating the trend observed with ellipsometry. It also suggests that high-molecular-weight PVP has an increased protein resistance *in situ* when compared to the values given by the former technique. But in the case of the already quite thick PVP film the difference measured by ellipsometry of 0.5±0.2 nm is not relevant, since the dry film thickness before exposure to protein varies by ±0.9 nm. These variations are not taken into account in the *in situ* QCM-D measurement and therefore we also consider the high-molecular-weight PVP as being fully protein resistant.

3.3.3.2 Marine bacteria

Two strains of bacteria were used, since they have been reported to present different surface energies: *Cobetia marina* has been considered hydrophilic, while *Marinobacter hydrocarbonoclasticus* is a hydrophobic species⁴⁸.

Results show that some differences in attachment do exist between the two species (Table 3.5 and Figure 3.2). Exposure to *C. marina* leads to a significantly higher number of attached bacteria on the adhesion promoter (11086 ± 102 bacteria per mm^{-2}) than on the bare SiO_2 control (7606 ± 85 bacteria per mm^{-2}). The remaining functionalized surfaces showed a considerable decrease in cell attachment whereas PVA, PEG and dextran-containing chemistries showed the lowest number of bacteria per unit area with over 90% decrease in attachment and there was no statistical difference between them. Regarding *M. hydrocarbonoclasticus*, the data show equally high attachment on the adhesion-promoter-coated surface (12000 ± 29 bacteria per mm^2), with a significant decrease in attachment on almost all other surfaces, including bare SiO_2 . The unexpected result here is the surface modified with dextran, on which a high attachment of *M. hydrocarbonoclasticus* was obtained (9034 ± 28 bacteria per mm^2). One common result between both strains is the surface leading to minimum settlement: PEG was characterized by 90 ± 6 and 182 ± 4 bacteria per mm^2 for *C. marina* and *M. hydrocarbonoclasticus*, respectively. However, these values were not significantly different (one-way ANOVA, $p < 0.05$) from the next best performing surfaces for either species, (hydroxylated PVA and Dextran in the case of *C. marina*, PEOXA and PVP 55kDa in the case of *M. hydrocarbonoclasticus*).

3.3.3.3 Zoospores of *Ulva linza*

By comparing settlement of zoospores between surfaces, it can be observed that a significant decrease was achieved on the substrates functionalized with hydrophilic polymers, compared with the bare SiO_2 surface (Table 3.5 and Figure 3.2). The same did not occur on the slightly more hydrophobic adhesion-promoter layer where 689 ± 60 spores per mm^2 were attached versus the 595 ± 93 spores per mm^2 that characterized the bare SiO_2 . The PEG-functionalized surface showed a significantly higher settlement

of zoospores than expected, with 365 ± 99 zoospores per mm^2 . This can be a consequence of stability issues associated with this polymer, namely its thermal/oxidative degradation⁶⁰, which were already observed in the study performed in section dedicated to the short-term stability of the coatings. The hydroxylated chemistries of PVA and dextran appeared to be extremely resistant to the settlement of spores, with a settlement density of 24 ± 10 and 2 ± 1 spore per mm^2 , respectively. Nevertheless, according to Tukey test they were not statistically different from the nitrogen-containing chemistries of PEOXA and both PVPs.

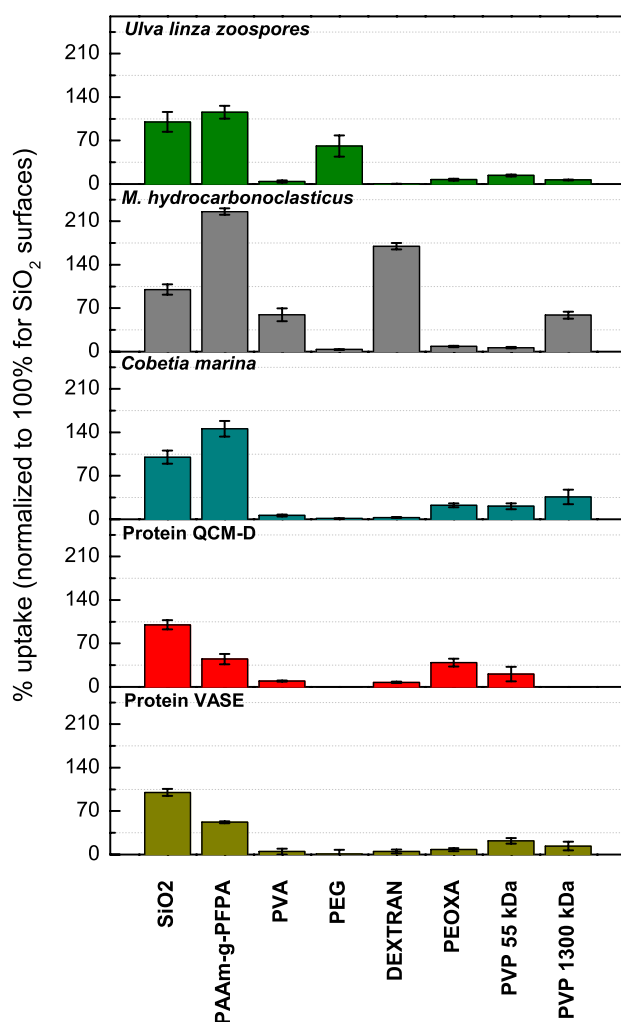


Figure 3.2 Normalized uptake results for tested nonfouling polymers regarding protein adsorption (provided by both VASE and QCM-D), bacteria (both *C. marina* and *M. hydrocarbonoclasticus*) and settlement of zoospores of *U. linza*. All data have been normalized against the results obtained from the bare SiO₂ (set to 100%).

3.4 Discussion

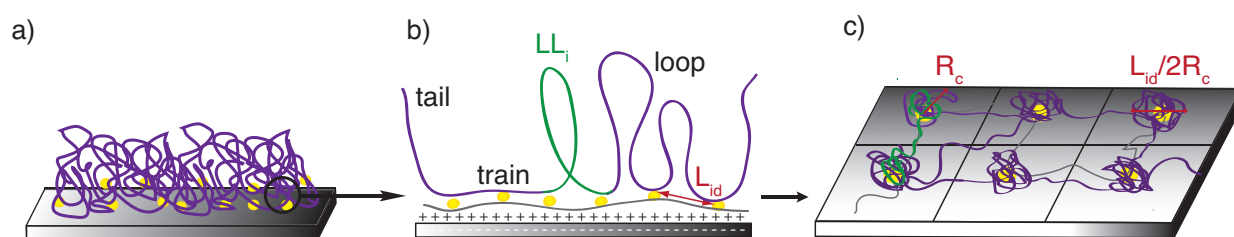
We have developed both a highly versatile surface-functionalization method and a comparative protocol for investigating the influence of different surface chemistries on different fouling stages, from proteins to cells, over different length scales (nm to μm for protein and bacteria/spores, respectively). Different coatings provided different relative responses, depending on the fouling species. In order to determine if those differences are material (chemistry) or architecture (conformation) dependent, we first need to build a conceptual model for our coatings.

3.4.1 Study of novel, multiply-tethered polymer coatings

The conformation of the organic layer that is created via azide chemistry and described in this work is primarily determined by two factors. The first one is related to the polymeric backbone, PAAm-*g*-PFPA, which spontaneously adsorbs onto the SiO_2 surface due to an electrostatic interaction between the positively charged amine groups of the polymer and negatively charged deprotonated silanol groups of the silicon oxide substrate. The use of polyelectrolytes on opposite charged substrates is a well-known strategy that has found applications in diverse areas such as lubrication,²⁰⁸ colloidal stabilization,²⁰⁹ wetting,²¹⁰ induced protein resistance. In order to better control the adsorption stability of polyelectrolytes, factors⁴⁴ such as pH and ionic strength were tuned. To guarantee full coverage, physiological pH (7.4) was used, since this value lies between the isoelectric point of the substrate (1.7-3.5) and the pK_a of polyallylamine (9.5), providing a negatively charged substrate and a positively charged polymer backbone. The role that ionic strength plays is related to the conformation adopted by the polymer when adsorption occurs. At lower ionic strength, polyelectrolytes tend to adopt an extended conformation due to the high repulsion between the charged groups. By slightly increasing ionic strength, the polymer adopts a coiled configuration, due to reduced repulsion between charges, allowing more macromolecules to be adsorbed. By further increasing ionic strength, electrostatic screening between charges on the polymer and on the surface increases, and consequently adsorption is reduced. In the reported case, a low-ionic-strength medium (HEPES I – 10 mM) is used for adsorption,

which results in a planar conformation of our adsorbed polymeric backbone,²¹¹ which is confirmed by the measured thickness.

The second conformational condition is schematically represented in Scheme A. Upon activation, the azide groups of the backbone will covalently bind to random segments of the polymer adlayer via insertion reactions. Three different situations for the bound polymer chain can be postulated: loops, trains and/or tails. The first comprises unbound segments that are further away from the surface but are constrained by neighbouring bonded segments, the second consists of successive bonds to the polymeric backbone and the third is when a sequence of bonded polymer (either in the configuration of a train or a loop) has one or both free chain ends stretched away from the surface.²¹² This resembles the frequently used loop-train-tail model for adsorbed polymers.²¹³



Scheme A Expected polymer architecture a) and simplified model b) and c) for the multi-tethered system described in this work, in which loops, trains and/or tails can be formed. For each surface attachment point, an average loop length LL_i can be calculated, from which the radius for a collapsed sphere R_c and the overlap of these polymer spheres on the surface, described by the parameter $L_{id}/2R_c$, can be determined, where L_{id} corresponds to the average distance between attachment points.

Literature on architectural studies of polymer brushes is fully based on end-grafted entities. A few theoretical studies have been performed on double-tethered brushes^{214,215} but due to its complexity, no work so far has been done on multi-tethered ones. The aim of this paper is not to provide a fundamental study on the behaviour and limitations of this new class of brushes, as both the random nature of the nitrene insertion and the difficulty to experimentally distinguish between loops, trains or tails do

not allow a reliable quantitative study. Nevertheless by using a simplified model, in which only loops are considered, structure-property relationships can be compared with those of end-tethered polymer brushes and possible advantages and/or disadvantages can be extrapolated. To this end, and based on the proposed model, the equations for the physicochemical properties presented in Table 3.6 have been deduced and calculated (more detail is provided in the Appendix) in order to obtain the final parameter $L_{id}/2R_c$, which correlates average distance between attachment points (L_{id}) and coiled radius of a collapsed loop (R_c).

Table 3.6 Physicochemical properties of the model surfaces used assuming 100% PFPA binding efficiency (Eff=1).

	Grafting density σ (1/nm ²)	Monomer density σ (1/nm ²)	σ_{attach}	LL_i (nm)	L_{id} (nm)	R_c (nm)	$L_{id}/2R_c$
PAAm- <i>g</i> -PFPA	0.067	1.65	-	-	-	-	-
PVA 27 kDa	0.028	16.9	59.8	2.6	0.84	0.51	0.82
PEG 20 kDa	0.141	64.2	11.7	17.1		0.83	0.51
Dextran 2000 kDa	0.003	42.4	480.3	16.7		1.01	0.41
PEOXA 50 kDa	0.009	4.4	189.6	1.0		0.45	0.93
PVP 55 kDa	0.026	12.8	63.7	1.9		0.65	0.64
PVP 1300 kDa	0.007	77.3	250.0	11.7		1.19	0.35

σ_{attach} : attachment density

LL_i : average loop length

L_{id} : average distance between attachment points

R_c : coiled radius

$L_{id}/2R_c$: degree of overlap between loops

When correlating R_c with the distance between chains of grafted polymer (L_{id}), the regimes in which these loops are found can be directly compared to those that an

end-tethered polymer brush can adopt. This is because, in a similar way, if one increases the surface density of loops, these will tend to stretch away from the surface in good solvent once the compensation between osmotic (excluded volume effect) and elastic (stretching entropy) pressure is reached. Since $L_{id}/2R_g$ (where R_g is the radius of gyration of the polymer chains in good solvent) is an indicator of the potential for forming brushes on the surface, $L_{id}/2R_C$ can be used as an upper limit of this quantity, since the polymer will swell upon exposure to solvent, i.e. $R_g > R_C$. Therefore, mirroring the generally accepted guidelines for $L_{id}/2R_g$, a conservative condition for brush formation is $L_{id}/2R_C < 0.5$.

According to the calculated values displayed in Table 3.6, it was found that the distance between attachment points, or length between PFPA units, was around 0.84 nm. The degree of overlap of each polymer loop, $L_{id}/2R_C$, was above the condition for brush formation ($L_{id}/2R_C < 0.5$), with the exception of dextran and PVP 1300 kDa. Although the brush conformation is well known to confer protein resistance to polymers due to the steric repulsion effects, the dependence of our polymer architecture, or a polymer's fouling ability, on the attachment efficiency of the PFPA units plays an important role in this system. The variation is presented in Figure 3.3 where it can be seen that significant changes in the conformation of the attached polymer only occur when efficiency reaches 20% or lower. Although a quantitative analysis of azide efficiency is difficult to study under the conditions presented here, if one considers that these chemical groups are known for their stability in the dark and at room temperature^{216,217} then it should be possible to assume that their binding efficiency is above the limit stated above.

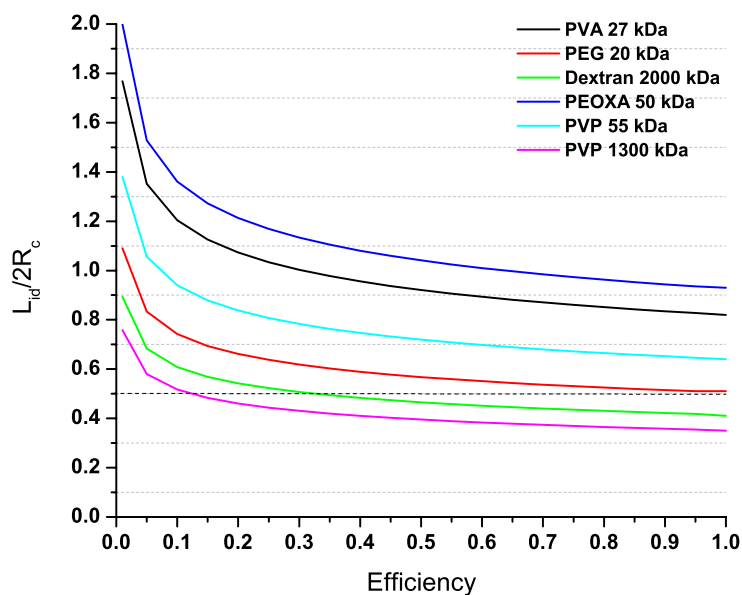


Figure 3.3 $L_{id}/2R_c$ variation with adhesion promoter efficiency.

3.4.2 Influence of polymer chemistry and proposed architecture on fouling response

In order to verify the abilities of the polymers tested in this work to withstand fouling, five assays covering different length scales were performed: protein resistance (3-20 nm) was analysed both *in situ* and *ex situ* and exposure to two strains of marine bacteria (2-3 μm long) and zoospores of *U. linza* (diameter 4-6 μm at widest point of motile pyriform-shaped spore) was carried out (see Table 3.5 and Figure 3.2).

In terms of protein resistance, the *ex situ* ellipsometry technique showed that the best performance was obtained by PEG and hydroxylated chemistries. However, since the uptake variability often lay within the instrumental error, another technique was needed in order to confirm this set of data. The *in situ* QCM-D was used and the experimental results obtained confirm that both dextran and PVA have very low protein uptake, supporting the information already provided by ellipsometry. A reason for this is the presence of OH groups in the latter polymers. These polymers will therefore be more likely to form a tightly bound water layer when compared to the nitrogen containing polymers. This consequently results in an improved protein resistance due to a more significant physical and energetic barrier being formed.⁴¹ The high-molecular-

weight PVP data, which implies full protein resistance, suggests that other parameters, such as mechanical stiffness (or lack of it), can equally affect the non-fouling performance of a polymeric film. The negative protein uptake that characterized PEG (due to loss of film mass) may be an indication that this specific coating is not stable, especially on the time scale over which these assays were performed. Some assays could take several hours, which contrasts with the few minutes needed to perform an ellipsometric analysis and such differences therefore influence the final outcome.

Regarding the other bioassays, spores of *U. linza* and the two strains of bacteria showed a higher settlement (attachment) on the slightly more hydrophobic surfaces (PAAm-*g*-PFPA, advancing contact angle of $70\pm 1^\circ$). Indeed, it has been observed that zoospores typically settle in higher numbers on hydrophobic surfaces and in lower numbers but with higher adhesion strength on hydrophilic surfaces.²¹⁸ In the same way, it has also been demonstrated that various marine bacteria show a tendency to attach on hydrophobic surfaces, irrespective of their surface chemistries.^{219,220}

However, regarding levels of settlement, different results were obtained for each species. While the two bacteria showed minimum settlement on the PEG-coated samples, spores settled in higher numbers on this sample compared to all the other non-fouling surfaces, which can be attributed to the lack of resistance of this specific coating towards the adhesives secreted by this species during the settlement process⁹². Both for spores of *U. linza* and cells of *C. marina*, settlement on the hydroxylated chemistries was minimal, which is in good agreement with the literature that suggests that hydration is also an important parameter in achieving decreased settlement/attachment for these specific species.⁴² Nevertheless, this latter hypothesis does not appear to hold for the results obtained for *M. hydrocarbonoclasticus*. Here, the lowest settlement was observed on samples coated with PEG, PEOXA and PVP 55 kDa, while PVA, PVP 1300 kDa and dextran showed considerably higher settlement (over 50% more than the low-settlement coatings). Dextran was the only 'nonfouling' surface that showed a higher settlement of bacteria than bare SiO₂, showing that for this specific strain of bacteria, dextran cannot be regarded as a fouling-resistant polymer. The preference of this bacterium for hydroxylated chemistries strongly suggests that hydration does not prevent its settlement. Instead, the presence of hydroxyl groups appears to play a key role in this process. The conditions under which bacteria are

cultured play a major role in cell physiology and the composition of extracellular polymeric substances produced, which determine how cells respond to surfaces.^{221,26} *M. hydrocarbonoclasticus* is known to produce wax esters (in EPS, extracellular polymeric substances) from alcohols by oxidation via the enzyme alcohol dehydrogenase.²²¹ This might be a reason for the preferential settlement of *M. hydrocarbonoclasticus* on hydroxylated chemistries, in contrast to *C. marina*, which is not known to produce this enzyme. Overall, these findings suggest that hydrophilicity, or surface energy, cannot be the sole responsible parameter for the adhesion of bacteria, which is consistent with previously reported results.^{48,221,222} Instead, since it is known that bacteria such as *E. coli*²²³ degrade dextran, one could postulate that the same happens with *M. hydrocarbonoclasticus*, hence explaining the preferential settlement on this polysaccharide. Interestingly the bacterium seems to attach preferentially to high-molecular-weight PVP 1300 kDa when compared to the low molecular weight PVP 55 kDa. The reason for the greater resistance of the lower-molecular-weight PVP indicates that *M. hydrocarbonoclasticus* attachment might also be regulated by other parameters, such as mechanical stiffness of the polymer substrate.

One other parameter this study allows us to evaluate is the polymer conformation of the developed organic films. As calculated, only dextran and PVP 1300 kDa were characterized as having a $L_{id}/2R_C < 0.5$ (i.e. brush), while all the others were above this limit in the collapsed state but still below 1. According to the literature, a more fouling-resistant performance is associated with polymers with $L_{id}/2R_g < 1$ ⁴⁴ when they start adopting a brush conformation. If one considers $R_g > R_C$, then once the polymers are hydrated they should all readily adopt a brush-like conformation. By analyzing Figure 3.2, the surface that presents the most consistent resistance to proteins and all tested organisms is the one that was functionalized with PVP 55 kDa. This indicates that while conformation and chemistry may play a key role in a polymer's resistance to biofouling, other additional physicochemical factors are equally important in conferring this ability.

All the findings stated above illustrate the complexity involved in marine biofouling but also indicate that the response of organisms to a particular surface chemistry is highly dependent on the test organism. There is not a single property that will dictate the fouling performance of a coating but more a combination of several

properties. Chemistry can help to increase resistance to fouling but cannot prevent it alone, thanks to the high adaptability of living organisms.

3.5 Conclusions

The adhesion promoter described in this paper provides a versatile approach to the functionalization of surfaces with a variety of polymers in a reliable and reproducible manner. By manipulating the stoichiometry of the adhesion promoter, grafting densities of the immobilized polymers and their conformational properties can be precisely tuned, enabling the impact of these properties on function to be readily studied. We have used this approach to test a range of hydrophilic uncharged polymers against both proteins and some of the most important marine-fouling test organisms.

The adhesion promoter possesses the ability to electrostatically bind to negatively charged substrates and, upon activation, covalently bind polymers in its close proximity. Validation of the functionalization method was achieved by means of different surface characterization techniques, such as dynamic contact angle, ellipsometry and XPS. Often, our non-fouling, coated surfaces were found to decrease protein uptake to such an extent that the experimental values were below the sensitivity of the instrument used, making it difficult to state which was the best-performing nonfouling chemistry. It was shown that the response to surface chemistry by marine fouling organisms strongly depends on the organism tested and cannot be simply related to a key property, or deconvoluted into general physicochemical conditions. PVP 55 kDa showed a more consistent resistance against all biological assays performed. Although it did not match PEG's low values for protein and bacteria attachment, it showed a higher stability and less variability in the results and should be considered as a promising candidate for nonfouling surfaces.

Chapter 4

Multimodal Binding of a Nonfouling Polymer

The work performed for this chapter has been included in the PCT patent application, Nr. PCT/EP2014/002453, submitted on 11/09/2014 entitled Functional Polymer by Serrano, Â.; Zürcher, S. and Tosatti, S. All experimental work was carried out by myself under the supervision of Dr. Zürcher and Dr. Tosatti, who also participated in manuscript preparation and in related scientific discussions, along with Prof. Spencer.

4 Multimodal Binding of a Nonfouling Polymer

4.1 Introduction

The work presented in this chapter had the aim of understanding how the combination of different binding groups present on a polymeric backbone influence the binding or adhesion strength of an ultrathin polymeric film spontaneously absorbed onto a solid support. In particular the adlayer thickness, and thus functional-group densities, and resistance to desorption when exposed to different media as a function of the foot combination and the substrates to be coated were investigated. The substrates of choice were silicon and titanium oxide for the reasons stated elsewhere (see section A.2 of the Appendix). To be able to investigate the coatings in term of their functionality, all coatings were tested for their ability to resist nonspecific protein adsorption upon exposure to full serum.

Working with several binding groups implies the simultaneous use of many different chemical functionalities, which necessitates a versatile and easy-to-handle platform. This was achieved by synthesizing a polymeric backbone that can be simply postmodified by any chemical functionality, provided it possesses a key end-group. The chosen system was an active-ester-containing polymer, poly(pentafluorophenyl acrylate) (PPFPAc), synthesized via a controlled polymerization technique—RAFT (Reversible Addition Fragmentation Radical Transfer – see section A.5 of the Appendix). This is a well-known approach to postmodification, as active esters react selectively with amine-bearing functionalities (see Figure 4.1).

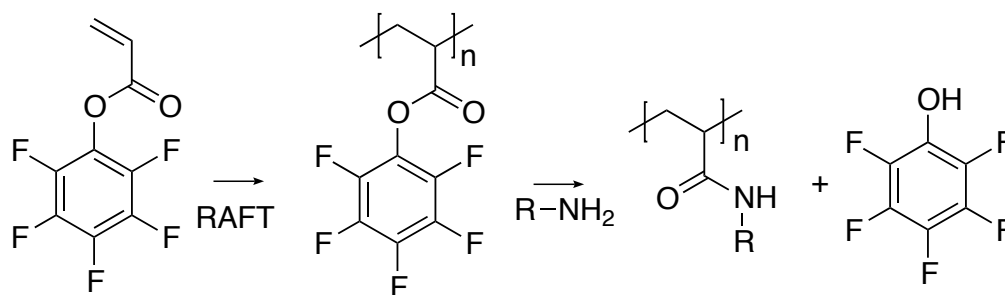


Figure 4.1 Schematics of the synthesis and postmodification of poly(pentafluoro-phenyl acrylate) – PPFPAc.

First, the backbone was postmodified with poly(ethylene glycol) side chains (mPEG-NH₂). These should impart resistance to non-specific protein uptake, provided their surface density reaches a certain level (formation of the brush – see Chapter 2). The PEG grafting ratio (the ratio between PEG chains and surface binding groups per polymer backbone) was chosen to be similar to that of previously described systems, such as PLL-*g*-PEG. Further, using hydrophilic PEG provides a guarantee that the polymer can be further processed in aqueous solution—a key feature for applied coatings in industrial applications. Secondly, various groups were grafted at different grafting ratios and in distinctive combinations, depending on their affinity to the model substrates used: for long-range electrostatic interactions to both substrates amines were used, for a covalent/coordination bond to titanium oxide catechol and phosphonate groups were grafted, while for the covalent bond to silicon oxide silane chemistry was applied. A non-binding, hydroxyl-functionalized compound (ethanolamine) was used as a quencher group.

Bulk characterization of the synthesized backbone included gel-permeation chromatography (GPC), nuclear magnetic resonance (¹H NMR, ¹⁹F NMR and ¹H-¹H NMR COSY), Fourier transform – infrared spectroscopy (FT-IR) and elemental analysis (EA), while for the subsequent analogous polymers only the latter and ¹H NMR were used. Surface characterization of the manufactured coatings was performed with variable-angle spectroscopic ellipsometry (VASE). Quartz crystal microbalance with dissipation (QCM-D) was used for *in situ* real-time adsorption studies on the most promising combinations.

4.2 Experimental

4.2.1 Substrates

Wafers

The TiO₂ substrates (22 nm thick film) were obtained from Powatech, GmbH (Switzerland). Information regarding the supply of SiO_x wafers and their cleaning protocol can be found in section 3.2.1 of the previous chapter.

QCM-D sensors

Details regarding the sensors used are described in section 3.2.1 of Chapter 3.

Well plates

The well plates used for storage and incubation are the same as those described in section 3.2.1 of Chapter 3.

4.2.2 Chemicals

All chemicals listed herein were used as received unless stated otherwise.

Solvents

Toluene ($\geq 99.9\%$), 2-propanol ($\geq 99.8\%$), methanol and N,N-dimethylformamide (DMF, $\geq 99.8\%$) were obtained from Merck (Switzerland); dichloromethane (99+%) was purchased from Acros Organics (Switzerland) and ultrapure water (purified with a water-treatment apparatus from Millipore, $\geq 18.2 \text{ M}\Omega \text{ cm}^{-1}$ resistivity, total organic content ≤ 5 ppb) was used throughout the experiments. For NMR experiments the solvents deuterium oxide (99.9 at.% D) from Aldrich (Switzerland) and deuterated chloroform (99.8 at.% D) from Armar Chemicals (Switzerland) were used.

Salts

Sodium chloride (NaCl, $\geq 99.5\%$) was provided by Merck (Switzerland) and magnesium sulphate (MgSO₄, $>99\%$) was acquired by Fluka (Switzerland).

Polymers

Methoxy-poly(ethylene glycol)-amine·HCl (average $M_w = 2000 \text{ g mol}^{-1}$) was acquired from JenKem Technology (USA) and poly(L-lysine)-*g*-poly(ethylene glycol) (PLL(20000)-*g*[3.5]-PEG(2000)) was provided by SuSoS AG (Switzerland).

Protein solutions

Lyophilized human serum (Precinorm U, Roche Diagnostics, Switzerland) was dissolved in ultrapure MilliQ water in order to obtain a solution with 160mM of ionic strength for use in the protein-adsorption tests. The protein concentration of the final solution is approximately 80 mg/mL.

Other used reagents

3-(Ethoxydimethylsilyl)propylamine, N-Boc-1,6-hexanediamine ($>98\%$), N-Boc-1,6-hexanediamine hydrochloride ($\geq 98\%$), acryloyl chloride ($\geq 97\%$), 2-(dodecylthiocarbonothioylthio)-2-methylpropionic acid (98%) and glycine ($\geq 99\%$) were obtained by Sigma Aldrich (Switzerland); trifluoroacetic acid, 2,6-dimethylpyridine, sodium dodecyl sulphate, triethylamine and fuming hydrochloric acid (37%) from Merck; pentafluorophenol (99%) and cetyl trimethylammonium bromide (CTAB, 98%) from ABCR (Germany); 12-aminododecylphosphonic acid·HCl from Sikémia (France); hexamethyldisilazane and potassium bromide puriss. (KBr, $\geq 99.5\%$), 2'2'-Azobis(2-methylpropionitril) (AIBN, recrystallized from Ethanol) from Fluka (Switzerland); N-hydroxysuccinimide perfluorophenylazide, and nitrodopamine sulphate were provided by SuSoS AG (Switzerland);

4.2.3 Buffers

All buffers used were prepared using ultrapure water (MilliQ) and stored in the dark at 4°C.

- *HEPES I*: 10 mM *N*-(2-hydroxyethyl)piperazine-*N'*-(2-ethanesulfonic acid) (HEPES), pH was adjusted to 7.4 with NaOH.
- HEPES 0: Prepared from HEPES I by diluting 10 times.
- *HEPES II*: 10 mM *N*-(2-hydroxyethyl)piperazine-*N'*-(2-ethanesulfonic acid) (HEPES) and 150 mM of NaCl were dissolved and the pH adjusted to 7.4 with NaOH.

4.2.4 Synthesis of pentafluorophenyl acrylate monomer

The monomer was synthesized according to the previously reported protocol²²⁴ (see Figure 4.2). Briefly, pentafluorophenol (87.21 g, 0.47 mol) was dissolved in 150 mL of CH₂Cl₂ at 0°C and 2,6-dimethylpyridine (60.55 mL, 0.52 mol) was added slowly through a dropping funnel, which was afterwards rinsed with another 150 mL of CH₂Cl₂. This second portion was added to the reaction mixture. Acryloyl chloride (42.14 mL, 0.52 mol) was then added dropwise to the reactor, still under cooling, and left to react overnight under N₂ atmosphere at room temperature. The resulting 2,6-dimethylpyridine hydrochloride salt was removed by filtration and the subsequent solution was washed three times with 100 mL of water, dried with MgSO₄ and the solvent evaporated under reduced pressure. The product was purified by distillation (in two portions) under reduced pressure (10 mbar) to give a colorless liquid (97.09 g, 78%) with the expected structure as confirmed by ¹H NMR.

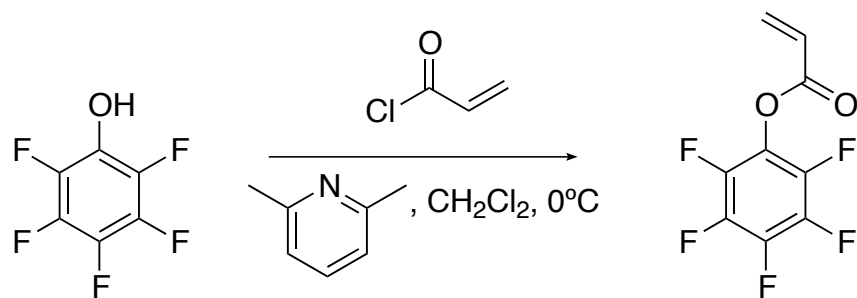


Figure 4.2 Synthesis scheme for the preparation of the monomer pentafluorophenyl acrylate.

4.2.5 Synthesis of poly(pentafluorophenyl acrylate) - PFPAC

The monomer pentafluorophenyl acrylate (14.31 g, 60.13 mmol), the initiator AIBN (23.83 mg, 0.15 mmol) and the chain-transfer agent 2-(Dodecylthiocarbonothioylthio)-2-methylpropionic acid (158.45 mg, 0.43 mmol) (see Figure 4.3) were dissolved in 15 mL of toluene inside a Schlenk tube. The solution was degassed via three freeze-pump-thaw cycles and left to react under a nitrogen atmosphere at 80°C in an oil bath for 18h. After the polymerization was completed, the mixture was left to cool to room temperature and the resulting polymer was isolated by precipitation in methanol and dried under vacuum for 48h (12.90 g, 90%). Bulk characterization was performed by gel-permeation chromatography, Fourier transform – infrared spectroscopy, NMR (^1H and ^1H - ^1H COSY) and elemental analysis.

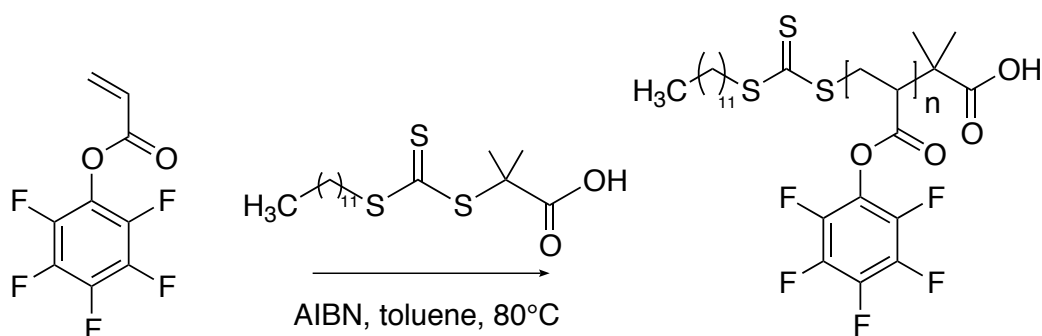


Figure 4.3 Polymerization of pentafluorophenyl acrylate via RAFT.

4.2.6 Matrix generation and postmodification reactions

4.2.6.1 Matrix generation

As stated before, the rationale behind the creation of this work's matrix was to evaluate the influence of different adhesive groups, and therefore of different binding strengths, onto a particular substrate by assessing the overall functionality of the deposited coating. To that end, the investigated polymers were divided in four different groups:

1. polymers with only long-range-interacting side groups;
2. polymers with only strongly binding side groups;
3. polymers with mixtures of long-range-interacting and strongly binding side groups;
4. polymers with only non-binding side groups.

The resulting matrix is presented below (see Table 4.1).

Table 4.1 Stoichiometric grafting densities of the studied postmodified polymers.

Designation	Stoichiometric grafting density (d)						Group
	mPEG	N-Boc-1,6-hexanediamine hydrochloride	3-aminopropyl dimethylethoxy silane	nitrodopamine	12-aminododecyl phosphate	ethanolamine	
A	0.15	0.85	-	-	-	-	1
B		0.425	0.425	-	-	-	3
C		0.425	-	0.425	-	-	3
D		0.425	-	-	0.425	-	3
E		0.425	-	-	-	0.425	1
F		0.425	0.2125	0.2125	-	-	3
G		-	0.425	0.425	-	-	2

Designation	Stoichiometric grafting density (d)						Group
	mPEG	N-Boc-1,6-hexanediamine hydrochloride	3-aminopropyl dimethylethoxy silane	nitrodopamine	12-aminododecyl phosphonate	ethanolamine	
H		-	0.85	-	-	-	2
I		-	-	0.85	-	-	2
J		-	-	-	0.85	-	2
K		-	-	-	-	0.85	4

4.2.6.2 First stage postmodification of PFPfAc: PEGylation for nonfouling functionality

In order to obtain nonfouling properties, the PFPfAc backbone was modified with the polymer methoxy-poly(ethylene glycol)-amine hydrochloride (mPEG-NH₂•HCl, 2000 gmol⁻¹). Briefly, 79.4 mg (0.333 mmol per monomer) of PFPfAc was dissolved in dimethylformamide (DMF) under stirring at a temperature of 50°C. Separately, 100 mg of mPEG-NH₂•HCl was dissolved in DMF (0.050 mmol) together with a 2 to 3-fold excess of triethylamine. The PEG solution was then added to the initial reactive mixture drop-wise and left to react overnight to obtain a PEG grafting density of 0.15. The resulting solution of poly(acrylic acid)-*g*-(PFPfAc, PEG) (238.11:2000 M_r ; 0.85:0.15 d), was used for further postmodification as described in the following section.

4.2.6.3 Second stage postmodification of PFPfAc: binding side groups

All polymer combinations presented below started from the pegylated version of poly(acrylic acid)-*g*-(PFPfAc, PEG) (238.11:2000 M_r ; 0.85:0.15 d) described in the previous section of the current chapter.

Polymer A or poly(acrylic acid)-*g*-(PEG, 1,6-hexanediamine) (2000:116.2 M_r ; 0.15:0.85 *d*)

107.43 mg (0.425 mmol) of N-Boc-1,6-hexanediamine hydrochloride were dissolved in 1 mL of DMF with an excess of triethylamine (177.71 μ L, 1.275 mmol). The mixture was added drop-wise to the poly(acrylic acid)-*g*-(PFPAc, PEG) (238.11:2000 M_r ; 0.85:0.15 *d*) solution and left to react overnight under stirring at 50°C. DMF was evaporated under reduced pressure, the mixture re-dissolved in dichloromethane (DCM, 2 mL, 4 equivalents) and trifluoroacetic acid (0.5 mL, 1 equivalent) and left to react under stirring overnight. The resulting mixture was again evaporated under reduced pressure and re-dissolved in ultrapure water (5 mL). This solution was purified by dialysis against water for two days using a membrane with a MWCO of 3,500 Da and subsequently freeze dried to obtain the polymer as a white powder (113.77 mg, 77.24%).

Polymer B or poly(acrylic acid)-*g*-(PEG, 1,6-hexanediamine, 3-aminopropyldimethylethoxysilane) (2000:116.2:161.3 M_r ; 0.15:0.425:0.425 *d*)

35.81 mg (0.142 mmol) of N-Boc-1,6-hexanediamine hydrochloride were dissolved in 1 mL of DMF with an excess of triethylamine (59.2 μ L, 0.425 mmol). The mixture was added drop-wise to the Poly(acrylic acid)-*g*-(PFPAc, PEG) (238.11:2000 M_r ; 0.85:0.15 *d*) solution and left to react overnight under stirring at 50°C. A new solution containing 45.71 mg (0.283 mmol) of 3-aminopropyldimethylethoxysilane and triethylamine (118.47 μ L, 0.85 mmol) was dissolved in 1 mL of DMF and, added drop-wise to the previous solution still at 50°C and under stirring overnight. Deprotection of the amine and purification followed as described for polymer A (118.08 mg, 77.91%).

Polymer C or poly(acrylic acid)-*g*-(PEG, 1,6-hexanediamine, nitrodopamine) (2000: 116.2:198.2 M_r ; 0.15:0.425:0.425 *d*)

Postmodification with N-Boc-1,6-hexanediamine hydrochloride was as described in polymer B. An excess of nitrodopamine was dissolved separately (83.94 mg, 0.283 mmol) in 1 mL of DMF with 118.47 μ L of triethylamine (0.85 mmol). The latter solution was added slowly to the polymer solution and left stirring overnight at the same

temperature. Deprotection of the amine and purification followed as described for polymer A (66.99 mg, 83.33%)^a.

Polymer D or poly(acrylic acid)-*g*-(PEG, 1,6-hexanediamine, 12-aminododecylphosphonate) (2000:116.2:265.3 *M_n*; 0.15:0.425:0.425 *d*)

Postmodification with N-Boc-1,6-hexanediamine hydrochloride was as described in polymer B. To this a solution containing 12-aminododecylphosphonate-bis(trimethylsilyl)ester²²⁵ and 118.47 μ L of triethylamine (0.85 mmol) in 1 mL of DMF (85.33 mg, 0.283 mmol) was added drop-wise. The resulting polymer solution was left reacting overnight at 50°C while stirring, followed by the deprotection of the amine and phosphonate and purification as described for polymer A (243.86 mg, 143.23%)

Polymer E or poly(acrylic acid)-*g*-(PEG, 1,6-hexanediamine, ethanolamine) (2000: 116.2:61.1 *M_n*; 0.15:0.425:0.425 *d*)

Postmodification with N-Boc-1,6-hexanediamine hydrochloride was as described in polymer B, after which an excess containing solution of ethanolamine (17.31 mg, 0.283 mmol) and triethylamine (118.47 μ L, 0.85 mmol) in 1 mL of DMF was slowly added. The resulting polymer solution was left reacting overnight at 50°C while stirring, followed by the deprotection of the amine and purification as described for polymer A (113.69 mg, 80.43%).

Polymer F or poly(acrylic acid)-*g*-(PEG, 1,6-hexanediamine, 3-aminopropyl-dimethylethoxysilane, nitrodopamine) (2000:116.2:161.3:198.2 *M_n*; 0.15:0.425:0.2125: 0.2125 *d*)

Postmodification with N-Boc-1,6-hexanediamine hydrochloride was as described in polymer B. Afterwards a solution of 3-aminopropyl-dimethylethoxysilane (11.43 mg, 0.071 mmol) and triethylamine (29.62 μ L, 0.21 mmol) in 1 mL of DMF was added dropwise and left stirring overnight at 50°C. A last solution of excess nitrodopamine (41.97 mg, 0.142 mmol) in DMF (1mL) and triethylamine (59.24 μ L, 0.43 mmol) was

^a Unlike the other postmodifications, polymer C was initiated with half of the starting material due to its limited availability at the time.

added dropwise. The resulting polymer solution was left reacting overnight at 50°C while stirring, followed by the deprotection of the amine and purification as described for polymer A (125.72 mg, 80.51%).

Polymer G or poly(acrylic acid)-*g*-(PEG, 3-aminopropyl-dimethylethoxysilane, nitrodopamine) (2000:161.3:198.2 M_r ; 0.15:0.425:0.425 *d*)

22.85mg (0.142 mmol) of 3-aminopropyldimethylethoxysilane previously dissolved in 1 mL of DMF and containing excess triethylamine (59.24 μ L, 0.425 mmol) was added to a solution of poly(acrylic acid)-*g*-(PFPAc, PEG) (238.11:2000 M_r ; 0.85:0.15 *d*). After reacting overnight at 50°C under stirring a new solution of excess nitrodopamine (83.94 mg, 0.283 mmol) and triethylamine (59.24 μ L, 0.43 mmol) in 1 mL of DMF was added dropwise. The resulting polymer solution was left to react overnight at 50°C while stirring, followed by the deprotection of the amine and purification as described for polymer A (135.95 mg, 82.39%).

Polymer H or poly(acrylic acid)-*g*-(PEG, 3-aminopropyl-dimethylethoxysilane) (2000:161.3 M_r ; 0.15:0.85 *d*)

Excess of 3-aminopropyldimethylethoxysilane (0.425 mmol, 68.56) and triethylamine (1.275 mmol, 177.71 μ L) was added to a 2 mL solution of poly(acrylic acid)-*g*-(PFPAc, PEG) (238.11:2000 M_r ; 0.85:0.15 *d*) as prepared in Example 2. The reaction was left overnight stirring at 50°C. Purification was performed as described for polymer A (132.65 mg, 85.14%).

Polymer I or poly(acrylic acid)-*g*-(PEG, nitrodopamine) (2000:198.2 M_r ; 0.15:0.85 *d*)

167.88 mg of excess nitrodopamine (0.57 mmol) and 236.95 μ L of triethylamine were dissolved in 2 mL of DMF and added to a solution of poly(acrylic acid)-*g*-(PFPAc, PEG) (238.11:2000 M_r ; 0.85:0.15 *d*) and left to react at 50°C under stirring overnight. Purification was performed as described for polymer A (80.81 mg, 92.75%)^b.

^b Same situation as polymer C.

Polymer J or poly(acrylic acid)-*g*-(PEG, 12-aminododecylphosphonate) (2000:265.3 M_r ; 0.15:0.85 *d*)

170.66 mg of excess 12-aminododecylphosphonate-bis(trimethylsilyl)ester (0.57 mmol) and 236.95 μL of triethylamine (1.7 mmol) were dissolved in 2 mL of DMF and added to a solution of poly(acrylic acid)-*g*-(PFPAc, PEG) (238.11:2000 M_r ; 0.85:0.15 *d*) and left to react at 50°C under stirring overnight. Purification was performed as described for polymer A (321.56 mg, 166.42%).

Polymer K or poly(acrylic acid)-*g*-(PEG, ethanolamine) (2000:61.1 M_r , 0.15:0.85 *d*)

34.61 mg of excess ethanolamine (0.57 mmol) and 118.47 μL of triethylamine (0.85 mmol) were dissolved in 2 mL of DMF and added to a solution of poly(acrylic acid)-*g*-(PFPAc, PEG) (238.11:2000 M_r ; 0.85:0.15 *d*) and left to react at 50°C under stirring overnight. Purification was performed as described for polymer A (115.72 mg, 85.47%).

Solutions of polymers containing nitrodopamine were adjusted to a basic pH prior to dialysis, in order to guarantee full dissolution in water. All polymers described in this section were characterized via ^1H NMR and elemental analysis.

4.2.7 Surface Modification

All samples were functionalized as follows: clean substrates (see section 3.2.1) were immersed in a polymer solution of 0.1 mg/mL dissolved in HEPES 0 overnight at room temperature, after which they were rinsed once with HEPES 0, ultrapure water and dried under a stream of N_2 .

4.2.8 Surface Characterization

The functionalized surfaces were characterized via ellipsometry by measuring the thicknesses of the clean metal substrate prior to adsorption and the subsequent

polymer coating afterwards. Experimental details can be found in section A.1 of the Appendix.

4.2.9 Stability assays

Ionic Strength

All polymer coatings were tested for stability by immersing the samples overnight at room temperature in sodium chloride solutions at pH 7.4 with different ionic strengths. Two ionic concentrations were used: a low-concentration version of 0.15 M dissolved in a 10 mM HEPES buffer (HEPES II) and a high-concentrated version of 2 M. The samples were then removed from the salt solution, rinsed twice with ultrapure water and dried under a stream of N₂. The adlayer thickness variation was then measured by ellipsometry.

Surfactants

Stability against surfactants of the polymer adlayer was tested by exposing surfaces functionalized with polymer A (full electrostatic binding to both SiO₂ and TiO₂) and polymer F (mix of electrostatic and covalent bonds to the metal surfaces) to an anionic and cationic surfactant: SDS and CTAB, respectively, at 0.5% w/v for 30 min at room temperature. Afterwards, the samples were rinsed twice with ultrapure water, dried under a stream of N₂ and the thickness variation measured via ellipsometry.

Acid

The influence of pH on stability/desorption of polyelectrolytes is a well-known and common assay. In this assay, substrates coated with the same two polymers as described in the previous test (Polymer A and Polymer F) were immersed in a glycine-HCl (10mM-pH=2.4) buffer for 30 min at room temperature. The samples were then rinsed twice with ultrapure water, dried under a stream of N₂ and the thickness monitored by ellipsometry.

4.2.10 Protein adsorption assays

By Ellipsometry

Prior to the assay in question, the thickness of the samples was measured (see experimental details in section A.1 of the Appendix). Afterwards they were immersed in HEPES II for 15 min, followed by exposure to a human serum solution for 30 min. The rinsing process included washing once with HEPES II and once with ultrapure water. They were then dried under a stream of N₂ and the thickness was again measured. Throughout the incubation, samples were stored at room temperature with no agitation.

By Quartz Crystal Microbalance with Dissipation

All steps described here were continued until a stable baseline was reached, under a flow of 20 µL/min at 25°C, with the exception of the human serum exposure which was performed under static conditions.

The cleaned sensors were exposed to a HEPES 0 solution until a stable baseline was established followed by the injection of a polymer solution of 0.1 mg/mL in HEPES 0 until a new plateau was reached. In order to remove loosely adsorbed molecules, the sample was rinsed with HEPES and allowed to equilibrate until a stable baseline was reached. The stability test could then be started: buffer was first replaced with ultrapure water followed by injection of a concentrated NaCl solution of 1 M pH=7.4 and final rinsing with ultrapure water. For testing the protein resistance of the modified sensors, the buffer was yet again exchanged, now for HEPES II, and a human-serum solution injected. Exposure continued for 30 min, followed by rinsing with the HEPES II buffer.

4.3 Results

4.3.1 Pentafluorophenyl acrylate monomer characterization

As stated before, it was our aim to use a chemical approach that would allow for easy postmodification of the synthesized polymer. To that end, active ester chemistry

was chosen although it is still not as commonly used as other postmodification techniques such as cycloaddition²²⁶ or thiol-ene reactions.²²⁷ The reason for this choice is related to the fact that active esters undergo a selective and rapid substitution in the presence of amines, yielding values close to 100% for amide conversion²²⁸ (see Figure 4.1). Furthermore, this reactivity can be enhanced in the presence of strongly electron-withdrawing groups, such as are found in the pentafluorophenyl group, under mild reaction conditions and in various organic solvents. Another design parameter that needed to be addressed was the choice of an acrylate over a methacrylate type of monomer. Studies have already been performed in order to understand which is associated with a higher reactivity and it was found that the polymer containing the acrylate version of the pentafluorophenol-substituted active ester can be modified either by primary or secondary amines at high conversion rates (100% and 80%, respectively) and by aromatic amines at lower rates (14%). This is in contrast to the methacrylate version, which only achieves 65% of modified polymer with both primary and secondary amines, and undergoes no conversion when exposed to an aromatic amine.²²⁹

¹H NMR characterization

The product was characterized by ¹H NMR (see Figure 4.4).

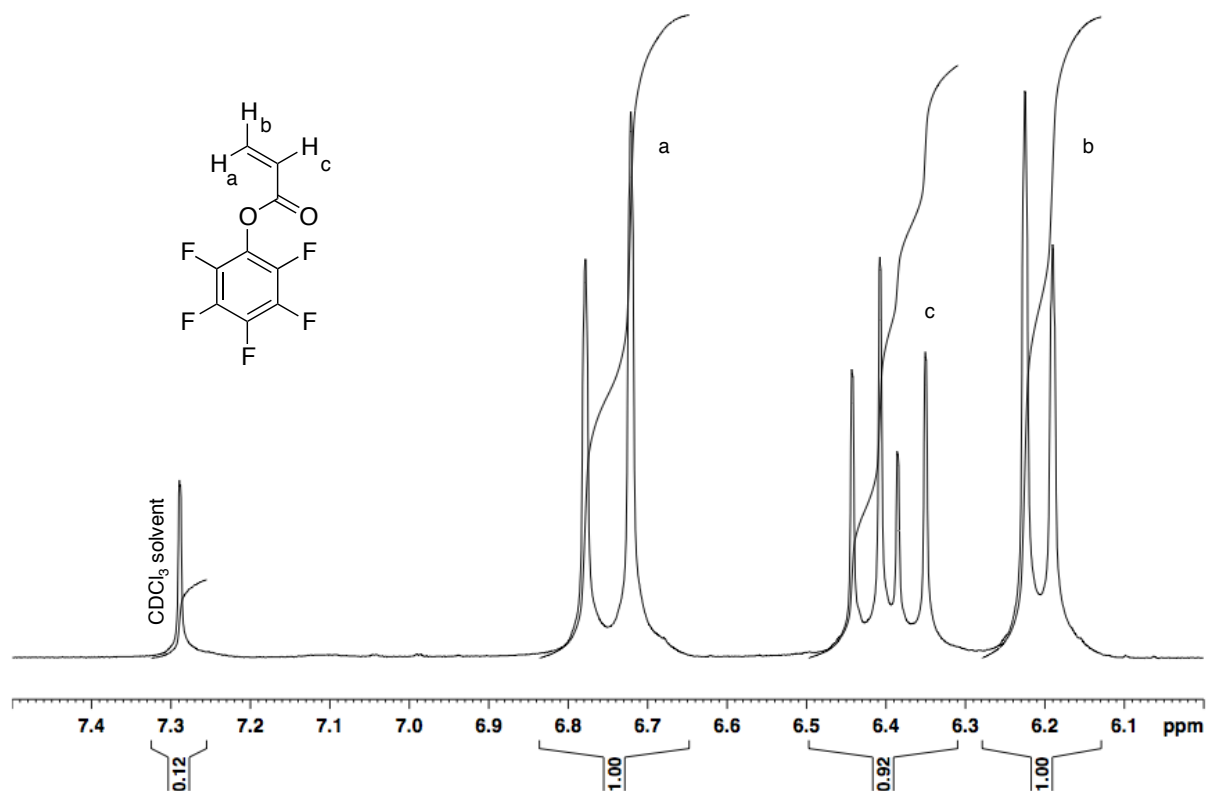


Figure 4.4 ^1H NMR spectrum of the pentafluorophenol acrylate monomer in CDCl_3 .

Solely the region of interest is shown, as no other peaks were observed in the remaining range of the spectra. There are three sets of peaks relevant to the synthesis in question: the doublets at 6.2 ppm, 6.7-6.8 ppm and the double doublet around 6.4 ppm. This is an expected result as only the hydrogens of the non-symmetrically substituted olefin are present. The reason why H_c results in a double doublet is related to the fact *cis* and *trans* protons have slightly different coupling constants (J) – usually *cis* suffers a shift upfield and *trans* is shifted downfield. The different chemical environment that both H_a and H_b are exposed to also accentuates this variation, as the strong electronegativity of the pentafluorophenyl group causes a proton in its close proximity to have reduced electron density and consequently be deshielded (higher chemical shift).

4.3.2 Poly(pentafluorophenyl acrylate) (PFPAc) characterization

After confirming the structure and composition of the pentafluorophenyl acrylate monomer, polymerization was carried out. Although no specific studies have been done as to understand the impact of polydispersity (PDI) on postmodification reactions, it is known that the properties of smaller polymer chains can strongly differ from those of longer ones. So in order to have a reproducible and accurate behaviour of the end-polymer, the living radical polymerization technique called RAFT was chosen to polymerize the pentafluorophenyl acrylate monomer into a well-defined, narrow polydisperse reactive polymeric backbone. Further information regarding mechanism and characteristic features of RAFT can be found in Appendix or elsewhere.²³⁰⁻²³³

Defining reaction conditions

Besides polydispersity (PDI) other features, such as degree of polymerization (DP) and consequent molecular weight, also had to be defined for the backbone. As a model for a comb-like co-polymer architecture we wanted to achieve, the well-studied poly(L-lysine)-*graft*-poly(ethylene glycol) (PLL-*g*-PEG) molecule was considered, more specifically when $M_{w,PLL}=20000 \text{ g mol}^{-1}$, $M_{w,PEG}=2000 \text{ g mol}^{-1}$ and $d_{PEG}=0.29$, where d stands for grafting density. Factors such as chain length of both backbone (PLL) and nonfouling function (PEG) or grafting density of the latter have been optimized in order to obtain a polymer-brush-like monolayer with optimal ability to resist protein adsorption¹²⁶. With the $M_{w,lysine \text{ monomer}}=128 \text{ g mol}^{-1}$ and the $PDI_{PLL}=1.3$, this will translate into a backbone with a polymerization degree of 120, which will be another aimed feature for the poly(pentafluorophenyl acrylate) backbone.

In order to define which concentrations of reagents should be used to attain the above-mentioned requirements, an initial set of reactions was designed to obtain a series of polymers with different degrees of polymerization based on equation 5 and considering total conversion (*conv*).

$$M_{n, \text{theo}} = \frac{M_{\text{monomer}} \times [\text{monomer}]_0 \times \text{conv}}{[\text{CTA}]_0} + M_{\text{CTA}} \quad (5)$$

The CTA-to-initiator ratio was kept constant while the monomer-to-(CTA-to-initiator) ratio was the variable one. Results from GPC are shown in Table 4.2.

Table 4.2 Reaction conditions and GPC (in THF, MW vs. PMMA standard) results for the first RAFT polymerization series.

Designation	Monomer: CTA:Initiator	Solvent	Temperature (°C)	Time (h)	M _w (g mol ⁻¹)	DP*	PDI	Yield (%)
FRP	100:0:1	Toluene	80	18h	54400	61	3.7	85.6
RAFT#18	18:3:1				3180	5	2.45	12.7
RAFT#210	210:3:1				12500	37	1.47	73.4
RAFT#415	415:3:1				23800	68	1.43	77.0
RAFT#831	831:3:1				33500	72	1.95	72.8

*(based on GPC's M_n values)

As a comparative control, the same polymerization procedure was performed in the absence of CTA. As one can see, in this latter case, the control over polydispersity was absent as a value of 3.7 was obtained although the highest molecular weight was achieved with a broad molecular weight distribution (see Figure 4.5a). These are typical outcomes of free-radical polymerization (FRP).

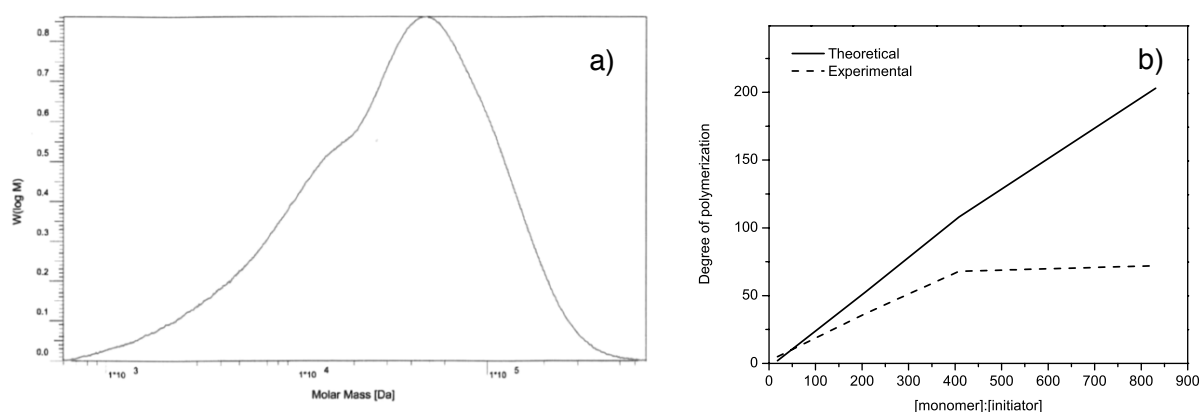


Figure 4.5 a) Molar-mass distribution of FRP polymer; b) Degree of polymerization dependence on monomer-to-initiator ratio during RAFT polymerization based on M_n values. All experimental values were obtained by GPC in THF.

Regarding the RAFT series, under these experimental conditions, it is clear that by increasing the monomer-to-(CTA-to-initiator) ratio the polydispersity decreases and the molecular masses and yield increase. This trend however is not fully observed with the highest ratio (RAFT#831). In this latter case, both yield and polydispersity showed poorer values than with the previous polymer. This might be a consequence of the limited range of control of the CTA used towards this specific monomer. Supporting this suggestion are the overall lower molecular weights obtained compared to the theoretical values (see Figure 4.5b).

Since a higher degree of polymerization could not be reached without losing control over the PDI, a compromise was reached by choosing the reaction conditions corresponding to the RAFT#415 example. These were then the conditions chosen for the scaled-up synthesis of the pentafluorophenyl acrylate polymerization. Results are shown in Table 4.3.

Table 4.3 Reaction conditions and GPC (in THF) results for the poly(pentafluorophenyl acrylate) PFPAC backbone.

Designation	Monomer: CTA:Initiator	Solvent	Temperature (°C)	Time (h)	M _w (g mol ⁻¹)	DP*	PDI	Yield (%)
PFPAC final	415:3:1	Toluene	80	18h	19300	53	1.51	90

*(based on GPC's M_n values)

¹H NMR characterization

Characterization of poly(pentafluorophenyl acrylate) was performed by NMR where the resulting spectra of the region of interest can be found in Figure 4.6, as no other relevant peaks were found. Solely the signals related to the polymeric backbone will be discussed, as the remaining ones have been attributed to the end groups belonging to the CTA used.

It is known that polymer ¹H NMR spectra are often characterized by broad and poorly defined peaks as a consequence of a proton experiencing more than one environment on the timescale used for the measurement – *chemical exchange broadening*.²³⁴

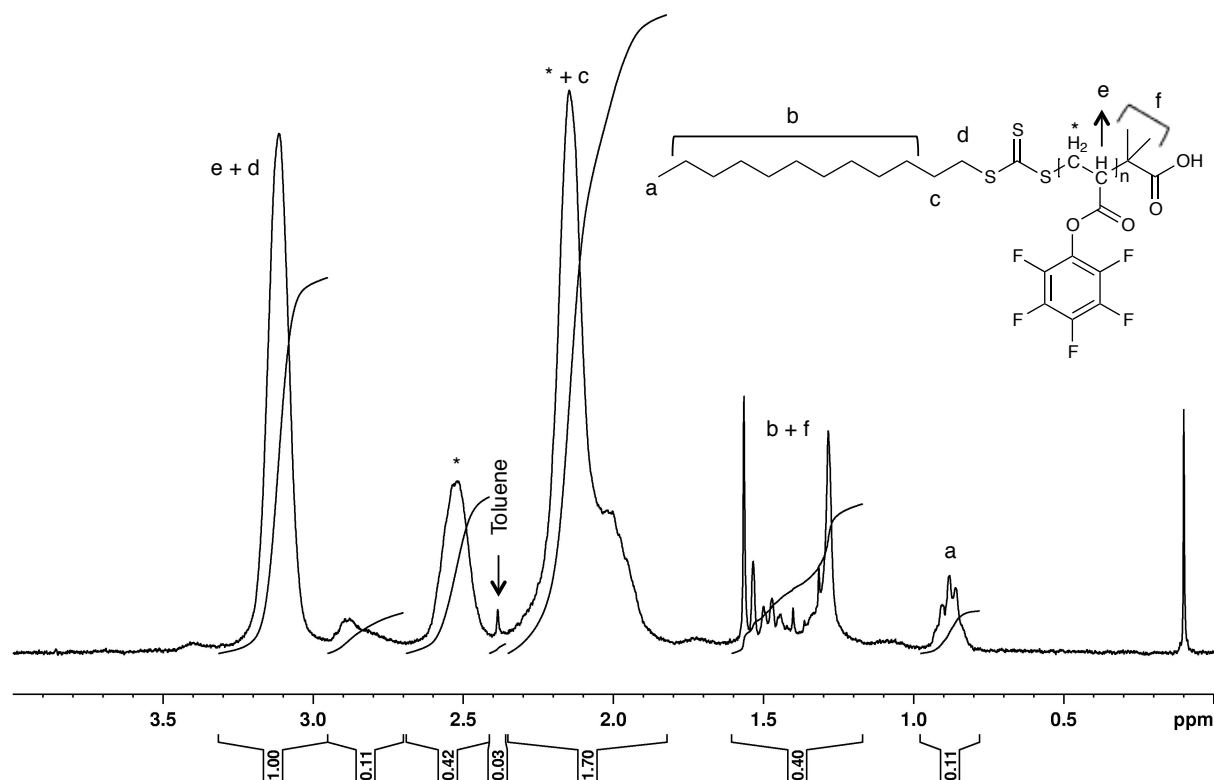


Figure 4.6 Region of interest of the ^1H NMR spectrum of poly(pentafluorophenol acrylate) in CDCl_3 .

It is reported in the literature that the expected peaks of the polymer in question should be found at 3.07 ppm (1H, s) and 2.09 (2H, br s)²²⁹. Nevertheless, integration of both these peaks does not fully account for the presence of the three hydrogens. More recent studies²³⁵ reveal that instead of two isolated peaks there is a region, roughly between 2 and 3 ppm, where three resonances arise—each one of them with different areas. To better understand why this occurred, 2D ^1H - ^1H Correlation Spectroscopy (COSY) was performed, as it provides information regarding spin-spin coupling (see Figure 4.7).

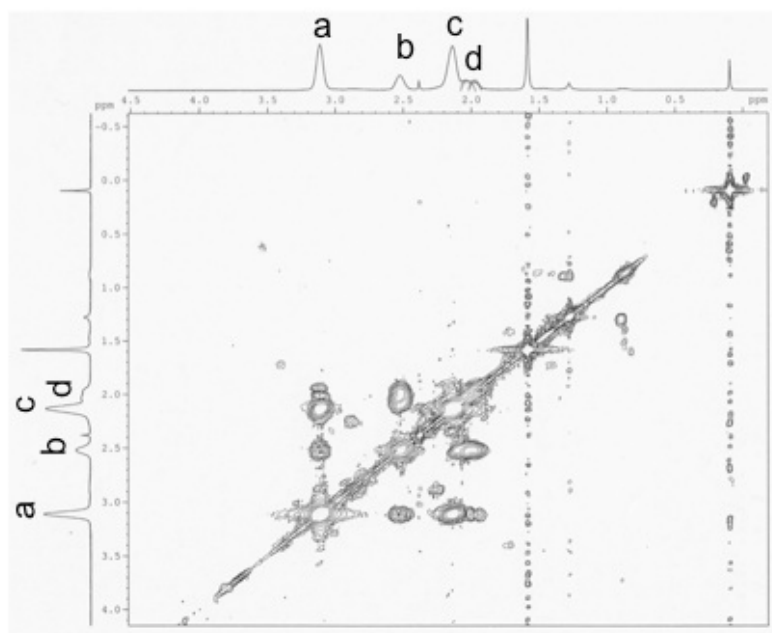


Figure 4.7 2D ^1H - ^1H COSY spectrum of poly(pentafluorophenyl) acrylate in CDCl_3 .

Considering the labelling on the COSY spectrum one can assume the following correlations:

- *a* couples to *b*, *c* and *d*;
- *b* couples to *a* and *d*;
- *c* couples to *a*;
- *d* couples to *a* and *b*.

These features bring us to the possible scenario that *a* is one proton ($-\text{CH}-\text{C}=\text{O}$), *b* and *d* are one form of the two hydrogens ($-\text{CH}_2-\text{CH}-$) and *c* is the other form of the latter. It is suggested that this peak splitting is due to the presence of syndiotacticity, where the groups in the chiral center ($-\text{CH}-\text{C}=\text{O}$) occupy opposite configurations every other chiral carbon (see Figure 4.8). Although the relative intensities of the relevant peaks might be compromised by the presence of other hydrogens that do not belong to the aliphatic part of the polymeric backbone, it is commonly found in poly(acrylates) a 1:2:1 proportion to give rise to 50% isotacticity and 50% syndiotacticity.²³⁶

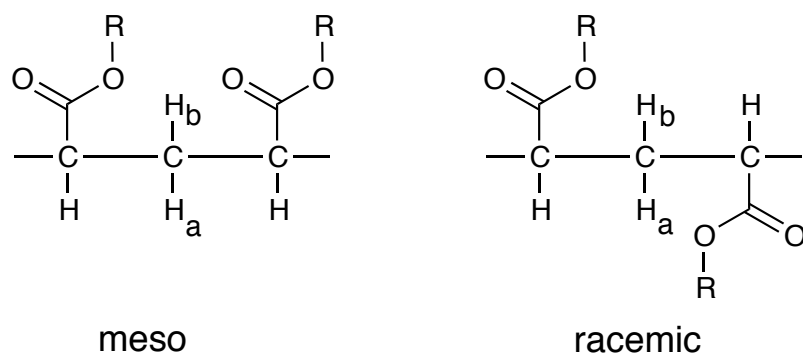


Figure 4.8 Meso and racemic diads of poly(pentafluorophenyl acrylate).

FT-IR characterization

Infrared spectroscopy was also performed in order to both characterize the polymer and verify if any hydrolysis of the ester group had occurred. The results are shown in Figure 4.9.

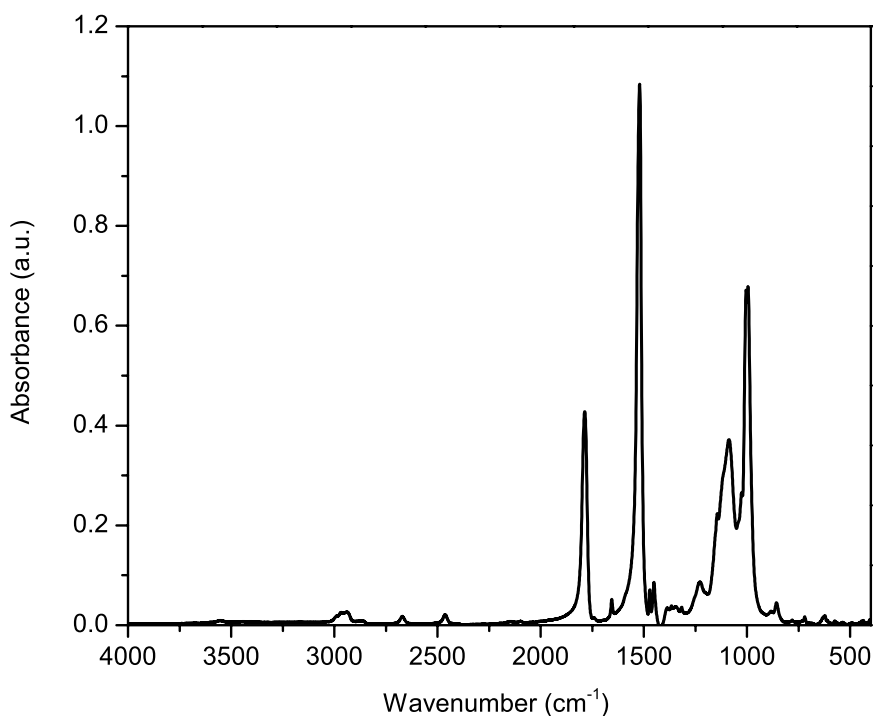


Figure 4.9 FT-IR spectrum of poly(pentafluorophenyl acrylate) in KBr pellets.

There are four relevant absorption bands that are typical of the polymer in question: C=O (stretch) found at 1800 cm^{-1} , aromatic C-C (stretch) at 1525 cm^{-1} , C-H (stretch) at 2950 cm^{-1} and C-F (stretch) $950\text{-}1250\text{ cm}^{-1}$. In addition, no strong broad bands were found between $2500\text{-}3300\text{ cm}^{-1}$ commonly associated to the presence of a carboxylic acid, which leads us to conclude no hydrolysis occurred and the predicted polymer absorption bands are present.

Elemental analysis characterization

Finally, the polymer, of formula $(\text{C}_9\text{H}_3\text{O}_2\text{F}_5)_n$, was also characterized via elemental analysis where the results can be found below in Table 4.4.

Table 4.4 Comparison between the calculated and experimental elemental analysis values respective to poly(pentafluorophenyl acrylate).

Elements	wt. %	
	Theoretical	Experimental
C	45.37	45.40
H	1.26	1.27
O	13.45	13.44
F	39.92	39.89

As it can be observed, there are no relevant differences between the theoretical and experimental values for the weight percentages of the present elements, which, in combination with all the results shown before, indicates the successful synthesis of the targeted polymer.

4.3.3 Postmodification matrix

4.3.3.1 Determination of the optimal PEG grafting density

After establishing that the intended backbone has been polymerized, the postmodification was carried out. In a first step, the backbone was modified with mPEG-NH₂ in order to (i) introduce the nonfouling functionality and to (ii) render the polymer water-soluble. Similar to the work performed for the PLL-*g*-PEG system, it was necessary to determine the grafting ratio (number of pentafluorophenyl acrylate units per PEG chain) at which this polymer would assume a brush-like conformation upon adsorption and so achieve best nonfouling behaviour. For that purpose an analogue of the model molecule PLL(20000)-*g*[3.5]-PEG(2000) was synthesized (see Figure 4.10).

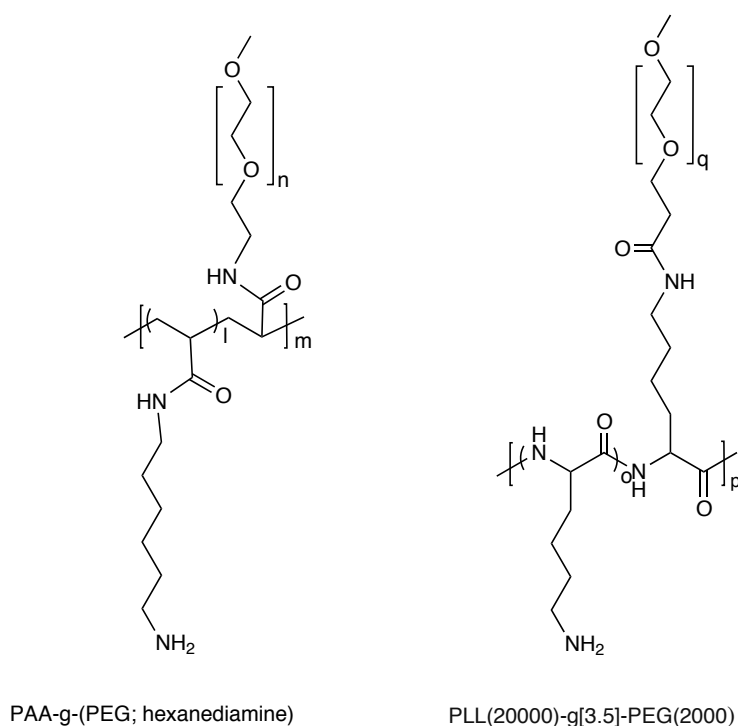


Figure 4.10 On the left structure of the PAA-*g*-(PEG; hexanediamine) used for the grafting density studies; on the right structure of the analogue PLL-*g*-PEG used as a model system to follow.

It is known that for PLL-*g*-PEG the grafting ratio of 3.5 provides the lowest protein uptake from human blood serum and resists cell attachment and this behaviour is

compromised when the grafting ratio increases as a result of lower PEG surface density⁵⁶. After considering the different lengths of both monomers (pentafluorophenyl acrylate and lysine), an equivalent grafting ratio of 5.1 (or a grafting density of 0.20) for the PAA-*g*-PEG architecture was estimated. A series of poly(acrylic acid)-*g*-(PEG, 1,6-hexanediamine) polymers with different grafting densities around the estimated value ($0 < d_{\text{PEG}} < 0.23$) was then synthesized in order to verify the influence of surface charge and PEG density on polymer adsorption and resulting reduction of non-specific protein adsorption. The synthesized polymers were adsorbed onto two different types of substrates (silicon oxide and titanium oxide) at a concentration of 0.1 mg/mL in HEPES 0 overnight. The coated samples were then immersed in HEPES II for equivalent time (overnight) to test for stability and finally exposed to human serum for 30 minutes. In between each step, ellipsometry was used to assess thickness variations. Results are shown in Figure 4.11.

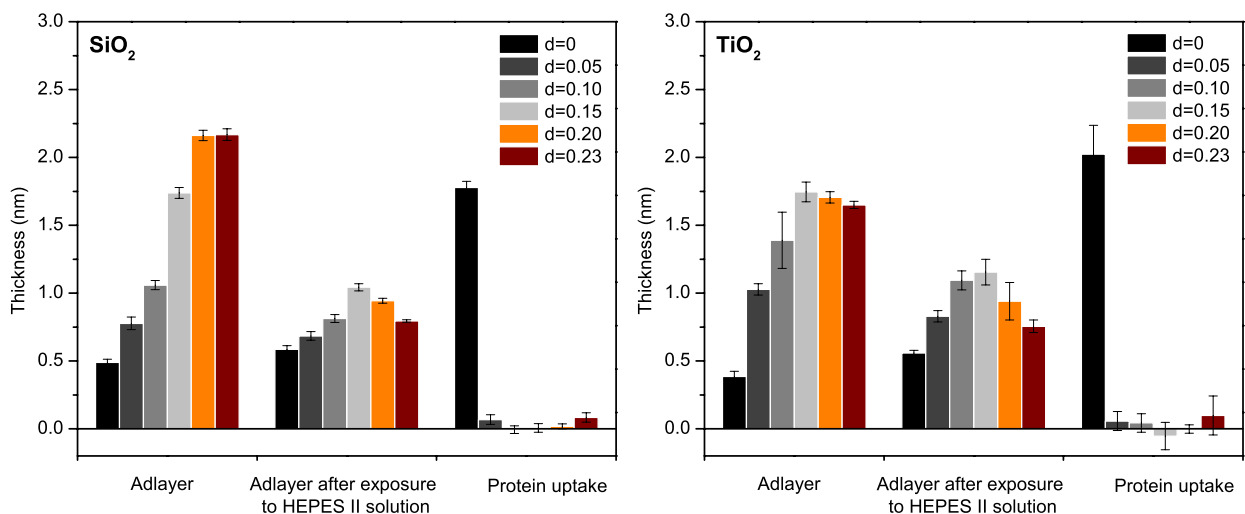


Figure 4.11 Adsorption, stability (exposure to HEPES II solution) and protein resistance ellipsometry results on silicon and titanium oxide surfaces of six post-modified polymers: poly(acrylic acid)-*g*-(PEG, 1,6-hexanediamine) was synthesized with different grafting densities ($0 < d_{\text{PEG}} < 0.23$).

As can be observed for both substrates, the absence of PEG ($d=0$) directly correlates with a minimum in adlayer thickness and maximum in protein uptake, as

expected. As soon as some PEG is grafted on the polymer backbone, the thickness increases, reaching a maximum when $d=0.20$ on SiO_2 and $d=0.15$ on TiO_2 . This is because if the surface density of PEG chains increases, these will tend to stretch away from the surface in a good solvent once the compensation between osmotic (excluded volume effect) and elastic (stretching entropy) forces is reached, leading to a brush-type conformation. Simultaneously, by increasing the monomer density of ethylene glycol units in the film, its resistance to protein uptake is also increased, as observed.

After exposure to the HEPES II salt buffer on both substrates, the thickest layers are obtained with a PEG grafting density of 0.15. This is possibly a consequence of the optimized ratio between binding positive charges and PEG chains still forming a dense brush. The protein uptake values between $d=0.10$ and $d=0.20$ for both substrates therefore reach a minimum.

Based on these findings, a grafting density of PEG of $d=0.15$ was chosen for the following tests, where different binding groups are compared with each other.

4.3.3.2 Order of addition of surface binding groups

The second stage of postmodification involved adding the surface-binding groups to the backbone. Defining their order of addition turned out to be crucial to the performance of the fully modified backbone. In the example below, two versions of polymer D poly(acrylic acid)-*g*-(PEG, 1,6-hexanediamine, 12-aminododecylphosphonate) (2000:116.2:265.3 M_r ; 0.15:0.425:0.425 d) were synthesized in parallel, with the only difference being the order of addition of the surface-binding groups: in version A the electrostatic component was added first while in the version B it was added last. Much like the previous assay, the resulting polymers were used to functionalize the two-model surfaces (SiO_2 and TiO_2) overnight, following the stability assay in HEPES II and the protein-resistance test with human serum. Ellipsometry values are shown in Figure 4.12.

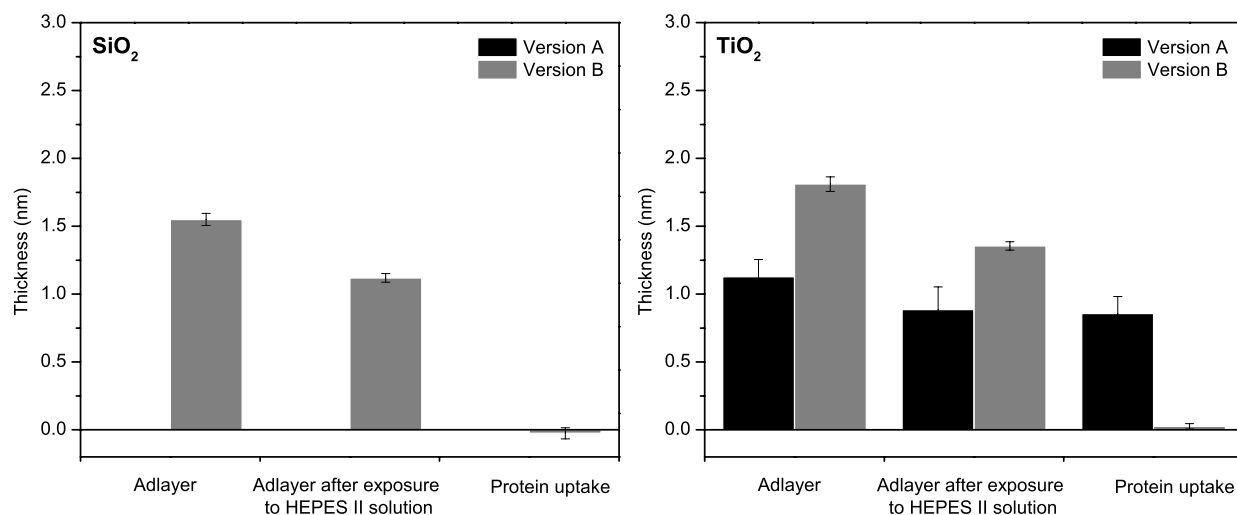


Figure 4.12 Adsorption, stability (exposure to HEPES II solution) and protein-resistance ellipsometry results on silicon and titanium oxide surfaces of two versions of polymer D poly(acrylic acid)-*g*-(PEG, 1,6-hexanediamine, 12-aminododecylphosphonate) (2000:116.2:265.3 M_r ; 0.15:0.425:0.425 d).

In the case of SiO₂, no adsorption was verified when using version A of polymer D and for that reason no further assays were performed on those surfaces. Nevertheless, a 1.5 nm thick film was registered with version B, which slightly decreases after exposure to HEPES II to values of 1.1 nm but reveals no protein uptake. Considering that at neutral pH, silicon oxide is negatively charged (isoelectric point of 2-3) and that the amine is positively charged (pKa around 11), an adsorption of electrostatic nature would be expected. This leads us to conclude that an insufficient amount of hexanediamine is present in version A to be able to drive the polymer onto the surface in a correct conformation, in contrast to what was observed in version B.

In the case of TiO₂, a difference can also be seen between versions: a protein-resistant, thicker adlayer was achieved in the case of version B, either before or after exposure to HEPES II, when compared to version A. In this latter case, however, adsorption was observed with the formation of a roughly 1 nm monolayer, which, based on the observations made in SiO₂, may be solely due to the affinity of the phosphonate groups to the substrate, although titanium oxide would be also negatively charged (isoelectric point = 6) and attract the positive amines. One explanation for these results

might be that the conformation of the polymers on the surface differs highly between versions A and B. The amount of hexanediamine in Version B is sufficient to force the polymer to adopt a stretched conformation due to segmental charge repulsion and, consequently, allows for a nonfouling, brush-like architecture. This seems not to be the case for Version A, where the presence of too many phosphonate groups, binding irreversibly to the surface, may prevent the polymers stretching out once adsorbed onto the surface.

Differences in the adsorption behaviour by varying the order of addition were found to be independent of the surface binding-group used. The hypothesis would be an increased compromised reactivity as the addition reactions proceeded due to steric hindrance. It is known that equilibrium constants and reactivity strongly decrease with increase in bulkiness of the substituents, particularly when there is already spatial crowding as pegylation is the first postmodification. Based on these results the following order of addition was adopted:

1. nonfouling PEG –to allow for a water soluble polymer;
2. hexanediamine – as the electrostatic component is suggested to be fundamental for polymer adsorption in the right conformation;
3. remaining surface-binding groups or quencher.

In all cases, the nomenclature of the polymer in question presents the order of addition of the reagents used for that postmodification.

4.3.3.3 Characterization of postmodified polymers

Characterization of the postmodified polymers was attempted by two techniques: elemental analysis and NMR. The intention of the latter was to determine the experimental grafting densities of the postmodified polymers. However, because of many components present the peak signals were too broad and overlapping to be able to isolate them (see ^1H NMR of combinations A to G in section A.7 of the Appendix). Therefore, solely a qualitative analysis can be performed (see Table 4.5).

Table 4.5 Assignment of characteristic NMR peaks of the chemical functionalities grafted to the postmodified polymers A to G, in terms of chemical shifts.

Polymer	Chemical Functionality	Peak Identification	Peak position (δ /ppm)
Polymer A	PEG	$-\text{CH}_2\text{-O-CH}_2-$	3.3 to 3.9
	1,6-hexanediamine	$-\text{CH}_2\text{-CH}_2\text{-CH}_2\text{-CH}_2-$	1.2 to 1.7
Polymer B	PEG	$-\text{CH}_2\text{-O-CH}_2-$	3.3 to 3.9
	1,6-hexanediamine (plus aliphatic contribution from the silane anchor)	$-\text{CH}_2\text{-CH}_2\text{-CH}_2\text{-CH}_2-$	1.2 to 1.7
	3-aminopropyl- dimethylsilanol	$-\text{Si}(\text{CH}_3)_2$	-0.9 to 0.1
Polymer C	PEG	$-\text{CH}_2\text{-O-CH}_2-$	3.3 to 3.9
	1,6-hexanediamine	$-\text{CH}_2\text{-CH}_2\text{-CH}_2\text{-CH}_2-$	1.2 to 1.7
	nitrodopamine	$=\text{C}(\text{H})-$ (aromatic ring)	two low intensity broad bands detected between 7 and 8
Polymer D	PEG	$-\text{CH}_2\text{-O-CH}_2-$	3.3 to 3.9
	1,6-hexanediamine (plus aliphatic contribution from the phosphonate anchor)	$-\text{CH}_2\text{-CH}_2\text{-CH}_2\text{-CH}_2-$	1.2 to 1.7
Polymer E	PEG	$-\text{CH}_2\text{-O-CH}_2-$	3.3 to 3.9
	1,6-hexanediamine	$-\text{CH}_2\text{-CH}_2\text{-CH}_2\text{-CH}_2-$	1.2 to 1.7
Polymer F	PEG	$-\text{CH}_2\text{-O-CH}_2-$	3.3 to 3.9
	1,6-hexanediamine (plus aliphatic contribution from the silane anchor)	$-\text{CH}_2\text{-CH}_2\text{-CH}_2\text{-CH}_2-$	1.2 to 1.7
	3-aminopropyl- dimethylsilanol	$-\text{Si}(\text{CH}_3)_2$	-0.9 to 0.1
	nitrodopamine	$=\text{C}(\text{H})-$ (aromatic ring)	two low intensity broad bands detected between 7 and 8

Polymer	Chemical Functionality	Peak Identification	Peak position (δ /ppm)
Polymer G	PEG	$-\text{CH}_2\text{-O-CH}_2-$	3.3 to 3.9
	1,6-hexanediamine (plus aliphatic contribution from the silane anchor)	$-\text{CH}_2\text{-CH}_2\text{-CH}_2\text{-CH}_2-$	1.2 to 1.7
	nitrodopamine	$=\text{C}(\text{H})-$ (aromatic ring)	two low intensity broad bands detected between 6.7 and 7.7

As one can observe, key peaks associated with the grafted chemical functionalities were obtained with the exceptions of the phosphonate and ethanolamine anchor groups in polymers D and E, respectively. Concerning polymer E (control polymer without adhesive groups), no further efforts were made to characterize it since its adsorption results (barely zero) matched our predictions. In the case of polymer D, although no characteristic peak was found on ^1H NMR, elemental analysis did detect the presence of phosphorus (see Table 4.6). The wt.% determined with the latter method shows differences between the experimental and the theoretical values. It is possible to hypothesize that the reason for such a deviation might be due to the synthetic procedure.

Table 4.6 Comparison between the calculated and experimental elemental analysis values respective polymer D.

Elements	wt.%	
	Theoretical	Experimental
C	56.05	51.15
H	9.38	9.11
N	3.81	2.85
O	28.24	35.35
P	2.51	1.55

Indeed, the polymeric combinations that contained the phosphonate anchor group (polymer D and polymer J) gave yields above 100%, which can be a consequence of a potential contamination associated to this specific binding group. As yield calculations were performed by gravimetric analysis, an unexpected increase in mass of the phosphonate due to contamination could lead to the unexpected high masses obtained in the end product. Furthermore, no $-\text{Si}(\text{CH}_3)_3$ signal was detected in the ^1H NMR spectra which would account for a potential failed deprotection of 12-aminododecylphosphonate-bis(trimethylsilyl)ester and unreacted monomer (pentafluorophenyl acrylate), having a lower molecular weight than the grafted phosphonate binding group, could not account for an increase in the final mass. Nevertheless, ^{19}F NMR was performed for the combinations discussed in this section in order to verify if full substitution had occurred in the pentafluorophenyl acrylate monomers.

In all cases no fluorine peaks were detected in the region of interest for poly(pentafluorophenyl acrylate): ^{19}F NMR (CDCl_3) δ : -161.77 (d, 2F), -156.88 (t, 1F), -151.79 (d, 2F).²³⁷ An example is shown in the left graph of Figure 4.13. The only fluorine peak found in the polymeric combinations that were modified with 1,6-hexanediamine, was the one associated to trifluoroacetic acid (see right graph in Figure 4.13), indicating that even after 2 days of dialysis, a certain portion of the amino groups remain in the form of an ammonium trifluoroacetate salt.

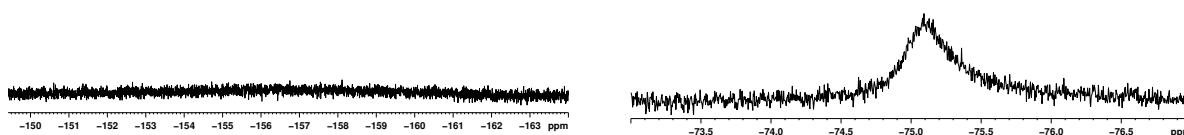


Figure 4.13 ^{19}F NMR spectra in CDCl_3 of Polymer A as an example of the observations found in all other polymer combinations subjected to this analysis. On the left is the region of interest for the presence of fluorine peaks associated with poly(pentafluorophenyl acrylate), on the right is the region of interest for trifluoroacetic acid.

4.3.4 Surface modification

4.3.4.1 Polymer adsorption

The adlayer thickness of the different postmodified polymers on both silicon oxide and titanium oxide was investigated via ellipsometry (VASE). Adsorption parameters are described in the Experimental section of this chapter and results are displayed in Figure 4.14.

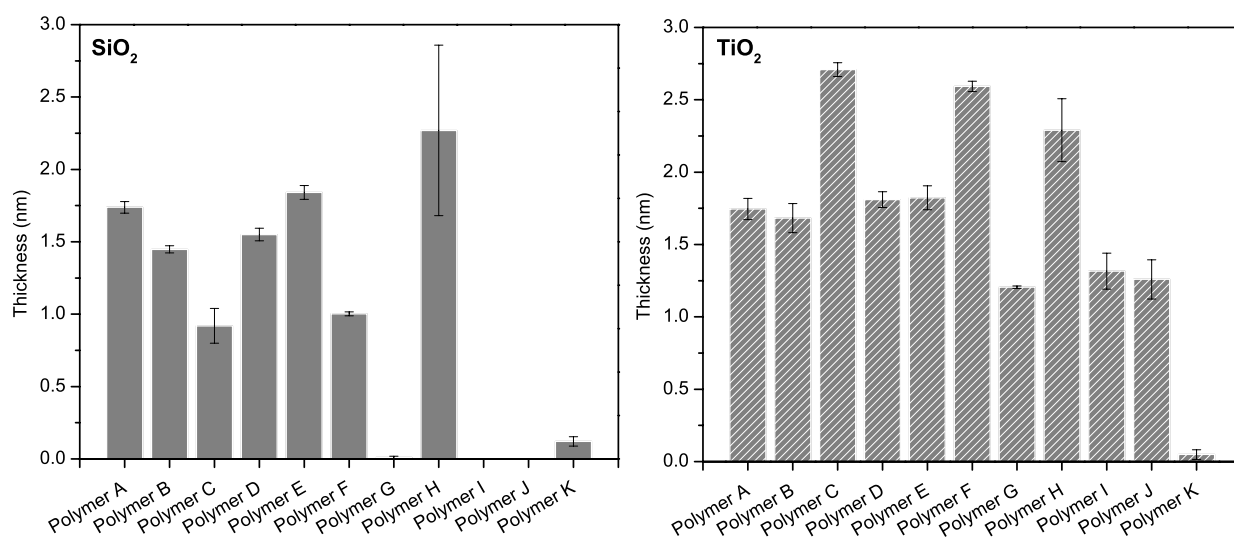


Figure 4.14 Adsorption thickness results of all postmodified polymers (A to K) on SiO₂ (left) or TiO₂ (right) substrates.

Results show the predictable formation of a polymeric film thickness that depends on the type of chemistry used for binding. For instance, polymer combinations containing amine and/or silane binding groups, known for their electrostatic or covalent binding to SiO₂, respectively, show a similar thickness on this type of substrate (roughly between 1.5 to 2.2 nm) even in the presence of the titania-binding phosphonate group or the quencher ethanolamine. This is not the case when nitrodopamine is present (polymers C and F), presumably due to its bulkiness and/or the presence of negatively charged hydroxyl groups, which influences the access of the amine and/or silane groups to the surface, affecting the adsorption conformation of the polymer. This can be easily observed by the lack of adsorption of polymers I and J.

Regarding the attachment to TiO₂, maximum thicknesses are reached when the catechol group (nitrodopamine) is present (polymers C and F) in combination with the positively charged hexanediamine. This suggests that covalent binding is more effective via the latter than with the phosphonate groups (case D) and also suggests that a rearrangement of the polymer on the surface takes place, in order to attain an optimal conformation. This might also be the reason why polymers I and J did not reach higher thicknesses. An adlayer is also verified even if none of the titanium oxide binding groups are present (cases A, B, E and H) due to the fact that adsorption is performed under neutral pH, which is higher than the isoelectric point of TiO₂ (~6). This now negatively charged surface can still bind electrostatically to the positively charged amine groups, present in the above-mentioned cases A, B and E. As for polymer H (full silane anchor moieties), it is known that silanization is possible due to the presence of an oxide layer²³⁸ hence the ~2.2nm layer obtained.

Regarding the quencher polymer K, which possesses the grafting densities $d_{\text{PEG}}=0.15$ and $d_{\text{ethanolamine}}=0.85$, some adsorption is registered on both substrates. This is however within the instrumentation's sensitivity and can thus be neglected.

4.3.4.2 Role of long-range interactions

In the previous section 4.3.3.2 there was already an indication that the role of the charged group hexanediamine might be critical to a correct self-assembly and consequent good performance of the postmodified polymers. Electrostatic forces, or coulombic interactions between charges, are known to be long-range interactions, and in order to better understand their role in our system's adsorption behaviour, two polymers (polymer F poly(acrylic acid)-*g*-(PEG, 1,6-hexanediamine, 3-aminopropyl-dimethylethoxysilane, nitrodopamine) (2000:116.2:161.3:198.2 M_r ; 0.15:0.425:0.2125:0.2125 d) and polymer G poly(acrylic acid)-*g*-(PEG, 3-aminopropyl-dimethylethoxysilane, nitrodopamine) (2000:161.3:198.2 M_r ; 0.15:0.425:0.425 d) were compared for adlayer formation, consequent stability against HEPES II and protein resistance. The main difference between them is that the latter did not possess any positively charged amine groups that are responsible for electrostatic adsorption on the surfaces. Results are shown in Figure 4.15.

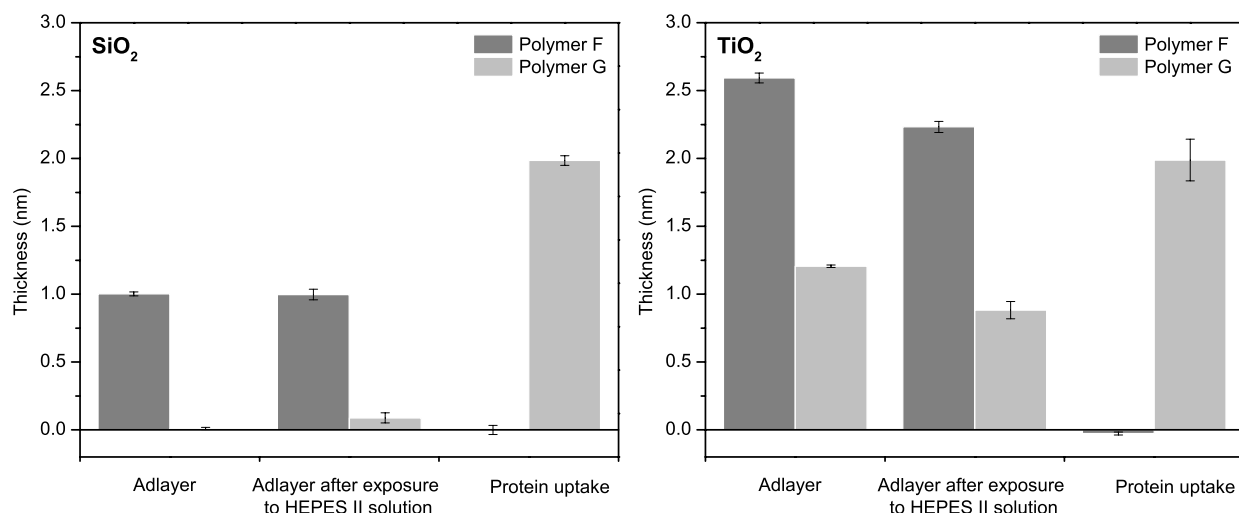


Figure 4.15 Adsorption, stability (exposure to HEPES II solution) and protein resistance ellipsometry results on silicon and titanium oxide surfaces of polymer F poly(acrylic acid)-*g*-(PEG, 1,6-hexanediamine, 3-aminopropyl-dimethylethoxysilane, nitrodopamine) (2000:116.2:161.3:198.2 M_r ; 0.15:0.425:0.2125: 0.2125 d) and polymer G poly(acrylic acid)-*g*-(PEG, 3-aminopropyl-dimethylethoxysilane, nitrodopamine) (2000:161.3:198.2 M_r ; 0.15:0.425:0.425 d).

In the case of SiO₂, no adlayer formation was verified for polymer G, indicating that long-range interactions are necessary to act as a driving force for the polymer to reach the substrate and assemble itself. Predictably, the absence of any nonfouling-containing structure directly translated in a high protein uptake for the non-amine-containing polymer. For the substrate TiO₂, although considerably lower coverage, an adlayer was formed regardless of the presence of amine groups. One could postulate that the catechol groups might have faster assembly kinetics than those of the silanes towards SiO₂ or even that the silanolates need ammonium groups to be stable in water and protect them from intramolecular Si-O-Si condensation. Despite the fact that this adlayer was formed, it was found not to be protein resistant, as possibly the polymer did not assemble under the needed conformation for such behaviour.

Overall, as already suggested, long-range interactions appear to be fundamental in the assembly in the correct conformation of the postmodified polymers.

4.3.4.3 Stability towards ionic strength and protein resistance assays

All postmodified polymers have been tested for stability against a low and high ionic strength medium and subsequent protein resistance, as described in the experimental section of this chapter. In order to further investigate the impact of electrostatic and/or covalent binding, polymers have been grouped according to the chemical functionality introduced, for the aimed model substrate. The controls have been chosen considering the stoichiometric grafting density used for the surface-binding groups. In short, groups have been arranged according to the following generic descriptions:

- polymer A (control) with 100% of electrostatic surface binding groups;
- polymer E (control) with 50% of electrostatic surface binding groups and 50% quencher;
- polymer with 50% of electrostatic and 50% of covalent surface binding groups;
- polymer with 100% covalent surface binding group.

Consequently, the results obtained have been divided into four groups, according to Table 4.7.

Table 4.7 Organization of the stability and protein resistance assays.

Group	Composition	Adsorption, stability and protein resistance results showed on:
Group I (controls and nitrodopamine containing polymers)	Polymer A poly(acrylic acid)- <i>g</i> -(PEG, 1,6-hexanediamine) (2000:116.2 M_r ; 0.15:0.85 <i>d</i>)	TiO ₂
	Polymer E poly(acrylic acid)- <i>g</i> -(PEG, 1,6-hexanediamine, ethanolamine) (2000: 116.2:61.1 M_r ; 0.15:0.425:0.425 <i>d</i>)	
	Polymer C poly(acrylic acid)- <i>g</i> -(PEG, 1,6-hexanediamine, nitrodopamine) (2000: 116.2:198.2 M_r ; 0.15:0.425:0.425 <i>d</i>)	
	Polymer I poly(acrylic acid)- <i>g</i> -(PEG, nitrodopamine) (2000:198.2 M_r ; 0.15:0.85 <i>d</i>)	
Group II (controls and silane containing polymers)	Polymer A	SiO ₂
	Polymer E	
	Polymer B poly(acrylic acid)- <i>g</i> -(PEG, 1,6-hexanediamine, 3-aminopropyl-dimethylethoxysilane) (2000:116.2:161.3 M_r ; 0.15:0.425:0.425 <i>d</i>)	
	Polymer H poly(acrylic acid)- <i>g</i> -(PEG, 3-aminopropyl-dimethylethoxysilane) (2000:161.3 M_r ; 0.15:0.85 <i>d</i>)	
Group III (controls and phosphonate containing polymers)	Polymer A	TiO ₂
	Polymer E	
	Polymer D poly(acrylic acid)- <i>g</i> -(PEG, 1,6-hexanediamine, 12-aminododecylphosphonate) (2000:116.2:265.3 M_r ; 0.15:0.425:0.425 <i>d</i>):	

Group	Composition	Adsorption, stability and protein resistance results showed on:
Group III (controls and phosphonate containing polymers)	Polymer J poly(acrylic acid)- <i>g</i> -(PEG, 12-aminododecylphosphonate) (2000:265.3 M_r ; 0.15:0.85 d)	TiO ₂
Group IV (controls and both silane and nitrodopamine containing polymers)	Polymer A	SiO ₂ and TiO ₂
	Polymer E	
	Polymer F poly(acrylic acid)- <i>g</i> -(PEG, 1,6-hexanediamine, 3-aminopropyl-dimethylethoxysilane, nitrodopamine) (2000:116.2:161.3:198.2 M_r ; 0.15:0.425:0.2125: 0.2125 d)	
	Polymer G poly(acrylic acid)- <i>g</i> -(PEG, 3-aminopropyl-dimethylethoxysilane, nitrodopamine) (2000:161.3:198.2 M_r ; 0.15:0.425:0.425 d)	

Group I - nitrodopamine containing polymers

Results (see Figure 4.16) show the predictable formation of a polymeric film thickness depending on the type of chemistry used for binding as already seen in the Polymer Adsorption section. In the case where solely electrostatic binding was involved (amine and amine-ethanolamine) the initial adlayer thickness, around 1.75 nm, was not maintained even after overnight exposure in low ionic strength medium (HEPES II – 0.16M). This is an expected result, as the salts are known to screen the repulsion between charged segments of the polymer and the electrostatic interaction between the film and the substrate. Losing the electrostatic attraction to the surface, the polymers start to coil and eventually desorb from the surface, leading to a decrease in thickness. However, the value obtained after immersion in HEPES II (around 1nm) seems sufficient to maintain the protein resistance of the functionalized surface, while after exposure to the 2M salt solution, the samples are no longer protein resistant.

The maximum thickness was obtained when both the amine and the nitrodopamine were present and it prevailed after exposure to both low- and high-ionic-strength media. Similar stability was also observed in the case where only nitrodopamine was used as a binding group to the titanium oxide, but with lower thickness values. Nevertheless, total protein resistance was obtained only in the former case, independently of the ionic strength the surfaces were exposed to. This fact suggests yet again that the presence of long-range interactions (electrostatic forces) is needed, both to act as a driving force for the polymer to reach the substrate and assemble itself but also for it to adopt the optimal conformation for a nonfouling surface with PEG exposed to the solution-surface interface. Covalent binding is equally necessary, especially to enhance the stability of the adlayer under harsh conditions such as high ionic strength.

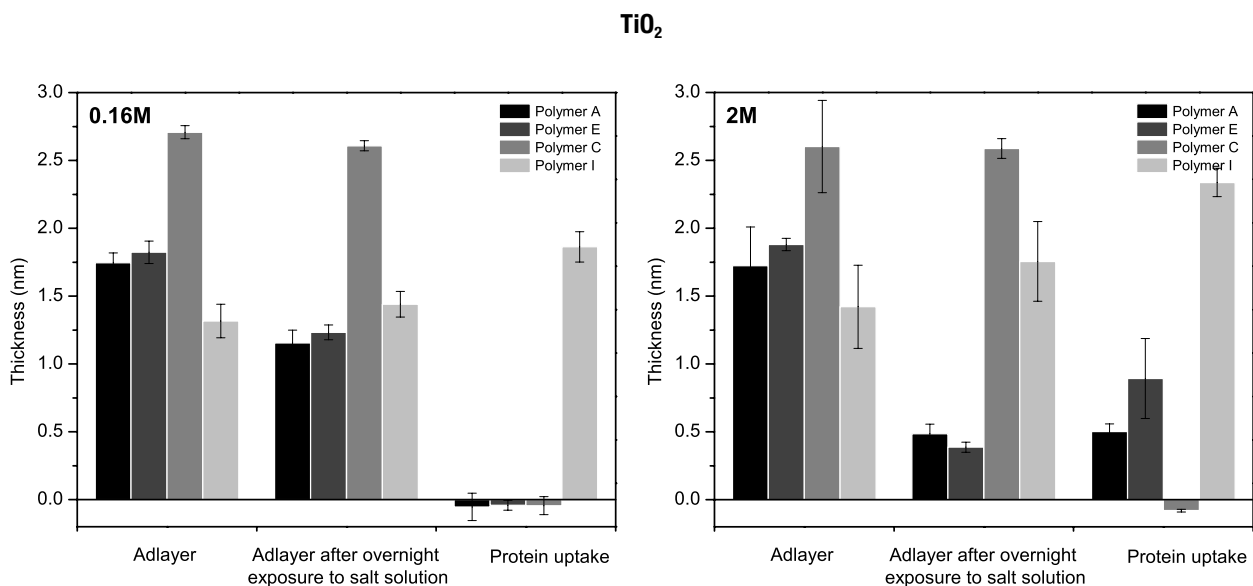


Figure 4.16 Adsorption, stability (exposure to solution) and protein resistance results on titanium oxide surfaces of four post-modified polymers: polymer A, polymer E, polymer C and polymer I. The graph on the left shows the results of the polymeric coatings when exposed to a low-ionic-strength medium (HEPES II 0.16 M) during the stability test step, while on the right they were exposed to a high-ionic-strength medium (NaCl 2M).

Group II - silane containing polymers

The trend observed in Figure 4.17 and in the previous example for the first two tested polymers A and F (amine and amine-ethanolamine) is the same as for SiO₂. When silane is added to the reactive backbone along with amine (polymer B) there is a slight reduction of the thickness of the adlayer after the stability test but protein resistance is maintained, irrespective of whether the functionalized surface has been exposed to low- or high-ionic-strength medium. This shows that the adlayer formed has ideal conformation and adhesion stability, even when compared to the previous case (polymer C on TiO₂ - see Figure 4.16). Polymers having only silane as a binding group, form an adlayer with a higher thickness than all the other polymers, indicating that a different conformation of the polymer is obtained. Those layers are however not protein resistant. It is polymer B, having both electrostatic and covalently linking groups, that outperforms all the other combinations for the same reasons as stated in the previous example.

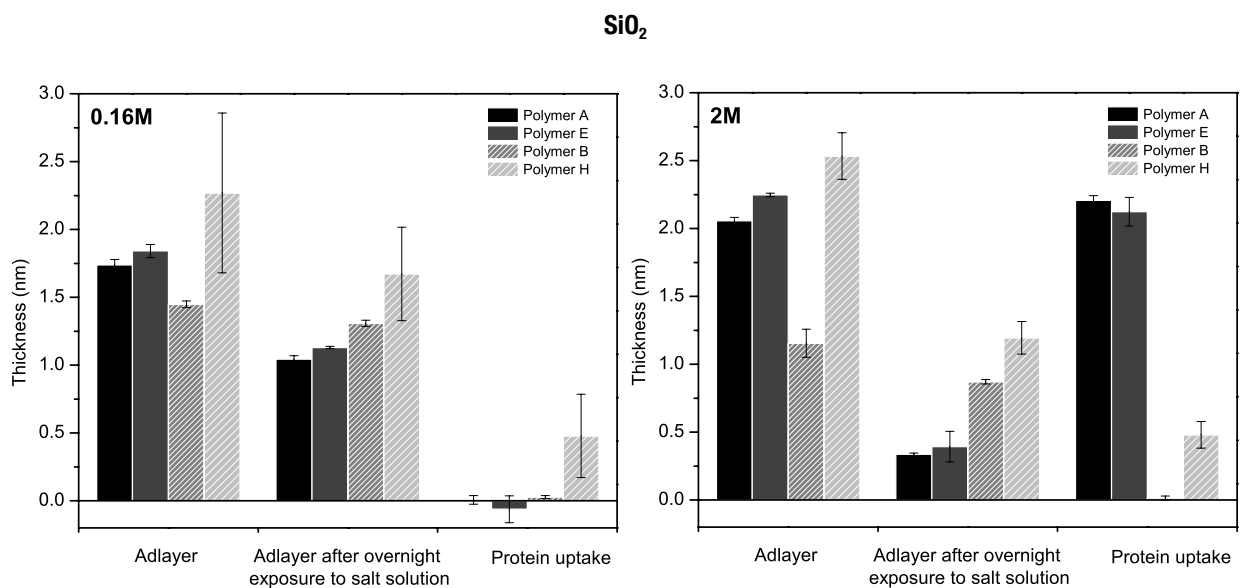


Figure 4.17 Adsorption, stability (exposure to solution) and protein-resistance results on titanium oxide surfaces of four post-modified polymers: polymer A, polymer E, polymer C and polymer H. The graph on the left shows the results of the polymeric coatings when exposed to a low-ionic-strength medium (HEPES II 0.16 M) during the stability test step, while on the right they were exposed to a high-ionic-strength medium (NaCl 2M).

Group III - phosphonate containing polymers

Similarly to the results obtained for Group I, in the case where the surfaces were exposed to HEPES II (0.16M) for stability (see Figure 4.18), there is an overall loss in initial thickness but all combinations containing the electrostatic contribution appeared to be protein resistant. This again shows that the latter has an important role when it the polymer is required to adopt the optimal conformation to this end (nonfouling). When exposing the surfaces to a higher ionic strength medium, then all surfaces lose their ability to prevent fouling. The same did not happen with the other titania-selective group nitrodopamine, which indicates that nitrodopamine forms a more stable bond with the substrate than the phosphonate group.

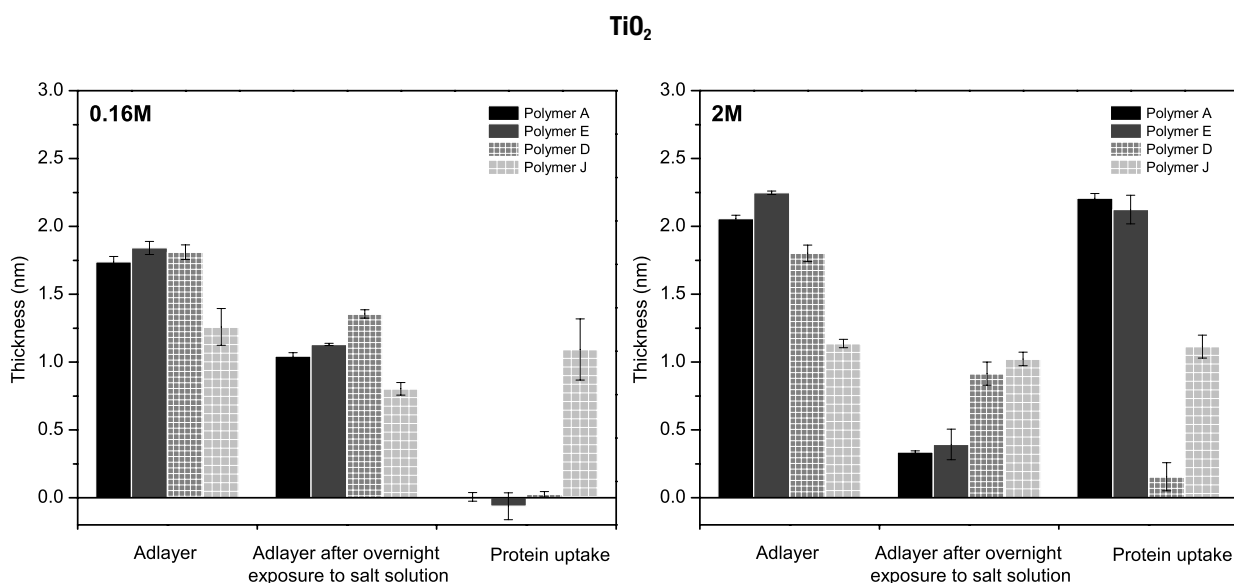


Figure 4.18 Adsorption, stability (exposure to solution) and protein-resistance results on titanium oxide surfaces for four post-modified polymers: polymer A, polymer E, polymer D and polymer J. The graph on the left shows the results of the polymeric coatings when exposed to a low-ionic-strength medium (HEPES II 0.16 M) during the stability test step, while on the right they were exposed to a high-ionic-strength medium (NaCl 2M).

Group IV –silane- and nitrodopamine-containing polymers

For both substrates (see results for silicon oxide in Figure 4.19 and for titanium oxide in Figure 4.20), and as already explained before, the surfaces that possess an

electrostatically driven polymeric conformation showed no protein uptake after being exposed to the lowest ionic strength salt solution. Since polymer G contains no amines attached to the backbone, even though it adsorbs, the polymer is not organized in a way that the PEG side chains adopt a brush-like structure and hence the surface is not protein resistant.

After exposing the surfaces to a 2M salt solution, the polymers without groups that can attach to SiO_2 or TiO_2 covalently, or consist only of covalently linking groups with no electrostatic contribution (polymers A, E and G), do not retain their resistance to human serum. Polymer F, having all three adhesive groups on the backbone, resists protein adsorption on both substrates even after an exposure to a high-ionic-strength medium.

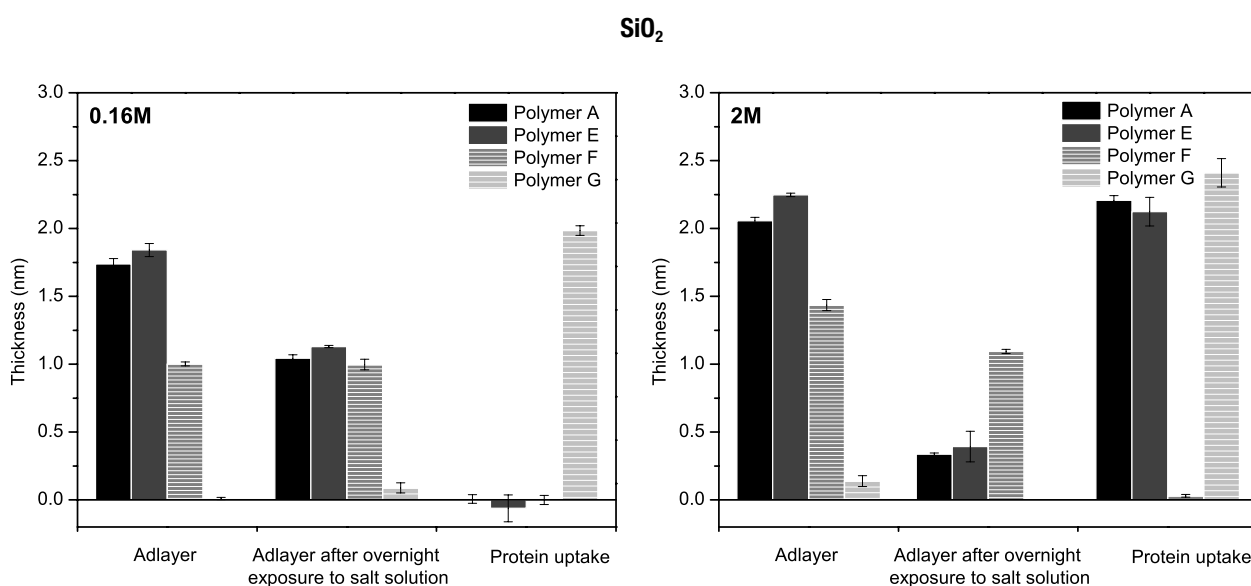


Figure 4.19 Adsorption, stability (exposure to solution) and protein-resistance results on silicon oxide surfaces for four post-modified polymers: polymer A, polymer E, polymer F and polymer G. The graph on the left shows the results of the polymeric coatings when exposed to a low-ionic-strength medium (HEPES II 0.16 M) during the stability test step, while on the right they were exposed to a high-ionic-strength medium (NaCl 2M).

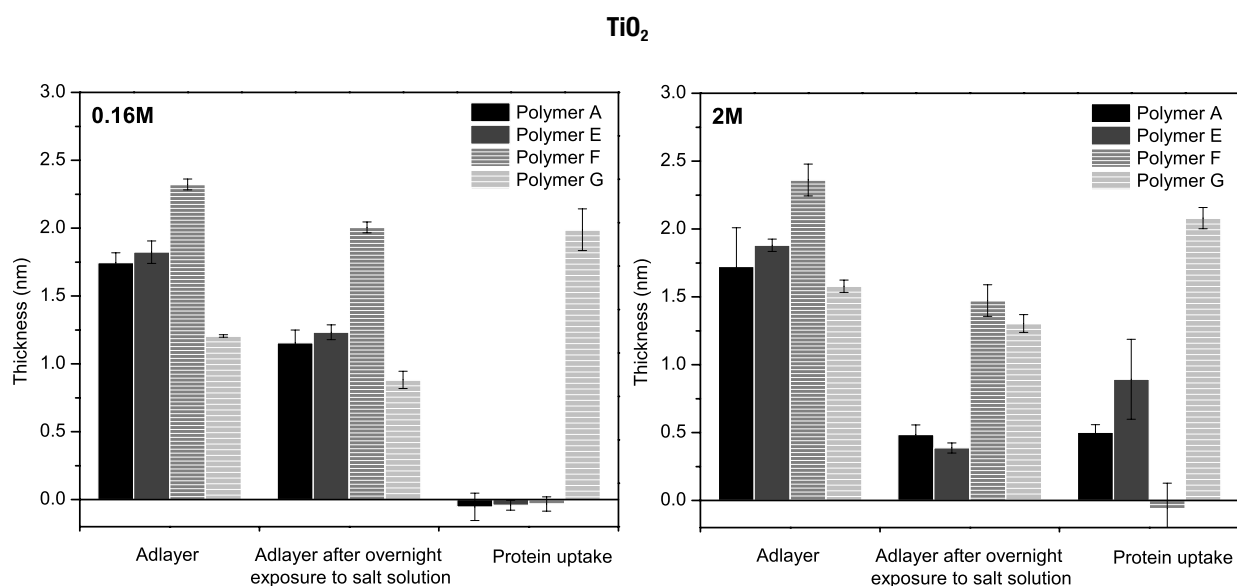


Figure 4.20 Adsorption, stability (exposure to solution) and protein-resistance results on titanium oxide surfaces for four post-modified polymers: polymer A, polymer E, polymer F and polymer G. The graph on the left shows the results of the polymeric coatings when exposed to a low-ionic-strength medium (HEPES II 0.16 M) during the stability test step, while on the right they were exposed to a high-ionic-strength medium (NaCl 2M).

4.3.4.4 Further stability against surfactants and acid and protein resistance assays

Based on the results obtained in the previous section where clearly polymer F revealed to be the most promising combination, as it retains its protein resistance even after exposure to a high-ionic-strength medium, different studies were performed in order to assess its stability and protein resistance under different conditions: (i) a cationic surfactant (CTAB), (ii) an anionic surfactant (SDS) and (iii) an acid solution (pH=2.4) (see section 4.2.9). Polymer A was used as a control.

Stability against surfactants

The effect of surfactants on polymer-adlayer stability was tested, and results can be observed in Figure 4.21 for the cationic CTAB and in Figure 4.22 for the anionic SDS.

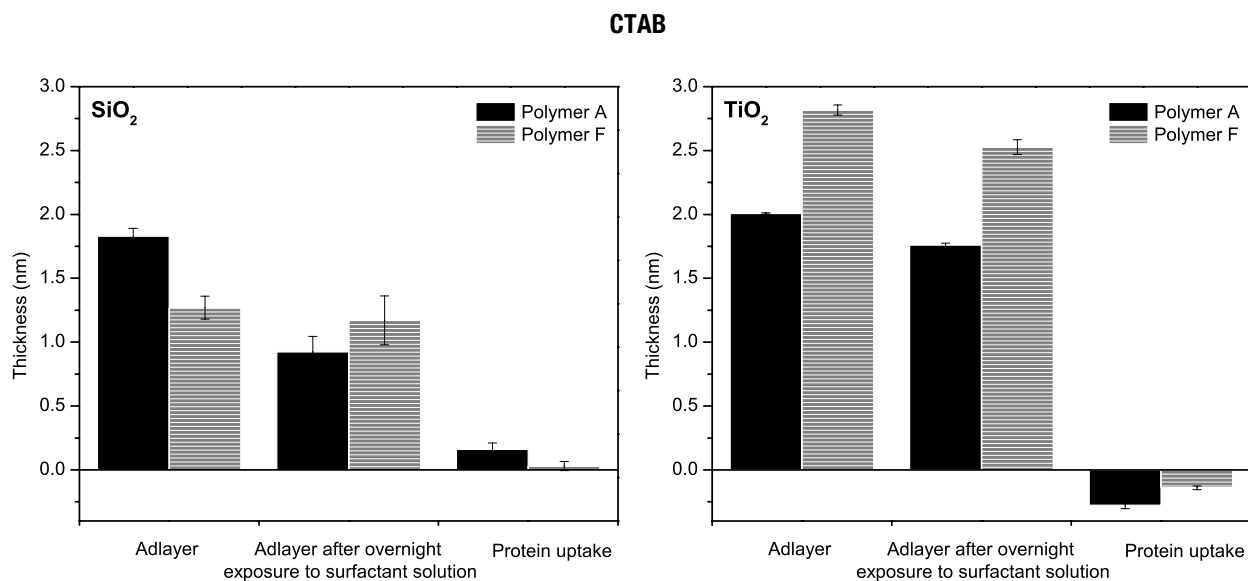


Figure 4.21 Adsorption, stability (exposure to the cationic CTAB surfactant) and protein resistance results of polymer A and polymer F. The graph on the left shows the results on silicon oxide surfaces while the graph on the right shows the data on titanium oxide surfaces.

As can be observed in Figure 4.21, polymer A's exposure to a cationic surfactant (CTAB) has a larger effect on the adlayer on SiO₂ than on TiO₂. In the first case the thickness obtained after the test was below 1 nm, which translated into protein uptake, while in the case of titania the thickness before and after CTAB exposure did not differ much, allowing the coating to maintain its protein resistance. One could state that there is a more relevant adsorption competition between surfactant and polymer in the case of the negatively charged silicon oxide than on titania, which is closer to its isoelectric point under these conditions.

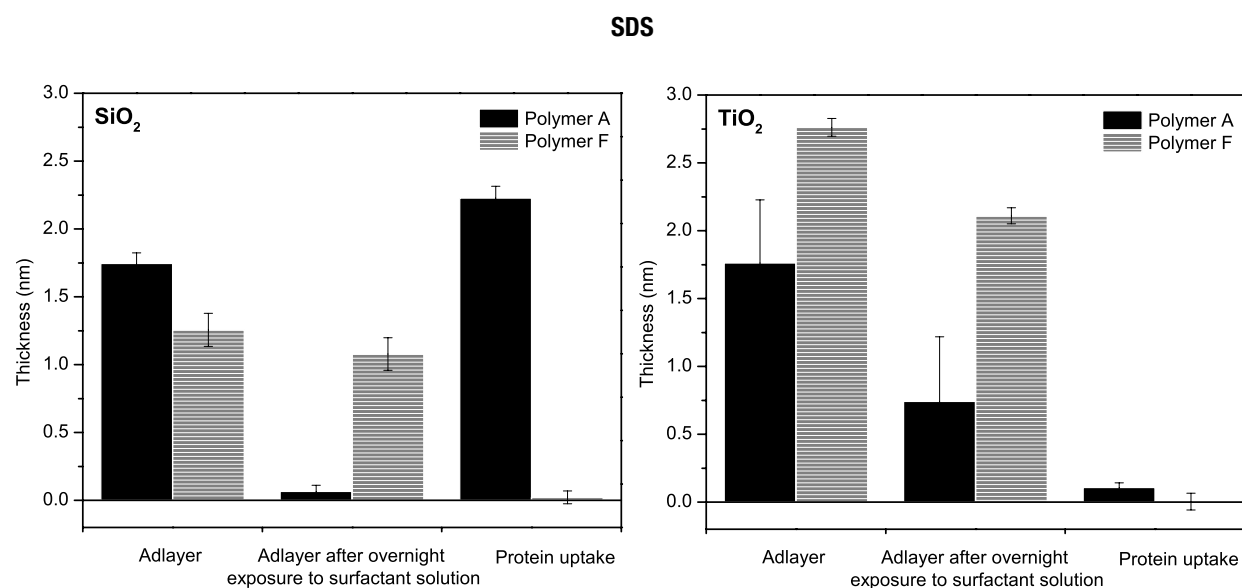


Figure 4.22 Adsorption, stability (exposure to the anionic SDS surfactant) and protein resistance results of polymer A and polymer F. The graph on the left shows the results on silicon oxide surfaces while the graph on the right shows the data on titanium oxide surfaces.

In the case of SDS (see Figure 4.22), polymer A results show a considerable decrease in thickness on both substrates (again more pronounced in the SiO₂ case), which explains the protein uptake. In this case the cationic polymer adlayer is now displaced from the substrate by the anionic surfactant. Although the polymer layer is just bound electrostatically to both metal surfaces, it is clear that in the two cases the layer's structure is more stable on TiO₂ than on SiO₂.

However when polymer F on SiO₂ or TiO₂ are exposed to the two surfactants (see both Figure 4.21 and Figure 4.22), the graphs clearly show that the stability of the polymeric coating is not compromised and it maintains its protein resistance. This is due to the covalent bonds formed (silane on SiO₂, nitrodopamine on TiO₂) which prevent significant polymer desorption from the surface during surfactant exposure.

Stability towards acid

The influence of pH on stability/desorption of polyelectrolytes is a well-known and common assay and results are displayed in Figure 4.23.

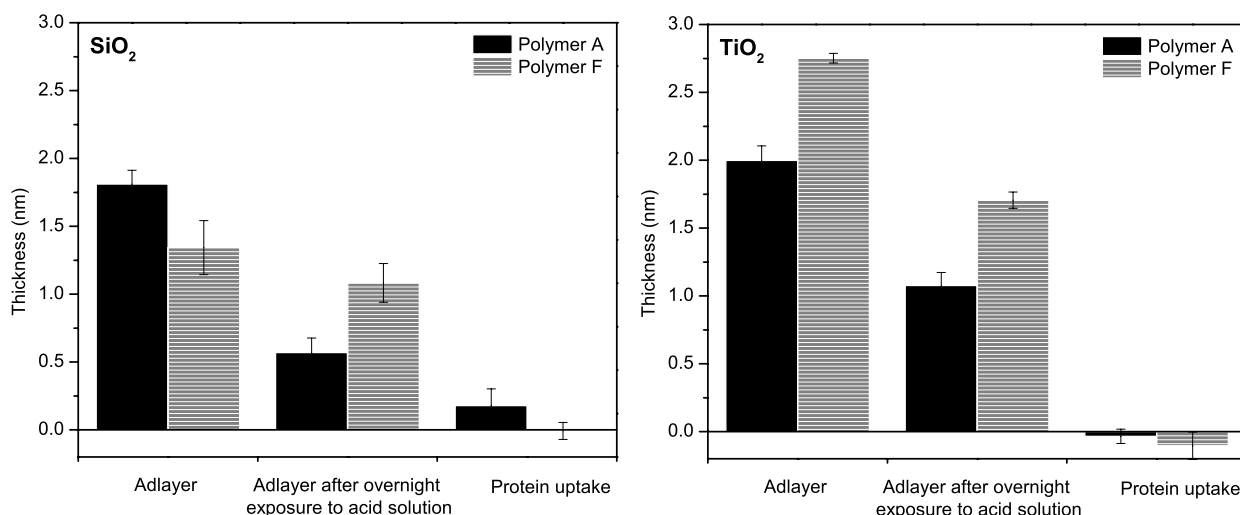


Figure 4.23 Adsorption, stability (exposure to an acidic solution glycine-HCl 10mM-pH=2.4 overnight) and protein resistance results of two post-modified polymers: polymer A and polymer F. The graph on the left shows the results on silicon oxide surfaces while the graph on the right shows the data on titanium oxide surfaces.

The data presented reveal that both polymeric combinations on both substrates suffer a reduction of their absolute thickness after exposure to the acid solution. Nevertheless, the cases where an adlayer of at least 1 nm remains after the stability test, protein resistance is maintained. The latter includes polymer F on both substrates and polymer A on TiO₂, confirming the importance of having a balance between electrostatic and covalent binding to both stabilize and maintain the nonfouling ability of the coating in this particular assay.

4.3.4.5 Crosslinking effect

In order to verify if the stability of the polymer architectures here described could be enhanced by introducing a crosslinker, a new polymeric combination was designed where, always maintaining the same amount of grafted PEG ($d_{\text{PEG}}=0.15$), an equal amount of crosslinker (perfluorophenylazide-NHS) and amine containing groups (1,6-hexanediamine) were added to the reactive backbone. A new postmodified polymer was created with the nomenclature poly(acrylic acid)-*g*-(PEG, 1,6-hexanediamine, N-(6-aminohexyl)-4-azido-2,3,5,6-tetrafluorobenzamide) (2000:116.2:334.2 M_r ;

0.15:0.425:0.425 *d*), or following a simpler nomenclature as polymer L, and its generic structure can be seen in Figure 4.24.

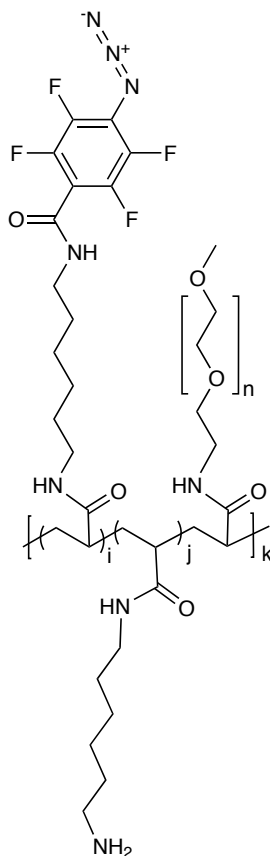


Figure 4.24 Structure of poly(acrylic acid)-*g*-(PEG, 1,6-hexanediamine, N-(6-aminohexyl)-4-azido-2,3,5,6-tetrafluorobenzamide) or polymer L.

Adsorption stability after exposure to a 2M salt solution and protein-resistance results were compared with the equivalent polymer that did not contain any cross-linker (polymer A) and according to the protocols described in the Experimental section of this and the previous chapter, as UV activation of the photochemical molecule is required). The data obtained is shown in the graphs of the Figure 4.25.

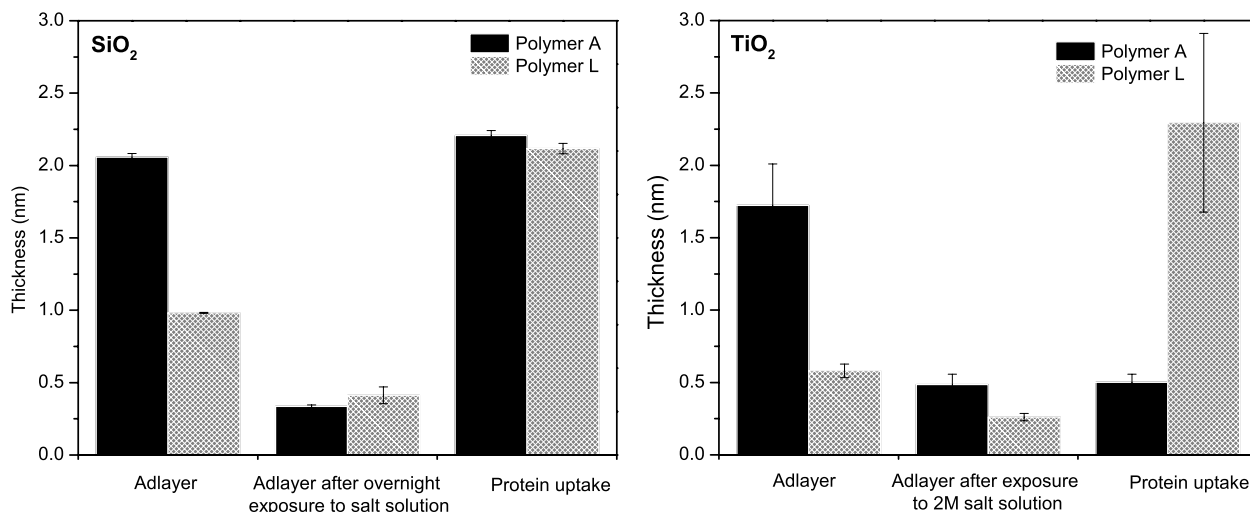


Figure 4.25 Adsorption, stability (exposure to a 2M salt solution) and protein-resistance results of two post-modified polymers: polymer A and polymer L. The graph on the left shows the results on silicon oxide surfaces while the graph on the right shows the data on titanium oxide surfaces.

It is clear that the introduction of a crosslinker does not improve the thickness of the adlayer, stability or protein uptake in either of the substrates. One of the reasons for this behavior might be related to the random nature of the azide binding: upon UV activation, this group decomposes into a nitrene intermediate that inserts preferentially and unspecifically into C-H and N-H bonds in any organic matter that is in its close proximity. This could be either the nonfouling function PEG or the amine binding groups, hence compromising its degrees of freedom to adopt the necessary conformation to perform their purposes. For this reason no further studies were developed regarding the introduction of a crosslinker in this system.

4.3.4.6 *In situ* adsorption studies

QCM-D studies were performed in order to assess if the data obtained for the most promising polymer (polymer F) during static *ex-situ* conditions would follow the same trend *in situ*. Besides the control measurement on a bare silicon oxide crystal, two other polymers were used as controls in a parallel manner: polymer E (surface binding entails 50% electrostatic and 50% quencher) and polymer B (surface binding entails

50% electrostatic and 50% covalent binding to silica via silane). Similarly to ellipsometry, adlayer formation, stability and protein resistance have been measured via QCM-D. Values have been calculated using the Sauerbrey equation (4), which does not take into account the viscoelastic nature of the polymers in the wet mass calculations. This in turn leads to an underestimation, since the signal from the shear wave of the oscillating crystal will be dampened due to viscoelasticity. Since the aim of this study was to look for a similar trend regarding the already shown values with ellipsometry, gross approximations can be used and a comparison between both techniques is shown in Figure 4.26. The raw data, however, can be consulted in section A.6 of the Appendix.

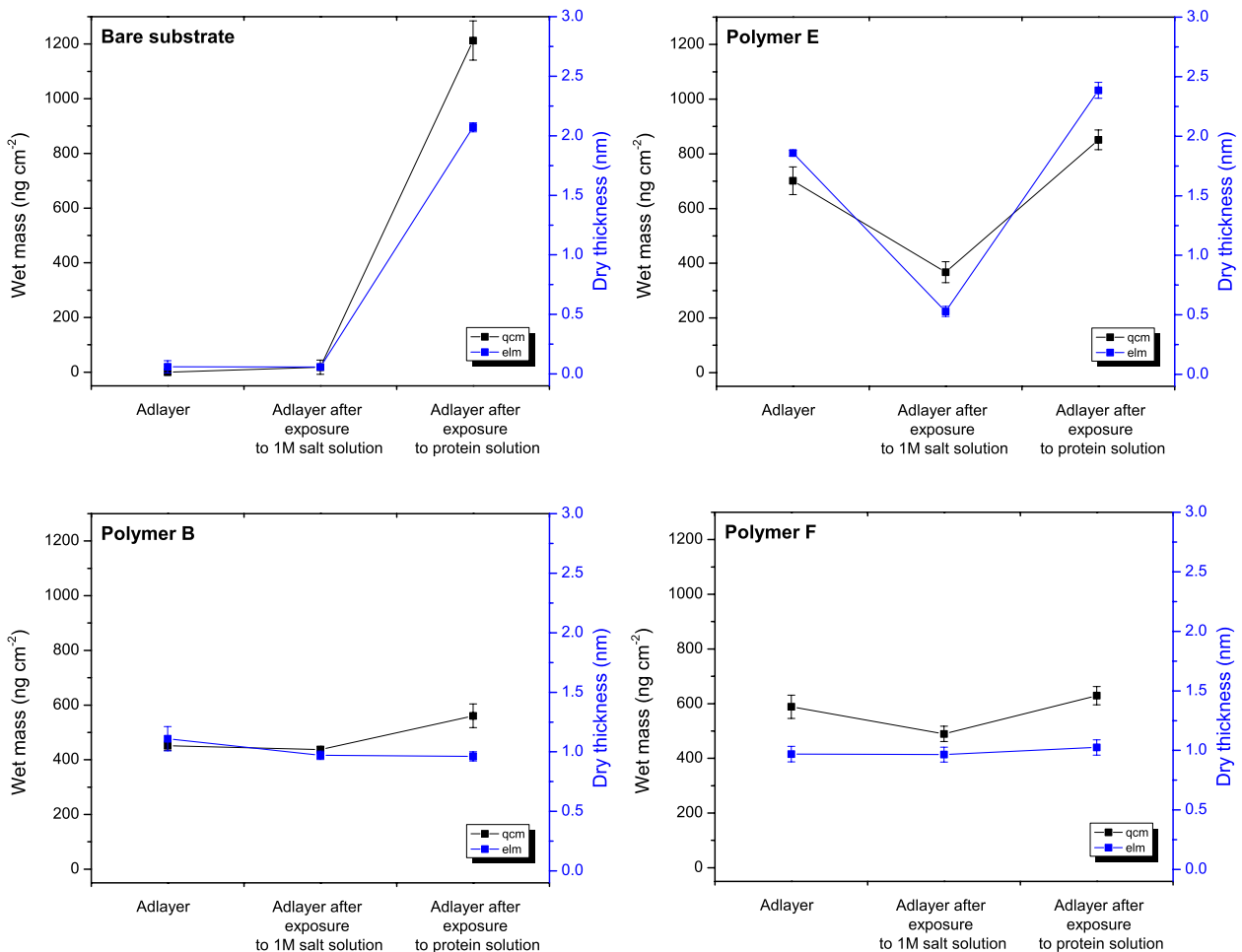


Figure 4.26 Comparison between the data obtained by QCM (black) and ellipsometry (blue) for adsorption, stability (exposure to a 1M salt solution) and protein resistance results on bare crystal (SiO₂) and three postmodified polymers: polymer B, polymer E and polymer F.

Although different quantities are being compared (wet mass and dry thickness), it is clear that in all four cases the trends are quite similar between the techniques.

In the case of the bare silicon oxide crystal, as expected, there is no adsorption in the first two steps of the assays (exposure to the solvent HEPES 0 and salt solution, respectively), which directly translates into protein uptake by high wet mass or thickness values as no nonfouling polymer is present on the surface. In case of polymer E, where only electrostatic forces are responsible for the adlayer formation on the crystal, in both cases there is a considerable loss of polymer upon exposure to salt as this will screen both the polymer and surface charges, causing its desorption. Consequently, assuming then that the PEG's surface density has diminished and/or the surface is partially exposed, an equally high protein uptake is verified when comparing to the values obtained with the bare crystal.

Better results were obtained with both polymer B and polymer F, where a covalent bond to silicon oxide (although in different grafting densities) is present. The biggest difference observed in both cases relates to the QCM results as it appears a slight trend for these two polymers to uptake protein, which is not observed in the ellipsometry results. A possible explanation could be that the polymers' rearrangement after exposure to salt (50% of the surface binding of both polymers is of electrostatic nature) may lead to the incorporation of more solvent molecules within the monolayer, which correlates to an increase of wet mass. Statistically, it is difficult to say which polymer has better protein resistance when adsorbed on silicon oxide, which indicates that having 50% (polymer B) or 25% (polymer F) of the surface binding groups covalently attached does not alter the stability of the monolayer. A possible interpretation is that the latter percentage already can be considered as a minimum threshold necessary for a stable coating under these specific conditions.

4.4 Discussion

A combinatorial polymeric matrix was successfully synthesized by means of postmodification by amidation of active esters. We were able to graft both polymers and

different chemical functionalities that allowed for a thorough investigation regarding the effect that surface binding has on a polymeric coating's performance. The further discussion about the system will be divided in three sections: assessment of the applied synthetic approach, explanation of the adsorption parameters used and analysis of the effect of the surface binding strength.

4.4.1 Synthetic approach for developing a combinatorial polymeric matrix

The synthesis of poly(pentafluorophenyl acrylates) for postmodification purposes is well known, and was primarily developed by Eberhardt *et al.*^{224,229} nearly a decade ago and used as a reference to develop the synthetic protocol reported here. Although these authors used free-radical polymerization, it was in our interest to synthesize the polymeric backbone using a living radical polymerization technique – RAFT - for the reasons already stated before. Bulk characterization techniques as NMR, FT-IR and elemental analysis all proved that the intended structure had indeed been achieved, although the GPC results revealed deviations from the targeted molecular weight and polydispersity indices. Several reasons can account for these results.

Regarding the variations in molecular weight, technically it is known that this type of chromatography, when using calibration standards different from those of the polymeric sample, will give relative molecular weights and not absolute ones. This feature can already account for some disparities between theoretical and experimental molecular weights. However, RAFTs' mechanistic conditions can also heavily contribute to this issue. For instance, it is possible that the core of the trithiocarbonate agent, upon reaching a certain critical degree of polymerization, will be sterically hindered and addition of further propagating chains will be compromised. This will consequently lead to early termination of the latter by combination or disproportionation—a fact that can be supported by the high polydispersity indexes obtained. The CTA-to-initiator ratio could also have affected the variability in our results, as it might have not been high enough. It is overall recommended to have a high number of chains derived from the CTA with respect to the chains resulting from the initiator (sometimes in the order of 10:1) so as to

keep a small amount of active propagating species and minimize potential side reactions involving the initiator. On the other hand, too high a CTA concentration can lead to retardation effects in the early stages of polymerization. This however is a more pronounced effect when using dithiobenzoates than trithiocarbonates as CTAs.

Considering the possibility that we might have used too high a concentration of an initiator characterized by a half-life of 75 minutes in toluene and at 80°C, an initially high polymerization rate is expected. Nonetheless, at long reaction times, such as ours, and considering the addition reactions of the propagating species to the CTA might become slower due to steric hindrance, a higher PDI can be expected as dead chains keep being generated with time. One possibility to investigate the behaviour of the polymerization rate would be to follow the monomer conversion with time by both NMR and GPC, bearing in mind that the RAFT mechanism follows a first order polymerization kinetics (M_n is linearly dependent on conversion). Despite the fact that the ^1H NMR of our synthesized backbone showed no peaks in the 6ppm region (localization of the protons belonging to the acrylate) does not mean we had full conversion. Remaining unreacted monomers or even some oligomers may have stayed in solution while doing the work-up of the polymer. Only an analysis of the reaction solution would be reliable enough to give such information.

All the hypotheses presented up to now assume an efficient chain-transfer process, which directly correlates to the use of a structurally appropriate CTA. Nevertheless, this might have not been the case. A crucial influence in the overall success of RAFT polymerization relies on the choice of chain transfer agent (CTA) used to mediate the polymerization between active and dormant chains (see structural details in section A.5 of the Appendix). In our case a commercially available trithiocarbonate was used (see Figure 4.3) as they are known to give good control over acrylate derivatives and possess good thermal stability.²³⁹ The role of the R (responsible for the fragmentation reactions of the radical adduct formed) and Z groups (responsible for the addition reactions of the radical adduct formed) however might have not been adequate towards our monomer and hence affected the effectiveness and transfer rates of the CTA. Usually R groups can see their fragmentation rate heightened by introducing radical-stabilizing and electron-withdrawing groups. In our case ($-\text{C}(\text{CH}_3)_2\text{CO}_2\text{H}$) there is a formation of a tertiary radical (stable) but there is no electron-withdrawing group

capable of further increasing its reactivity by destabilizing the CTA. Instead of the carboxylic acid, possibly a $-\text{CF}_3$ or $-\text{CN}$ group might increase the fragmentation rate of the R group. Regarding the Z group, it should activate the $\text{S}=\text{C}$ bond but also stabilize the adduct radical. Too much stabilization, however, can lead to slow fragmentation resulting in rate retardation. Our Z group ($-\text{S}-(\text{CH}_2)_{11}-\text{CH}_3$), in trithiocarbonate CTAs, is generally known to increase the addition rates (S-alkyl) as it does not over stabilize the radical.

Regarding the postmodification reactions, surface performance indicated that the order of addition of the side chains plays a role in the composition of the polymers. Although the attempt to quantify the postmodified polymers was not successful, the results showed no measurable difference between distinctive lots of the same polymer synthesized according to the same protocol (i.e. same order of addition). In order to quantitatively understand the postmodification reaction, one has to determine the differences between theoretical and experimental grafting densities. ^1H NMR at 300 MHz resulted in broad peaks that were difficult to analyse, which prevented us from performing such calculations. Future experiments using a higher frequency NMR or completely different techniques, such as XPS or UV for nitrodopamine detection, for example, may help to reach this goal.

4.4.2 Adsorption parameters

As one could point out, studies regarding the effect that ionic strength, temperature, pH, concentration or even incubation time, have on polymer adsorption could have been performed in order to better understand how to optimize the adsorption process. However, since we are investigating surface binding using several chemistries simultaneously, this would have not been a straightforward study. Instead, it was decided to use a very low ionic strength medium (HEPES 0 – 1 mM) for incubation, as we wanted to explore the role of electrostatic interactions between coating and substrate. As one could expect, by increasing ionic strength, the length of the double layer at surface decreases (Debye length) and charge screening takes place.²⁴⁰ Because of that, certain polymeric combinations (e.g. Polymer A or Polymer E) would be expected to display compromised adsorption. Regarding pH, it was in our interest to

maintain it at a physiological level, since we would be able to keep the charges present both in the amines and substrates and also simplify the adsorption method towards possible industrialization. Yet, this could have been an interesting study as silanes are known to hydrolyse quickly under acidic conditions, minimizing self-condensation reactions.¹⁶⁰ Comparing this with an adsorption at neutral pH could let us know if a silane containing polymer had already reached full hydrolysis and adsorption conformation (due to self-condensation reactions) during dialysis and, in case it hadn't, whether the full presence of silanols influenced the adsorption kinetics. Considering phosphonates, these are better known to increase their titanium oxide affinity by decreasing pH, as they become protonated allowing for the binding mechanism to take place and charge repulsion between both the negatively charged polymer and surface is no longer an issue.¹⁹⁹ Although their solubility would also decrease, the presence of PEG grafted chains, in our polymeric design, would account for this potential issue not to occur. For nitrodopamine, more specifically mPEG(5000)-nitrodopamine, it has been observed that a maximum thickness is obtained when pH is closer to both the isoelectric point of titanium oxide (~6) and the pKa (6.31) of nitrodopamine, as an optimal binding equilibrium is reached.¹⁷⁵ A temperature influence on adsorption kinetics could also be interesting to study as both rate of mass transfer (diffusion coefficient) and segmental motion are dependent of this parameter.^{241,242} However, besides potentially increasing the rate of adsorption of our polymers, varying the temperature parameter could again limit the applications of the developed coatings, which was not in our interest. This brings us to the incubation time factor. *Ex-situ* measurements continued overnight but when interpreting the *in situ* raw data obtained by QCM-D (see section A.6 of the Appendix), full mass was adsorbed on the surfaces in only a few minutes, indicating that the rate of adsorption at the polymer concentration used is quite fast. This is most probably again an effect of the long-range electrostatic interactions from the positive amine groups in the polymer.

4.4.3 Influence of surface binding on stability and protein resistance response

In order to understand if the strength of the surface binding can influence, in this case, the performance of nonfouling coatings, we postmodified several polymers and introduced different chemical functionalities that bind in a distinctive way to two model surfaces – SiO₂ and TiO₂. After adsorption, these manufactured coatings were subjected to stability and protein resistance assays.

The results suggests some interesting observations in respect to the initial thicknesses obtained. For instance, the control polymers A and E, which varied in the amount of positive charges, had quite similar thickness results. This indicates that the lower grafting density here represented by polymer E, but also by all other two-foot types polymers, is sufficient for an effective electrostatic binding.

Differences in the initial adlayer formation were observed when comparing a polymer with 50% of electrostatic and 50% of a covalent surface binding groups and the polymer with just the same covalent surface binding groups. For the nitrodopamine-containing polymers C and I, thicker layers were found for the former polymer, which contained an electrostatic binding component (~2.5 nm and ~1.4 nm, respectively). The same trend was observed with the phosphonate containing polymers D and J although not so pronounced (~1.7 nm and the latter ~1.2 nm). These differences should be related to different adsorption conformations of the polymers due to the presence of charged monomers. The fact that higher thicknesses are obtained in the latter case suggests a further stretching of the PEG chains, which can indicate that a denser packing was achieved and/or a different type of surface packing might be involved.

Table 4.8 PEG surface density values

		PEG surface density σ (chains nm ⁻²)	
		SiO ₂	TiO ₂
Controls	Polymer A	0.55	0.55
	Polymer E	0.59	0.58
Nitrodopamine containing polymers	Polymer C	-	0.73
	Polymer I	-	0.29
Phosphonate containing polymers	Polymer D	-	0.27
	Polymer J	-	0.14
Silane containing polymers	Polymer B	0.44	-
	Polymer H	0.62	-
Multi-covalent binding polymers	Polymer F	0.35	0.67
	Polymer G	0.02	0.32

By calculating the PEG surface density of each of the polymers in question (see Table 4.8) one can observe that indeed a more packed regime is found when positively charged amines are present in the backbone, although the difference is more pronounced in the nitrodopamine case than in the phosphonate. Considering that at the incubation pH each one of these entities possess one negatively charged oxygen (as their pK_as are below 7.4) randomly surrounded by amines' positive charge, we hypothesize that this will create in solution a more compact polymer structure than its linear stretched conformation due to charge attraction. This new way of packing, still in the brush regime, will allow for a higher amount of adsorbed polymer leading to a consequent stretching, and consequent thickness increase. The fact that this was not observed in the silane containing polymers B and H further supports our theory, since no negative charge is present in the backbone of those polymers. In fact the opposite trend occurred, as they were 1.2 and 2.5 nm thick, respectively. In case of polymer H, which did not possess any positively charged amines, a few possibilities can account for such thickness as it can be in a type of loop-train-tail system and/or some crosslinking

(intra- or intermolecular) might have occurred in case hydrolysis of the silanes was not complete during dialysis and self-condensation reactions took place. As for polymer F, the initial adlayers were considerably higher on TiO₂ than on SiO₂ (2.3 nm and ~ 1.2 nm, respectively), which translated into a denser packing according to Table 4.8. Although this correlation between thickness and surface density also corroborates our hypothesis, it gives further information regarding the importance of covalent binding. In the SiO₂ case, although a more compact polymer conformation might still be generated in solution due to the presence of opposite charges between monomers, since the nitrodopamine will not covalently bind to SiO₂ and furthermore contains negative charges that are repelled from the substrate, this will compromise the retention of that conformation upon adsorption. It is less packed but not so critically as to compromise its nonfouling abilities. This does not happen on TiO₂, as the nitrodopamine will bind covalently to the surface as soon as it is driven towards it.

One question that may arise from this proposed hypothesis is why in the case of polymer C and D, which have a theoretically zero net charge, adsorption is still possible. There are two possible explanations. One relates to the probability for the polymers to rearrange themselves in a way that the charges would be cancelled out and no longer be available to drive the polymer to the surface. This is very unlikely probably due to the stiffness of the alkyl chain present in the backbone and/or steric hindrance. The fact we have a random polymer also contributes to the lack of knowledge on how these charges are distributed along the backbone, which leads us to the other potential explanation: the pK_a values. The values obtained were measured for the single molecules not grafted to a polymer: pK_{a1} of nitrodopamine is 6.3 and for the dodecylphosphonate pK_{a1} ~2. Once both these groups are added to the backbone they can or not be surrounded by the positive charges of the amines, which affects differently the acidity of the hydroxyl protons. This is one of the reasons why quite often there is not a sharp transition in acid/base titration curves of polyelectrolytes but rather a gradual one is observed.²⁴³

Additionally, to further confirm we indeed had a more compact surface packing than the one obtained by grafting the model molecule, PLL-*g*-PEG, we decided to compare the surface density of (EG) units we manage to achieve on the surface with

respect to the ones achieved by grafting ultradense PLL-*g*-PEG(5) under the cloud-point method⁴⁹. Results are shown in Table 4.9 and Table 4.10.

Table 4.9 EG surface density (σ) of the postmodified polymers based on the initial adsorbed layer.

	EG surface density σ (units nm ⁻²)	
	SiO ₂	TiO ₂
Polymer A	25.09	25.19
Polymer B	20.14	-
Polymer C	-	33.20
Polymer D	-	12.19
Polymer E	26.60	26.34
Polymer F	15.92	30.33
Polymer G	0.89	14.56
Polymer H	28.09	-
Polymer I	-	13.37
Polymer J	-	6.43

Table 4.10 EG surface density (σ) of PLL-*g*-PEG(5) grafted at different temperatures.⁴⁹

PLL- <i>g</i> -PEG(5) on TiO ₂	
Temperature (°C)	EG surface density σ (units nm ⁻²)
20	15.91
40	18.18
60	43.18
80	55.68

As it can be observed quite consistently we reached an EG surface density that is found in between PLL-*g*-PEG(5) grafted between 40 and 60°C on TiO₂. Exceptions are:

- polymer D and J on TiO₂, which presented some solubility issues when postmodifying with the phosphonate group that could have compromised the ideal adsorption parameters;
- polymer F on SiO₂, most likely due to the charge repulsion between negative charges (nitrodopamine and substrate), which compromises the amount of polymer adsorbed;

- polymer G as it does not have the positively charged groups that act as a driving force for adsorption, again conditioning the amount of polymer that is actually adsorbed on the surfaces.

Regarding the stability and protein resistance of the synthesized polymers it was clear that the presence of an opposite charge to the substrate in their structures, besides acting as a strong driving force for adsorption, also allows for a brush-like conformation to be adopted upon adsorption, which is key to prevent protein uptake. However, the nature of this reversible binding can compromise the stability of the coating as an increase in ionic strength promotes charge screening between polymer and substrate, which leads to desorption. This can easily be seen in the QCM-D raw data of polymer E (see Figure A 5 in section A.6 of the Appendix), which was only bound electrostatically to the sensor, by a mass decrease upon exposing the coating to a 1M NaCl solution. However, if a polymer is partially covalently bound to the surface this desorption from the electrostatic groups is now reversible as no considerable mass loss was observed in the cases of polymer B and F (see Figure A 4 and Figure A 6 in section A.6 of the Appendix). This does not entirely match the ellipsometry values at high ionic strength medium (2M NaCl) as a thickness decrease was observed for these two polymers. Possible justifications for this difference between techniques are the fact that the salt solutions had different ionic strengths (higher for the ellipsometry assays) and the exposure times were also different: in the range of minutes for QCM and in the range of hours for ellipsometry. Nevertheless, if the polymer adlayer after exposure to salt solutions is at least 1 nm thick and it contains both electrostatic and covalent surface binding groups, sufficient surface density of PEG is present in the right conformation to maintain protein resistance. This was a common result throughout all adsorbed polymers.

4.5 Conclusions

In summary, with the results presented in this chapter we managed to prove that the key active-ester containing polymeric backbone PFPAc has been successfully

synthesized, characterized and postmodified with different chemical functionalities. Although the surface binding groups' grafting densities may have not been possible to determine, the reproducibility of the synthetic procedure allowed for the achievement of highly reproducible surface performances. The adsorption, stability and nonspecific protein resistance behaviours of the synthesized polymers were well predicted by the rationales used for developing their chemical design. Briefly, the combinations that contained positively charged groups were rapidly adsorbed on the surfaces in such a conformation that would allow for a brush type regime to be adopted. To increase their stability under high ionic strength medium, groups that bind covalently to the model surfaces used were added, which prevented the irreversible desorption of the electrostatically bound groups while still retaining their nonfouling abilities. This additional feature also allowed for a denser packing to be formed on the surfaces under mild conditions (room temperature, physiological pH and low ionic strength), provided these groups contained partially negatively charged monomers. By adding groups that targeted different chemistries, a multimodal binding polymer was obtained (polymer F) that still kept its surface functionality under various harsh conditions: low and high ionic strength media, exposure to acid and both cationic and anionic surfactants.

Chapter 5

Conclusions and Outlook

5 Conclusions and Outlook

The work presented in this thesis had two main aims. The first was to develop a platform that would allow comparison of the nonfouling properties of different hydrophilic uncharged polymers under similar conditions. The second was to design a generic and simple synthetic procedure that would allow the introduction of several different chemical functionalities into a single polymeric backbone. The motivation was to study the effect that the nature of surface binding has on the stability of a polymeric coating and simultaneously to develop a multifunctional polymer that would attach to several key model substrates.

Regarding the first aim, which is presented in Chapter 3, to develop such a versatile platform we used a cationic adhesion promoter, which would bind electrostatically to a negatively charged substrate, grafted with a photochemical group that upon activation results in covalent linkages to be formed with the closest organic molecule. This adhesion promoter, poly(allylamine)-*graft*-perfluorophenylazide (PAAm-*g*-PFPA), due to intramolecular segmental-charge repulsion, would be adsorbed in a stretched conformation allowing for the perfluorophenylazides to be positioned upwards. Upon spincoating a solution of a nonfouling hydrophilic uncharged polymer on top of the adhesion promoter and activation of the azides with UV light, insertion reactions would take place between these two layers. The linkage of the polymer was proven with a variety of surface-sensitive techniques. Ellipsometry showed dry thickness increase not only upon adhesion of PAAm-*g*-PFPA onto silicon oxide substrates but also after photochemically linking the functional polymers (PEG, PEOXA, low and high molecular weight PVP, PVA and dextran). Dynamic contact-angle measurements showed a transition from a hydrophilic substrate to a more hydrophobic one, upon functionalizing it with PAAm-*g*-PFPA, as the hydroxylated substrate is now covered with perfluorophenylazide groups, and a lowering of contact angles upon the successful attachment of the hydrophilic polymers. XPS data also chemically confirmed the different stages of surface functionalization. Silicon and oxygen peaks were found in the

bare substrate, which, after the monolayer adhesion of PAAm-*g*-PFPA, showed the presence of additional peaks of fluorine, nitrogen and carbon. Calculations from the F/N ratio indicated that the effective grafting ratio of PFPA on the PAAm backbone was 9.0 (1 unit PFPA per each 9 units of PAAm). This differs from the stoichiometric targeted value of 4. Reasons that account for such difference can be attributed to the strong deviation found in an increased oxygen content of the adhesion promoter, which would then decrease the atomic contents of the other elements, but it is also possible that the grafting reaction of PFPA to the PAAm backbone did not react stoichiometrically as expected. In order to assess which was the cause of the difference between theoretical and experimental grafting ratios, one could deposit a thick layer of the adhesion promoter (e.g. by spin coating) on a substrate that did not possess any chemical similarity, let it dry and measure chemical composition. In any case, this higher grafting ratio still allowed for the attachment of several nonfouling polymers—an increase in content of the expected elements was verified in all cases.

Considering the unspecific nature of the multiple binding between the adhesion promoter and the nonfouling polymers, the most probable conformation obtained in all cases was that of a loop-train-tail model. By simplifying our calculations to just the presence of loops, we found that $L_{id}/2R_c$ values (where L_{id} is the distance between chains of grafted polymer and R_c is the radius of the coil) could reach the typical limiting values of a brush regime (<0.5), particularly in the cases of high-molecular-weight polymers (PVP 1300 kDa and dextran 2000 kDa). This ratio can be interpreted as an equivalent of $L/2R_g$ for end-tethered polymer chains, as it is easy to conceive that by increasing the surface density of loops their stretching will also occur after an osmotic/elastic equilibrium is reached. Furthermore, although the lower-molecular-weight polymers were found to be below the condition for the loop-brush regime, one has to consider these calculations were performed based on dry thicknesses. Upon exposure to a good solvent it is expected that the loops will expand, increasing their R_c and hence lowering the overall $L_{id}/2R_c$.

Almost all hydrophilic uncharged polymers showed improved nonfouling properties compared to the bare substrate when exposed to a complex protein solution, marine bacteria or algae. The exception was for dextran-functionalized surfaces, when they were tested against the marine bacteria *M. hydrocarbonoclasticus*. Indeed, it was

found that this bacterium possesses an enzyme that reduces the sugar to wax esters. This enzyme is often found in extracellular polymeric substances (EPS) secreted by bacteria during the adhesion process.

Overall it was found that hydroxylated chemistries showed a better nonspecific protein resistance and lower *C. marina* settlement than the nitrogen-containing ones, most likely due to a higher ability to generate hydrated adlayers. As stated in section 1.1, surface hydration is key when preventing non-specific protein uptake, but our results also indicate that mechanical stiffness may play a role, as the high-molecular-weight PVP was found to resist uptake more efficiently than low-molecular-weight polymer. However, when our surfaces were exposed to the other marine fouling species, results were not straightforward. For *Ulva linza*, PEG registered the highest settlement among all surfaces functionalized with nonfouling polymers, and, as stated previously, for *M. hydrocarbonoclasticus* dextran did not render any nonfouling ability to the surface. Similarly to the potential explanation given for the latter event, PEG's lack of resistance may be correlated to the adhesives secreted by the *Ulva linza*. Although PVP 55 kDa did not show the lowest resistance in any of the bioassays made, it was the only that presented consistent low values in all tests. The only safe assumption to make based on all these findings is that, besides the importance of surface hydration, minimizing biofouling through chemical conditioning is highly dependent on the species tested.

The work accomplished in Chapter 3 proved that indeed we had developed a versatile platform that allows for surface modification using a variety of hydrophilic uncharged polymers. The coatings manufactured proved to be stable and appropriate for their use in short-term biofouling assessment assays. Further use of this platform within this topic would allow for complementary studies regarding the influence of chemistry (e.g. hydrophilic uncharged vs. zwitterionic polymers), chain length (e.g. different molecular weights of the same polymer), elasticity (e.g. varying the grafting ratio of perfluorophenylazide in order to induce more attachment points), and surface charge (e.g. uncharged dextran, cationic chitosan and anionic hyaluronan) in preventing biofouling.

However this platform is not limited to this particular study, as it has already been used to produce two-component polymer (hydrophobic and hydrophilic) concentration gradients,¹³⁴ to prepare chemical micropatterns for cell confinement,²⁴⁴ to perform studies regarding the difference between the lubricating properties of a grafting-to and grafting-from lubricious polymer¹⁰² and to study the impact of polymer architecture (loop-train-tail vs. brush) on the lubricity of a polysaccharide coated surface.²⁴⁵ It has also been verified that this platform can be used to functionalize polymeric coatings as the perfluorophenylazide is no longer just in an upward position and can simultaneously covalently bind to another polymer.^{246,247}

Considering that the only limitations of using this platform are:

- the nature of the functionalizing adlayer must be polymeric;
- the testing parameters do not include harsh conditions to the chemical integrity of the coating (e.g. in case of PAAm-*g*-PFPA, exposure to a high-ionic-strength medium that would allow for the adhesion promoter's desorption); it can be used in a wide range of applications involving surface modification at the nanoscale, as the nonspecificity of nitrene-binding chemistry conceptually allows for any polymer to be grafted to this adhesion promoter.

As for the second part of this project, which is presented in Chapter 4, an easy-to-postmodify polymeric backbone was synthesized, in order to graft different chemistries into it. The design of the studied postmodified polymers is presented in Table 4.1 of Chapter 4 and obeyed the following premises:

- fixed stoichiometric grafting density of a nonfouling polymer ($d_{\text{PEG}}=0.15$);
- stoichiometric grafting of silicon oxide targeting chemistry at varying densities ($0.2125 < d_{\text{silane}} < 0.85$);
- stoichiometric grafting of titanium oxide targeting chemistry at varying densities ($0.2125 < d_{\text{nitrodopamine}} < 0.85$ and $0.425 < d_{\text{phosphonate}} < 0.85$);
- stoichiometric grafting of negatively charged substrates targeting chemistry at varying densities ($0.425 < d_{\text{amine}} < 0.85$).

Sets of conditions were developed to allow a thorough study of the binding effect on a polymer's stability. Although further optimization needs to be done regarding the synthetic procedures, either polymerization or postmodification related, different polymers were synthesized, as their adsorption behaviour could be easily explained based on the chemistries involved in the correspondent postmodification procedures and on the substrates used (silicon and titanium oxides). In sum, all polymers containing positively charged amines were adsorbed onto the negatively charged surfaces in a stretched type of conformation. The polymers that did not contain this type of binding contribution, although adsorbed on the expected surfaces, did not show any protein resistance, most likely because they were not adsorbed in a stretched fashion, but more like a coil. This inhibits the stretching of the PEG polymer chains in a brush-like conformation—a key feature for the resulting coating to resist nonspecific protein uptake.

As for the remaining polymeric combinations, in addition to the mandatory presence of electrostatic binding, also a presence of a covalent or coordinative bond greatly enhanced their stability towards high-ionic-strength medium (NaCl 2M). This feature limited the irreversible desorption from the electrostatic component, allowing the coatings to maintain their conformation and protein resistance after exposure to such harsh conditions. The only exception was the amine and phosphonate-containing polymer (polymer D), which may have had some synthetic issues, as indicated by the yields superior to 100%. For all these reasons, a polymer with an anchor combination containing electrostatic binding to both substrates (amine), covalent binding to silicon oxide (silane) and coordinative binding to titanium oxide (nitrodopamine) was postmodified. Data showed that this combination resulted in an ultrastable coating that, upon exposure to high-ionic-strength medium, surfactants and acidic solution, still maintained its protein resistance on both substrates. This confirmed that by using this postmodification strategy we could easily synthesize polymers with an ability to simultaneously attach to different substrates. Preliminary tests showed that the polymers having the binding groups hexanediamine (polymer A), hexanediamine and silane (polymer B), hexanediamine and nitrodopamine (polymer C) and a combination of the three (polymer F) also adsorbed on gold substrates, most likely due to hydrophobic interactions with hexanediamine, or through weak coordination of the

aminogroups to gold.²⁴⁸ It also resisted exposure to high-ionic-strength. Furthermore, inspired by the results obtained in Chapter 3, we decided to further postmodify polymer A with the photoactive molecule perfluorophenylazide (see Figure 4.24) in order to verify if increased stability would be observed. Results did not confirm this rationale. This might be caused by the random type of nitrene binding, which could easily have linked to the anchor or PEG moieties thus compromising the brush conformation of the coating. Another possibility is that the grafting ratio targeted was too high ($d_{\text{perfluorophenylazide}}=0.425$) and, drawing a parallel with PAAm-*g*-PFPA, only a small degree of crosslinking is actually needed. Bearing this in mind, determination of an optimal grafting density of perfluorophenylazide would be of interest. Yet another possible application of this modified polymer, besides induced stability, is its potential use on polymeric substrates. Preliminary tests have showed that the same polymeric combination, though with a lower grafting density of the photochemical group ($d_{\text{perfluorophenylazide}}=0.2125$), was able to attach on polyethylene substrates and maintain its protein resistance even after exposure to a 2M salt solution.

The postmodification possibilities of the PFPAc backbone according to our protocol are wide and only require the existence of an amine group. We postulate that besides the nonfouling function of PEG, one could graft other polymers (that are nonfouling, end or side functionalized with groups of biotin), fluorescence markers, single-stranded DNA fragments or antibodies (to develop instrumental biosensors), or even hydrophobic polymers such as poly(dimethylsiloxane), perfluoroethers or perfluoroalkyls (as low-surface-energy coatings or lubricant additives). Besides altering the functional component of the coating, it is safe to assume, as far as anchors are concerned, that the combinations tailored to titanium oxide could easily be extrapolated to oxides of tantalum (Ta_2O_5), niobium (Nb_2O_5) and zirconium (ZrO_2) as they are characterized by similar reactivities with respect to titanium oxide.²⁴⁹

Furthermore, we have proven to achieve denser packing when both negatively and positively charged monomers are present in our backbone. This causes a relative compression of the polymer in solution, due to charge attraction, which is directly translated into a denser adsorption. EG surface density values were calculated and compared with those obtained with PLL-*g*-PEG adsorption under cloud-point grafting conditions on titanium oxide substrates. Results indicated that the density reached with

our polymer when adsorbed at room temperature was found to be between the EG surface density obtained when grafting PLL-*g*-PEG between 40 and 60°C.

Overall, both topics developed throughout this thesis show the advantages and versatility associated to postmodification reactions of polymers, either by crosslinking or nucleophilic substitution. We have proven that a loop-train-tail conformational system could easily match the classical end-tethered approach of polymer chains in order to obtain brush conformations and consequent protein resistance, but also that a clever polymer design can lead to enhanced performance.

Appendix

Appendix

A.1 Characterization Techniques experimental details

The current section provides details on the experimental conditions employed for each characterization technique used in this thesis. At the end of each paragraph, literature is recommended in order to better understand the theoretical principles behind each method.

Bulk Characterization Techniques

Nuclear Magnetic Resonance (NMR)

NMR experiments were performed with Bruker 300 and 500 MHz spectrometers (Bruker Corporation, Billerica, MA, U.S.A.). For sample preparation the deuterated solvents CDCl_3 and D_2O were used and specified in the related spectra.²⁵⁰⁻²⁵²

Gel Permeation Chromatography (GPC)

GPC measurements were performed by Polymer Standards Service GmbH (Mainz, Germany) using a PG04 instrument. Determination of M_w of polymers was performed by using PSS columns with a pore size from 10^2 - 10^5 Å and calibrated with poly(methyl methacrylate) standards. The detection system contained a differential refractive index detector where THF was used as an eluent at 23°C, with a flow rate of 1.0 mL/min and with a 3 g/L polymer sample concentration. Data were analyzed with PSS-WinGPC UniChrom Version 8.0 software.²⁵³

Elemental Analysis (EA)

Elemental analysis measurements were performed by the Micro-Laboratory of the Laboratory for Organic Chemistry at ETH Zurich. For determination of the C, H, N and O ratios, LECO machines were used. The first three elements were analysed by a combustion method where the products (CO_2 , H_2O and NO) are trapped and weighed and the latter by the difference between the total mass and the mass associated with the remaining analysed elements. For the determination of fluorine, the Schöniger oxidation method was applied followed by quantification via ion chromatography and for the analysis of phosphorous, an ICP-AES device (Perkin-Elmer and Thermo-Jarrel) was used and additionally quantified photometrically (as a colored complex) after digestion in a pressure-digestion device.²⁵⁴

Fourier Transform – Infrared Spectroscopy (FT-IR)

Data was obtained by measuring polymeric samples in the solid state (KBr pellet) and in transmission mode on a Bruker IFS 66v FTIR spectrometer (DGTS-KBr detector). Spectra were obtained under vacuum (< 2 mbar) in the spectral range of 400-4000 cm^{-1} at a resolution of 2 cm^{-1} and 128 scans. Data was both acquired and analyzed with OPUS software.²⁵⁵

Surface-Characterization techniques

Variable Angle Spectroscopic Ellipsometry (VASE)

Dry thickness measurements were performed using a M-2000F variable-angle spectroscopic ellipsometer from J. A. Woollam Co (Lincoln, NE, USA). All data presented here were recorded at a wavelength range from 370 to 1000 nm using focusing lenses at 70° from the surface normal. Data were analyzed with WVASE32 software using a three-layer (Si/SiO₂/Cauchy; $A_n = 1.45$ and $B_n = 0.01$, $C_n = 0$) or a four-layer model (Si/SiO₂/TiO₂/Cauchy; $A_n = 1.45$ and $B_n = 0.01$, $C_n = 0$), depending on the substrate used. All measurements were performed under ambient conditions.^{256,257}

Dynamic Contact Angle (dCA)

Surface-wettability measurements were performed by measuring advancing and receding contact angles with ultrapure water (6 μL) in a G2/G40 2.05-D from Krüss GmbH (Germany). Data were analyzed according to the tangent method 2 with DSA 3 Version 1.72 software from the latter company.^{258,259}

X-Ray Photoelectron Spectroscopy (XPS)

All spectra were recorded using a PHI5000 Versa probe (ULVAC-PHI, INC., Chigasaki, Japan). The spectrometer is equipped with a 180° spherical-capacitor energy analyzer and a multichannel detection system with 16 channels. Spectra were acquired at a base pressure of 5×10^{-8} Pa using a focused, scanning monochromatic Al K α source (1486.6 eV) with a spot size of 200 μm and 47.6 W power. The instrument was run in the FAT analyzer mode with electrons emitted at 45° to the surface normal. Pass energies used for survey scans was 187.85 and for the detailed spectra either 23.50 eV or 46.95 eV (the latter in case of angle resolved). The full width at half-maximum (FWHM) of this setup is <0.8 eV for Ag $3d_{5/2}$ for the latter pass energy.

Angle-resolved measurements were performed at three different take-off angles, specifically 15° , 45° and 65° , with respect to the surface normal.

The XPS spectra were evaluated using CasaXPS (version 2.3.12 and later). All binding energies are referenced relative to the hydrocarbon peak (from residual contamination in the case of the “clean” surfaces, or the $-\text{CH}_2-\text{CH}_2-\text{CH}_2-$ contribution of the polymers), set at a binding energy (BE) of 285.0 eV.

Normalized atomic percent (atom.%) concentrations were calculated from the detail spectra of each element present on the surface, corrected by the appropriate relative sensitivity factors (RSFs), the asymmetry parameter,²⁶⁰ the transmission function of the spectrometer, and inelastic mean free paths (IMFPs). The photoionization cross sections are normalized to C 1s according to Scofield,²⁶¹ except for Si 2p, where an experimentally determined factor of 1.06 was used, measured on a clean SiO_2 quartz reference material. This value is higher than the tabulated value from Scofield (0.817) and results in a better SiO_2 stoichiometry.²⁶²⁻²⁶⁵

Quartz Crystal Microbalance with Dissipation (QCM-D)

QCM-D measurements were recorded on a QCM-D E4 instrument and software from Q-Sense AB (Sweden). AT-cut polished crystals with a fundamental resonance of 5 MHz and SiO₂ coated were used (LOT-Oriel AG) and oscillated in shear mode. QCM-D data, Δf and ΔD , were acquired at 6 overtones ($i = 3, 5, 7, 9, 11$ and 13 , corresponding to resonance frequencies of $f_i \approx 15, 25, 35, 45, 55$ and 65 MHz). All experiments were performed at room temperature.²⁶⁶⁻²⁶⁸

A.2 Substrates

Throughout this thesis two model substrates, silicon and titanium oxide, have been used mainly due to the variety of fields they can be applied in. Hereafter, additional information about these substrates is provided:

- *Si/SiO₂*, or silicon-based materials, are widely used in the electronics industry, and are therefore well studied and characterized. They are used either as silicon (with a natural SiO₂ layer) or as sputter-coated oxide (SiO₂) layers. Similar to the Si/SiO₂ system there is fused silica glass, silicon nitride (Si₃N₄) and more generally glass. In all cases, the surface consists almost entirely of a silicon oxide layer. Literature reports two main approaches for functionalizing SiO₂: silane-based chemistry²⁶⁹ and spontaneous assembly of positively charged polyelectrolytes;²⁷⁰

- *TiO₂* substrates are among the most studied metal oxides due to their wide range of applications: medicine, solar cells, pigments, optical sensors, photocatalysts, electric devices or corrosion protection. They possess a highly regenerative dense oxide layer, which confers stability, and its coordinative structure can be found in three different forms: rutile, anatase and brookite, where the first is the thermodynamically stable one. The oxide layer is formed in presence of oxygen on any Ti or Ti alloy surface. Further, TiO₂ can be deposited by physical vapor deposition methods from a titanium source in an oxygen-rich low-pressure chamber. TiO₂ substrates are known to bind to phosph(on)ates,²⁷¹ catechols²⁷² and carboxylic acids.²⁷³ At physiological pH, they can also be functionalized using positively charged polyelectrolytes.²⁷⁰ The use of silanes

has been documented,²⁷⁴ however, in practice, due to poor reproducibility and lower stability compared to SiO₂ almost no application has found its way to the market. Oxides of tantalum (Ta₂O₅), niobia (Nb₂O₅), zirconia (ZrO₂) are similar to TiO₂ in terms of chemical reactivity.²⁴⁹

For protein adsorption, control measurements were performed on the bare substrates for the ionic strength assays according to the procedures described in section 4.2 of Chapter 4: clean substrates were immersed overnight (in dark at room temperature) in HEPES 0. The samples were then rinsed once with the above-mentioned buffer, once with water and dried under a stream of N₂. Thicknesses of the samples were measured before and after incubation by ellipsometry. Subsequently, the substrates were immersed overnight (at room temperature) in sodium chloride solutions at pH 7.4 with different ionic strength. Two ionic concentrations were used: 0.16M and 10mM HEPES buffer (HEPES II) and a 2M solution. The samples were then removed from the salt solution, rinsed once with 1mM HEPES buffer (HEPES 0), once with water and dried under a stream of N₂. The adlayer thickness was again measured by ellipsometry. Finally, the samples were re-immersed in HEPES II for 15 min and exposed to human serum (Precinorm Roche) for 30 min. During incubation, the samples were stored under ambient conditions without agitation. After exposure, the samples were rinsed twice with HEPES II buffer followed by ultrapure water and dried under a stream of N₂. The protein uptake was determined again by ellipsometry and results are displayed in Figure A 1

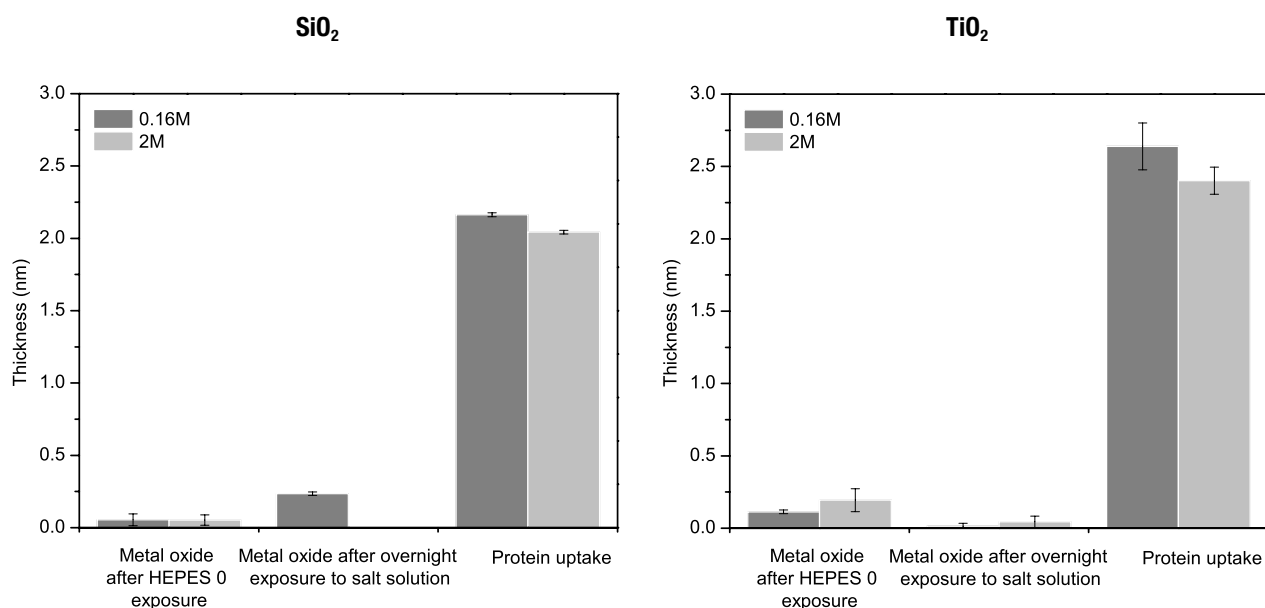


Figure A 1 Exposure to HEPES 0, salt solution (low ionic strength medium HEPES II 0.16 M and high ionic medium NaCl 2M) and protein resistance results on bare silicon oxide (left) and bare titanium oxide (right).

A.3 Basic properties of the tested polymers

For all the polymers used in Chapter 3 of this thesis, the following properties were either collected or calculated and finally summarized in Table A 1:

- monomer molecular weight ($M_{w,monomer}$) calculated according to the molecular structure of the polymer used (see Figure 1.4)
- monomer contour length, $L_{monomer}$, according to the following references: for vinyl based polymers PVA and both PVPs,¹¹⁶ PEG and PEOXA^{275,276} and dextran,²⁷⁷
- polymer molecular weight ($M_{w,polymer}$) was provided by the manufacturers and determined, when mentioned, either by light scattering, GPC or ¹H NMR end-group analysis;
- degree of polymerization was calculated according to equation (6)

$$DP = \frac{M_{w,polymer}}{M_{w,monomer}} \quad (6)$$

where $M_{w,polymer}$ (g mol^{-1}) is the average molecular weight of the polymer and $M_{w,monomer}$ (g mol^{-1}) is the average molecular weight of the respective monomer;

- average chain length ($\langle CL \rangle$) was obtained by applying equation (7)

$$\langle CL \rangle = DP \times L_{monomer} \quad (7)$$

where DP is the degree of polymerization and $L_{monomer}$ (nm) is the contour length of the monomer;

- the densities used as an approximation have been provided by manufacturer (PAAm-*g*-PFPA, PEOXA, PVP) or according to the following references: PVA,²⁷⁸ PEG²⁷⁹ and dextran.²⁸⁰

Table A 1 Properties of the polymers used.

	$M_{w, monomer}$ (g mol^{-1})	L_{mon} (nm)	$M_{w, polymer}$ (g mol^{-1})	DP (Degree of polymerization)	$\langle CL \rangle$ (nm)	ρ_{bulk} (g cm^{-3})
PAAm- <i>g</i> -PFPA	738	2.25	11,808	16	36	1.15*
PVA	44	0.25	27,000	613	153.25	1.35
PEG	44	0.44	20,000	454	199.76	1.20
Dextran	162	0.65	2,000,000	12345	8024.25	1.61
PEOXA	99	0.37	50,000	505	186.85	1.14
PVP	111	0.25	55,000	495	123.75	1.23
PVP			1,300,000	11711	2927.75	

* density of PAAm•HCl was used as an approximation of the density of PAAm-*g*-PFPA.

A.4 Calculation of the Average Loop Length as a Function of Coupling Efficiency E

For a loop-train-tail model, the average loop length (LL_i) of the different nonfouling polymers used in this work can be calculated according to equation (8)

$$LL_i = \frac{\langle CL \rangle_i}{\sigma_{attach,i}} \quad (8)$$

Where $\langle CL \rangle$ (nm) is the chain length of polymer i and $\sigma_{attach,i}$ is its probable attachment density to the polymeric backbone, PAAm- g -PFPA. This latter value is obtained by calculating the ratio between the PFPA units (see Figure 1.3) per surface area (σ (PFPA units nm^{-2})) and the grafting density of the different polymers (σ_i (chains nm^{-2})). Also a binding efficiency factor (Eff) needs to be introduced into the formula, to take into account the probability that an azide group becomes an attachment point, giving rise to equation (9).

$$\sigma_{attach,i} = \frac{\sigma(PFPA \text{ units } nm^{-2})}{\sigma(chains \text{ } nm^{-2})} \times Eff \quad (9)$$

Both PFPA and polymer i densities were calculated via a well-established formula. For the former we have equation (10)

$$\sigma(PFPA \text{ units } nm^{-2}) = \frac{h \times \rho_{bulk} \times N_{Av}}{M_{w,monomer \text{ PAAm-g9-PFPA}}} \quad (10)$$

where h (nm) is the dry thickness provided by ellipsometry, the ρ_{bulk} ($g \text{ } nm^{-3}$) is the density of the bulk polymer, N_{Av} (mol^{-1}) is the Avogadro number and M_w ($g \text{ } mol^{-1}$) is the

molecular weight of the PAAm-*g*-PFPA monomer. The same equation is then used to calculate the grafting density of the polymers by replacing the molecular weight of the monomer by that of the non-fouling polymer (equation (11)).

$$\sigma_i(\text{chains nm}^{-2}) = \frac{h \times \rho_{\text{bulk}} \times N_{\text{Av}}}{M_{w,\text{pol}_i}} \quad (11)$$

The average loop length (LL_i) can be used to calculate the coiled radius (R_c) according to equation (12), if one considers a coiled polymer to have a sphere-like structure. This assumption is proven valid since the basic experimental parameter used in these calculations is the dry thickness (collapsed state of a polymer brush) provided by *ex-situ* ellipsometry.

$$\begin{aligned} R_c &= \sqrt[3]{\frac{3 \times V_{\text{sphere}}}{4\pi}} \\ &= \sqrt[3]{\frac{3}{4\pi} \times \frac{m_{\text{loop}}}{\rho_{\text{dry}}}} \\ &= \sqrt[3]{\frac{3}{4\pi} \times \frac{M_{w,\text{monomer}} \times DP_{\text{loop}}}{\rho_{\text{dry}} \times N_{\text{Av}}}} \\ &= \sqrt[3]{\frac{3}{4\pi} \times \frac{M_{w,\text{monomer}} \times LL_i}{\rho_{\text{dry}} \times N_{\text{Av}} \times L_{\text{mon}}}} \end{aligned} \quad (12)$$

where V_{sphere} (m^3) is the volume of a sphere, m (g) is the mass associated to a loop and DP_{loop} is the degree of polymerization associated to the average loop length of polymer *i*.

The average distance between attachment points (L_{id}) in this particular case should be the same for all polymers since it is determined by the azide anchoring groups, assuming that the attachment efficiencies is independent of the polymer

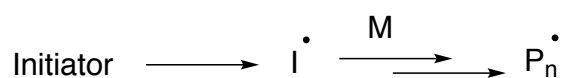
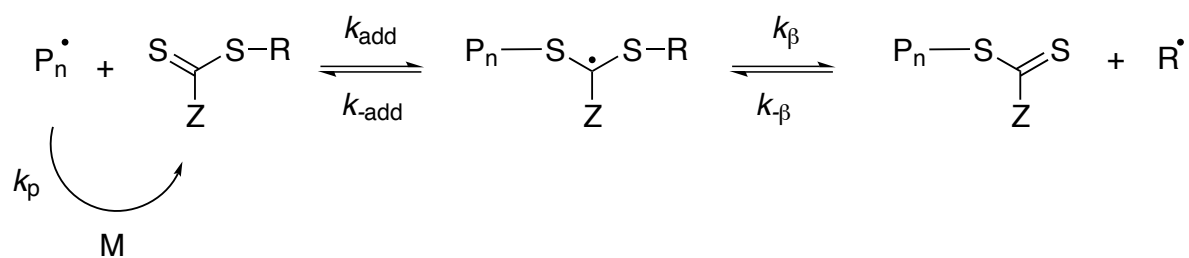
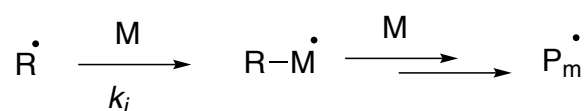
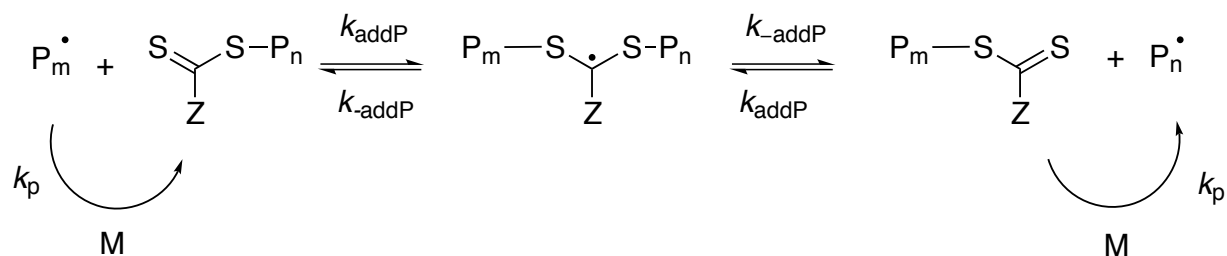
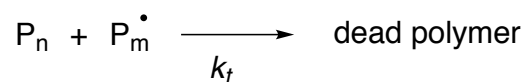
chemistry. It can be calculated according to equation (13), if hexagonal packing of the azide groups on the surface is assumed.

$$L_{id} = \left(\frac{2}{\sqrt{3} \times \sigma(\text{PFPA units nm}^{-2}) \times \text{Eff}} \right)^{0.5} \quad (13)$$

A.5 Radical Addition-Fragmentation Chain Transfer Polymerization (RAFT)

Within the class of living radical polymerization techniques there are three, which have been in the last years widely used to obtain homopolymers, copolymers and block copolymers with low polydispersities, while maintaining good control over the polymer architectures to be achieved and the end-groups to be used. These are the nitroxide-mediated polymerization (NMP), atom transfer radical polymerization (ATRP), and reversible addition–fragmentation transfer (RAFT) polymerization. Depending on the final goal one technique might be more suited than the others. For instance NMP, although it can be performed with minimal purification and is characterized by high conversion rates,²⁸¹ it is quite limited to only a few monomers that can be used (styrene derivatives, N,N-dimethylacrylamides, dienes, acrylonitriles),²⁸² it only works at high temperatures (120°C-150°C) and demands long polymerization times.²²⁴ For ATRP the list of monomers that can undergo this polymerization is wider than for NMP: substituted styrenes, acrylates, methacrylates, acrylamides, vinyl pyridine, acrylonitrile and dienes. Its tolerance to many functional groups and a multitude of available initiators are other advantages of ATRP.²⁸³ Nevertheless, this technique also possesses the disadvantage of using a catalyst that will contaminate the final product. The need to remove it is a major drawback specially when designing large-scale processes,²²⁴ RAFT polymerization has the advantage over ATRP and NMP of being tolerant to an even wider range of monomer functionalities and solvents, low influence on copolymer composition at low conversions and does not require a catalyst.²⁸⁴ RAFT is one of most

used polymerization techniques nowadays and it was first reported in the literature by Krstina *et al.*²⁸⁵ but only three years later its working mechanism was proposed²⁸⁶ (see Scheme A 1). The novelty of this technique when compared to conventional free radical polymerization relies on the use of a chain transfer agent (CTA), which controls the polymerization in a two-step addition-fragmentation process. The initiation step is as found in conventional radical polymerization, but in this case the resulting propagating radical species - P_n^* - reacts with the CTA leading to the formation of an intermediate adduct that is then fragmented creating a new radical species - R^* - and a dormant polymeric version of the chain transfer agent. The former will then react with the available monomers and a new propagating species - P_m^* - is generated. The living character of this method depends now on the transfer of the S=C(Z)S- moiety (in case a thiocarbonylthio is used as a CTA) between the propagating radical species and the dormant one. It needs to be faster than the propagation in order to allow the polymer chains to grow with the same statistical probability. Both the re-initiation and propagation step should also be fast in order to guarantee prevention of early termination,²⁸⁵ which follows the same mechanisms as free radical polymerization (combination or disproportionation). Once the polymerization is complete, most of the produced chain ends will retain the S=C(Z)S- moiety which allows RAFT to produce polymers with well-defined end-groups.²³⁹

Initiation**Reversible chain transfer/propagation****Reinitiation****Chain equilibration/propagation****Termination**

Scheme A 1 Mechanism for RAFT polymerization using a thiocarbonylthio chain transfer agent (CTA).

The design of the CTA agent is of crucial importance to obtain the living character of RAFT and its structure should follow certain guidelines: the presence of a reactive C=S bond that proceeds to give a high k_{add} , the fragmentation of the intermediate adduct should be quick (high k_{β}) and its equilibrium should be shifted towards the formation of products ($k_{\beta} \geq k_{\text{add}}$), and the new formed radicals - R - should be able to easily reinitiate polymerization.²³⁰ To better improve these rules one might deconstruct the chain-transfer agent into two different groups (see Figure A 2): group Z, which is responsible for the addition and fragmentation constant rates to the C=S reactive bond, and the R group which is a free radical leaving group (weak R-S bond) capable of reinitiating polymerization, as stated above.

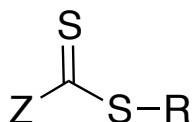


Figure A 2 General structure of the chain transfer agent (CTA) used in RAFT.

The most common CTAs used in RAFT are thiocarbonylthio compounds (or dithiobenzoates), trithiocarbonates, xanthates and dithiocarbamates. Examples of their structures and a general summary of their applications, depending on the monomer used, can be found elsewhere.^{231,232} The use of the correct CTA can prevent issues like inhibition and retardation, typically obtained when the re-initiation is slow and when the conversion rate of the CTA to its polymeric form is low, respectively.

The reasons why this specific living polymerization technique was chosen are based on the fact that NMP polymerization of acrylates (our monomer of choice) does not result in a good control of weight distribution²⁸⁷ and ATRP, due to the use of a metal catalyst, is a more O_2 sensitive technique than RAFT and its presence in the final product can pose both as an environmental and economic problem for scaling-up or large-scale production. Further general advantages of using this living polymerization technique are its versatility in the monomers used, as its tolerance towards a large number of functional groups. It can be applied under the same conditions as free radical polymerization (same initiators, solvents and temperatures) and can be used for both

homogeneous and heterogeneous polymerizations. Nevertheless, as for any technique, it possesses disadvantages, namely retardation when aiming at low molecular weight polymers²⁸⁸ and the overall Trommsdorff-Norrish effect when reaching high conversions.²⁸⁹

A.6 *In situ* adsorption studies - QCM-D raw data

The raw data obtained by the QCM-D measurements performed in section 4.2.10 of Chapter 4 are shown here. Although at least three measurements were performed for each surface-chemistry involved, only one example for each is shown here.

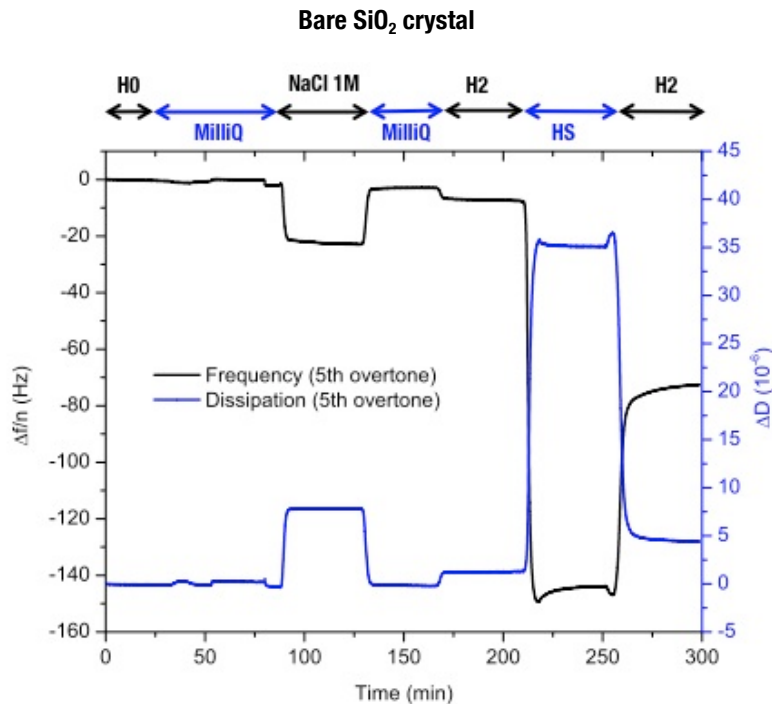


Figure A 3 Change in oscillating frequency and dissipation of QCM crystal coated with SiO₂ as function of time. The initial baseline was obtained in HEPES 0 for all experiments. After this a stability step was introduced where the solvent was exchanged for ultrapure water. The sensors were exposed to a concentrated NaCl solution of 1 M at pH=7.4 and were rinsed again with ultrapure water. For testing the protein resistance of the modified sensors the buffer was yet again exchanged, now for HEPES II, and a human serum solution was injected where static exposure continued for at least 30 min. Final rinsing was performed with the same HEPES II buffer.

Polymer B or poly(acrylic acid)-*g*-(PEG, 1,6-hexanediamine, 3-aminopropyltrimethoxysilane) (2000:116.2:161.3

M_n ; 0.15:0.425:0.425 d)

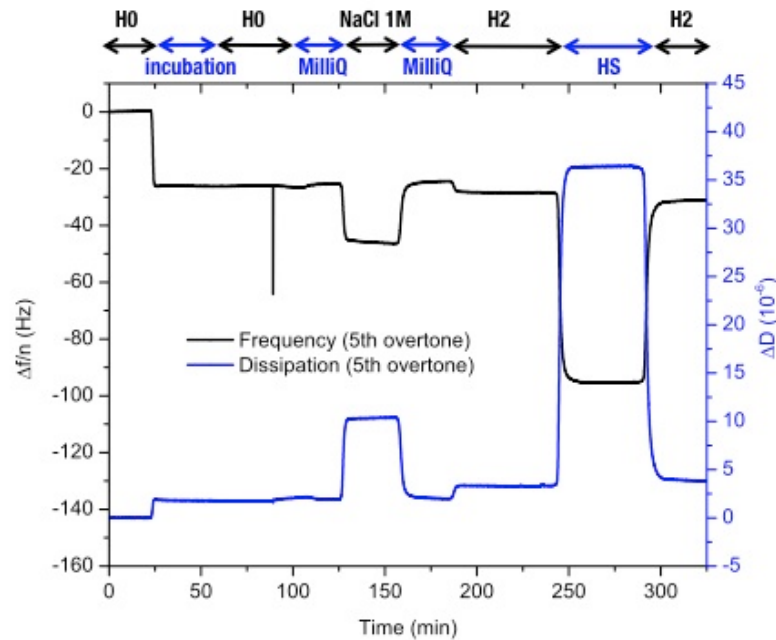


Figure A 4 Change in oscillating frequency and dissipation of QCM crystal coated with SiO_2 as function of time. The initial baseline was obtained in HEPES 0 for all experiments followed by the injection of a polymer B solution of 0.1 mg/mL in HEPES 0 until a new plateau was reached. After this a stability step was introduced where the solvent was now exchanged for ultrapure water. The sensors were exposed to a concentrated NaCl solution of 1 M pH=7.4 and were rinsed again with ultrapure water. For testing the protein resistance of the modified sensors the buffer was yet again exchanged, now for HEPES II, and a human serum solution was injected where static exposure continued for at least 30 min. Final rinsing was performed with the same HEPES II buffer.

Polymer E or poly(acrylic acid)-*g*-(PEG, 1,6-hexanediamine, ethanolamine) (2000: 116.2:61.1 *M*_r; 0.15:0.425:0.425 *d*)

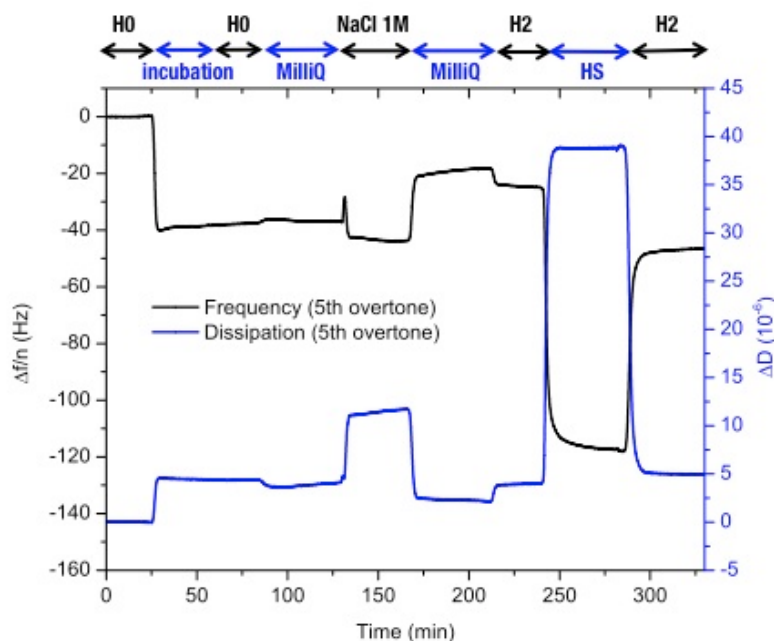


Figure A 5 Change in oscillating frequency and dissipation of QCM crystal coated with SiO_2 as function of time. The initial baseline was obtained in HEPES 0 for all experiments followed by the injection of a polymer E solution of 0.1 mg/mL in HEPES 0 until new plateau was reached. After this a stability step was introduced where the solvent was exchanged for ultrapure water. The sensors were exposed to a concentrated NaCl solution of 1 M pH=7.4 and were rinsed again with ultrapure water. For testing the protein resistance of the modified sensors the buffer was yet again exchanged, now for HEPES II, and a human serum solution was injected where static exposure continued for at least 30 min. Final rinsing was performed with the same HEPES II buffer.

Polymer F or poly(acrylic acid)-*g*-(PEG, 1,6-hexanediamine, 3-aminopropyl-dimethylethoxysilane, nitrodopamine)

(2000:116.2:161.3:198.2 *M*; 0.15:0.425:0.2125: 0.2125 *d*)

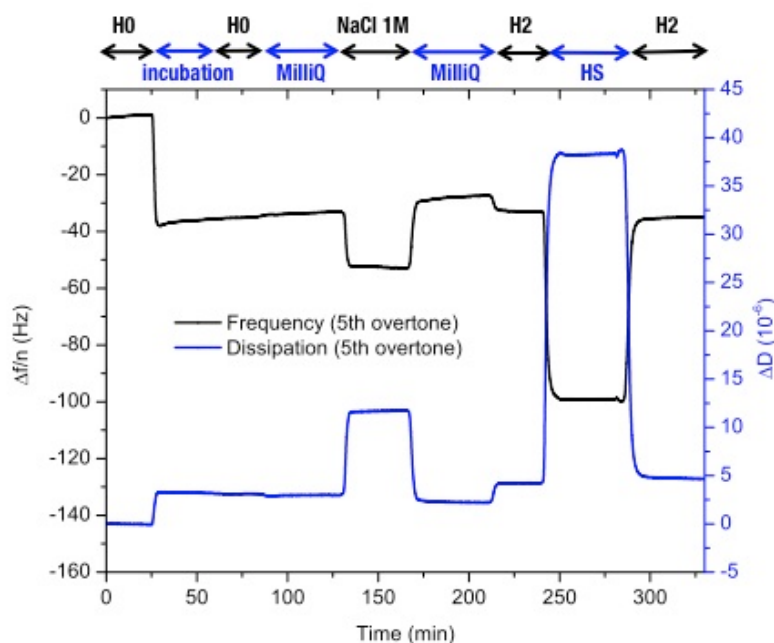


Figure A 6 Change in oscillating frequency and dissipation of QCM crystal coated with SiO₂ as function of time. The initial baseline was obtained in HEPES 0 for all experiments followed by the injection of a polymer E solution of 0.1 mg/mL in HEPES 0 until new plateau was reached. After this a stability step was introduced where the solvent was now exchanged for ultrapure water. The sensors were exposed to a concentrated NaCl solution of 1 M pH=7.4 and were rinsed again with ultrapure water. For testing the protein resistance of the modified sensors the buffer was yet again exchanged, now for HEPES II, and a human serum solution was injected where static exposure continued for at least 30 min. Final rinsing was performed with the same HEPES II buffer.

A.7 NMR spectra

The spectra obtained by ¹H NMR measurements in D₂O performed for section 4.3.3.3 of Chapter 4 are shown here.

Polymer A or poly(acrylic acid)-*g*-(PEG, 1,6-hexanediamine) (2000:116.2 M_n ; 0.15:0.85 d)

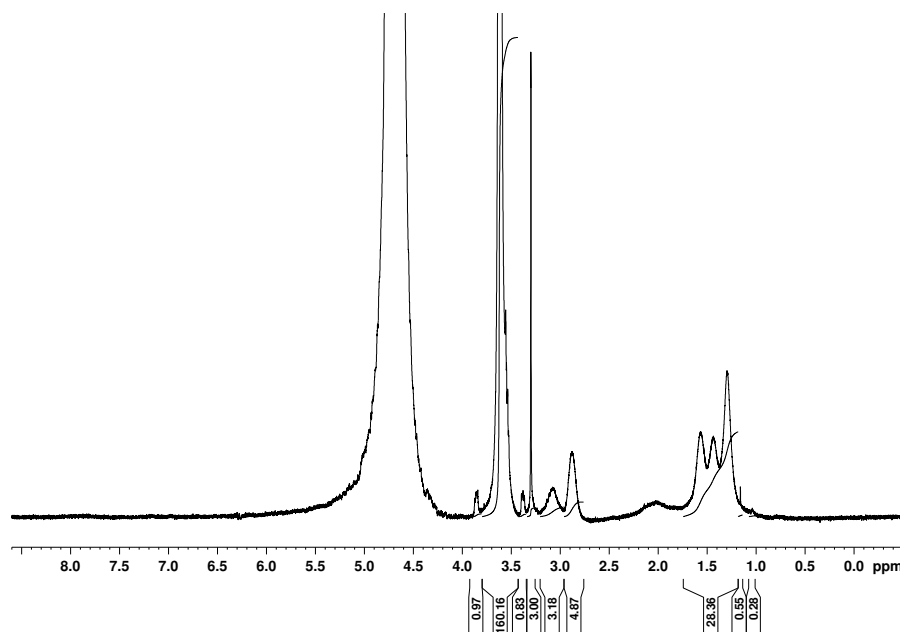


Figure A 7 ^1H NMR spectra of polymer A measured at 25 °C (128 scans) in D_2O at 300 MHz.

**Polymer B or poly(acrylic acid)-*g*-(PEG, 1,6-hexanediamine, 3-aminopropyldimethylethoxysilane)
(2000:116.2:161.3 M_n ; 0.15:0.425:0.425 d)**

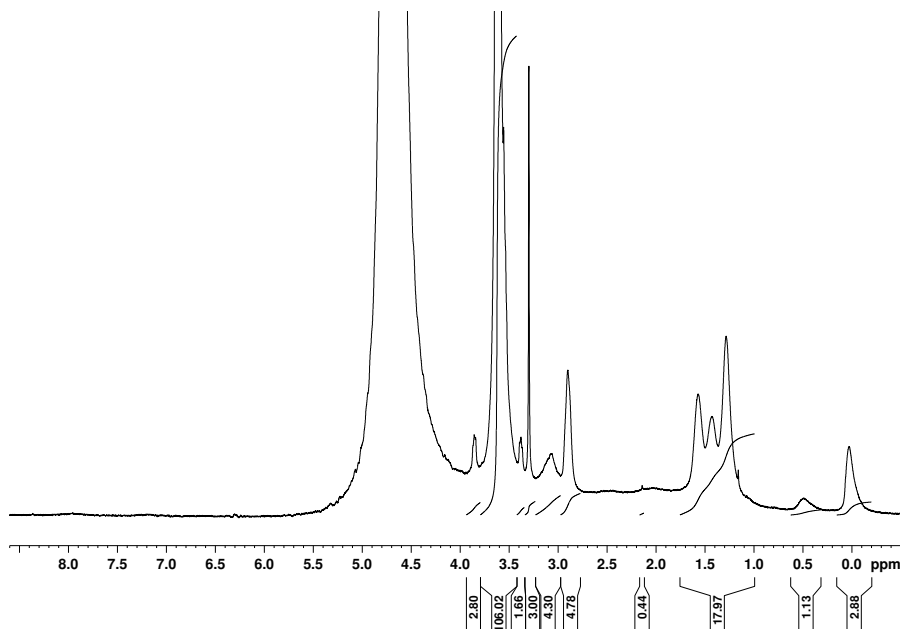


Figure A 8 ^1H NMR spectra of polymer B measured at 25 °C (128 scans) in D_2O at 300 MHz.

**Polymer C or poly(acrylic acid)-*g*-(PEG, 1,6-hexanediamine, nitrodopamine) (2000: 116.2:198.2 M_n ;
0.15:0.425:0.425 *d*)**

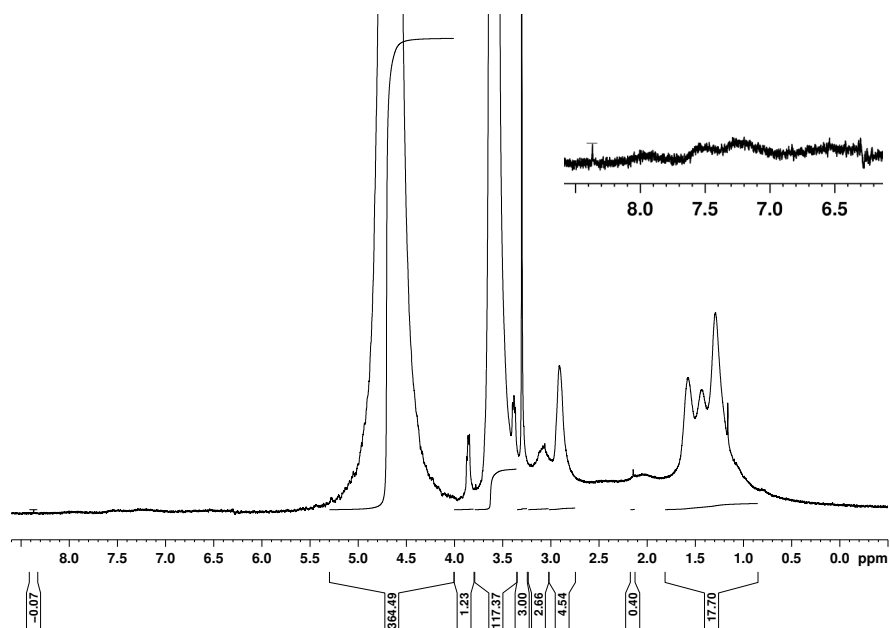


Figure A 9 ^1H NMR spectra of polymer C measured at 25 °C (128 scans) in D_2O at 300 MHz.

**Polymer D or poly(acrylic acid)-*g*-(PEG, 1,6-hexanediamine, 12-aminododecylphosphonate) (2000:116.2:265.3 M_n ;
0.15:0.425:0.425 *d*)**

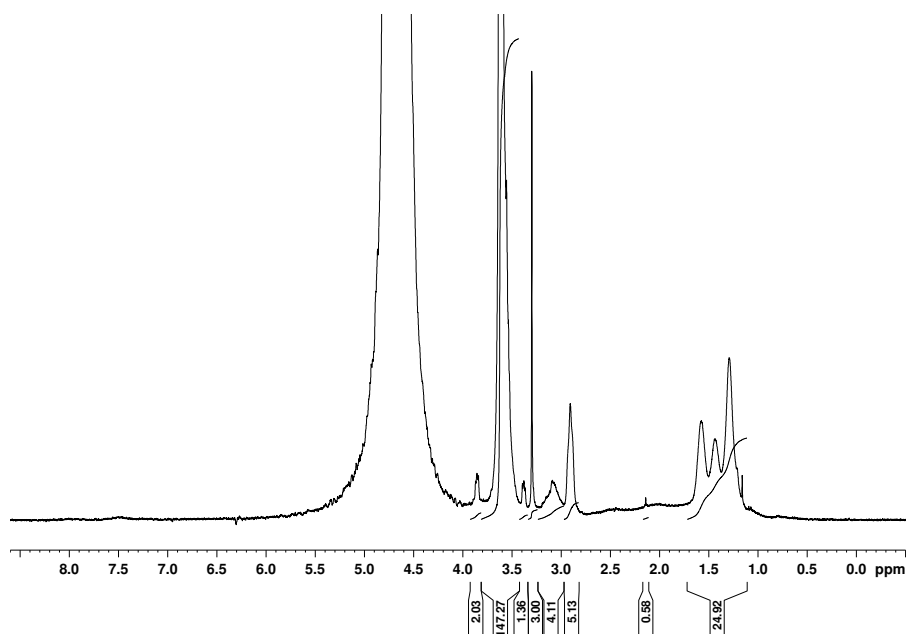


Figure A 10 ^1H NMR spectra of polymer D measured at 25 °C (128 scans) in D_2O at 300 MHz.

Polymer E or poly(acrylic acid)-*g*-(PEG, 1,6-hexanediamine, ethanolamine) (2000: 116.2:61.1 M_n ; 0.15:0.425:0.425 d)

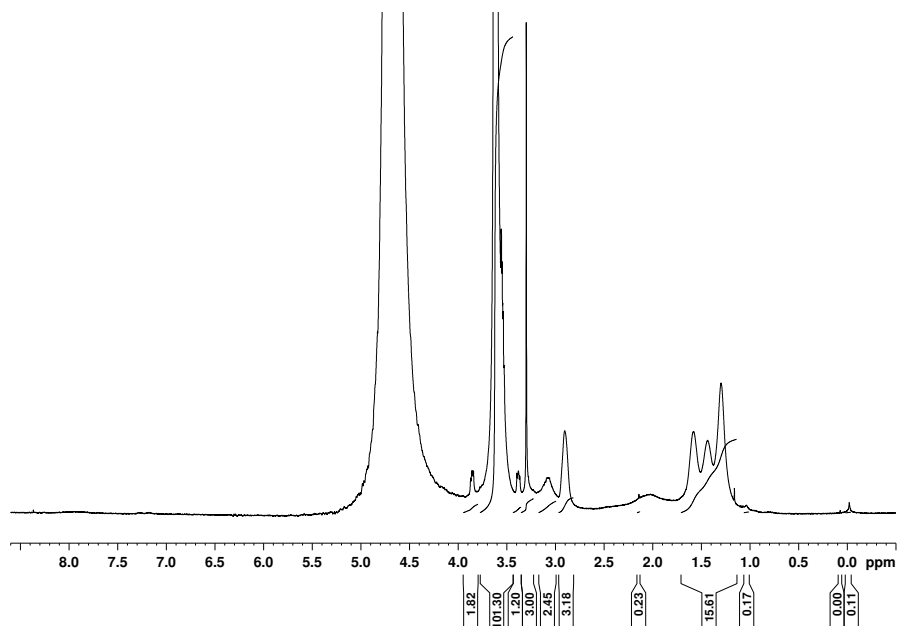


Figure A 11 ^1H NMR spectra of polymer E measured at 25 °C (128 scans) in D_2O at 300 MHz.

Polymer F or poly(acrylic acid)-*g*-(PEG, 1,6-hexanediamine, 3-aminopropyl-dimethylethoxysilane, nitrodopamine) (2000:116.2:161.3:198.2 M_n ; 0.15:0.425:0.2125: 0.2125 d)

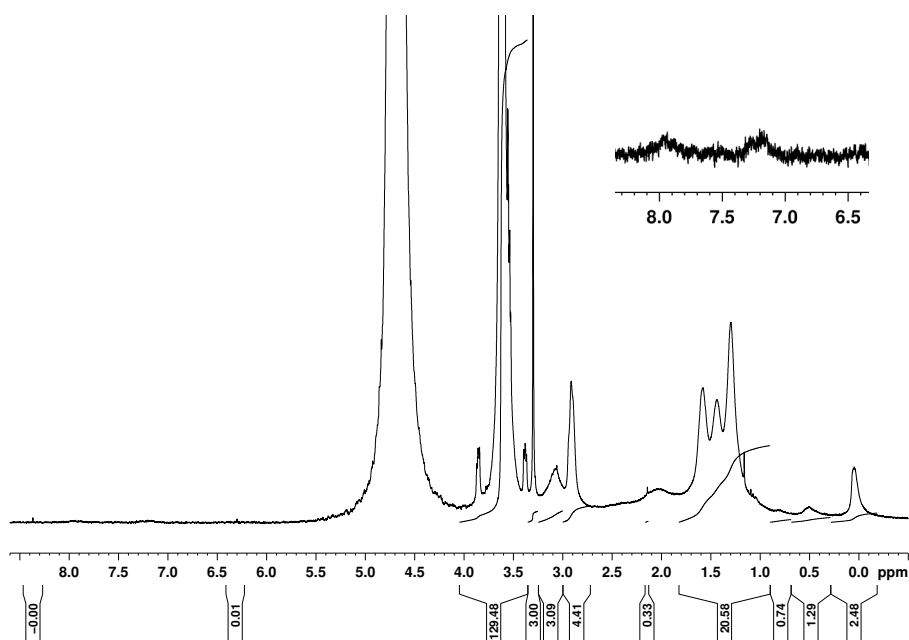


Figure A 12 ^1H NMR spectra of polymer F measured at 25 °C (128 scans) in D_2O at 300 MHz.

Polymer G or poly(acrylic acid)-*g*-(PEG, 3-aminopropyl-dimethylethoxysilane, nitrodopamine) (2000:161.3:198.2

M_i ; 0.15:0.425:0.425 *d*)

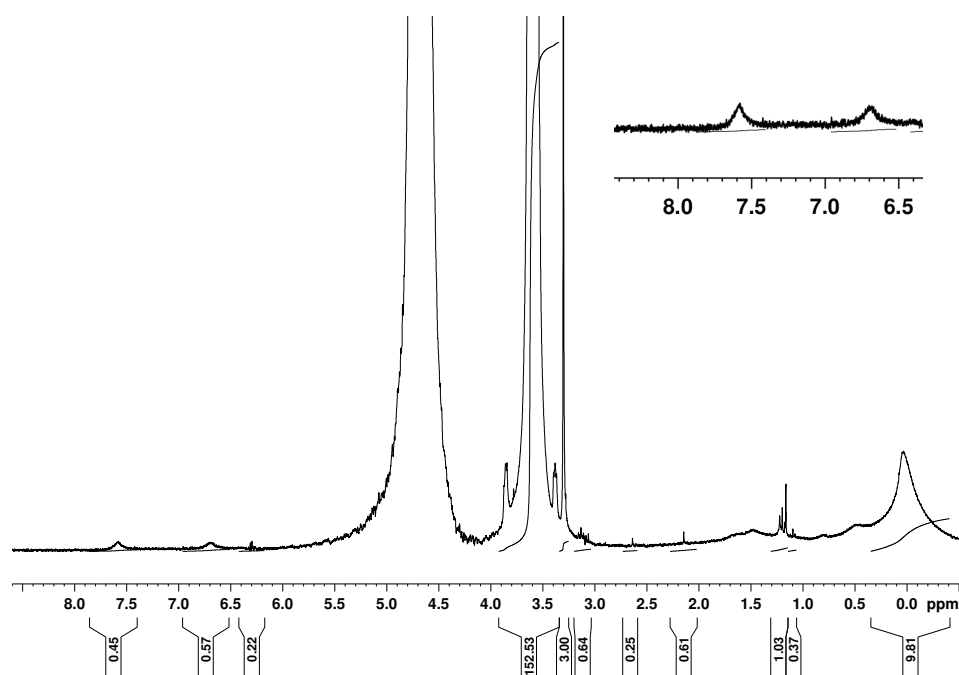


Figure A 13 ^1H NMR spectra of polymer G measured at 25 °C (128 scans) in D_2O at 300 MHz.

Bibliography

1. Statz, A., Meagher, R., Barron, A. & Messersmith, P. New peptidomimetic polymers for antifouling surfaces. *J Am Chem Soc* **127**, 7972–7973 (2005).
2. Hook, A. L. *et al.* Combinatorial discovery of polymers resistant to bacterial attachment. *Nature Biotechnology* 1–10 (2012). doi:10.1038/nbt.2316
3. Nguyen, T., Roddick, F. & Fan, L. Biofouling of Water Treatment Membranes: A Review of the Underlying Causes, Monitoring Techniques and Control Measures. *Membranes* **2**, 804–840 (2012).
4. Cao Shan, Wang JiaDao, Chen HaoSheng & Chen DaRong. Progress of marine biofouling and antifouling technologies. *Chin. Sci. Bull.* **56**, 598–612 (2011).
5. Fittridge, I., Dempster, T., Guenther, J. & de Nys, R. The impact and control of biofouling in marine aquaculture: a review. *Biofouling* **28**, 649–669 (2012).
6. Li, X., Xing, Y., Jiang, Y., Ding, Y. & Li, W. Antimicrobial activities of ZnO powder-coated PVC film to inactivate food pathogens. *International Journal of Food Science & Technology* **44**, 2161–2168 (2009).
7. Goode, K. R., Asteriadou, K., Robbins, P. T. & Fryer, P. J. Fouling and Cleaning Studies in the Food and Beverage Industry Classified by Cleaning Type. *Comprehensive Reviews in Food Science and Food Safety* **12**, 121–143 (2013).
8. Shirliff, M. & Leid, J. G. The role of biofilms in device-related infections. (2009).
9. Flemming, H. C. & Ridgway, H. in *Springer Series on Biofilms* **4**, 103–117 (Springer Berlin Heidelberg, 2009).
10. Walker, J., Surman, S. & Jass, J. Industrial biofouling. (2000).
11. Schultz, M. P., Bendick, J. A., Holm, E. R. & Hertel, W. M. Economic impact of biofouling on a naval surface ship. *Biofouling* **27**, 87–98 (2011).
12. Videla, H. A. Manual of biocorrosion. (1996).
13. Abarzua, S. & Jakubowski, S. Biotechnological investigation for the prevention of biofouling. I. Biological and biochemical principles for the prevention of biofouling. *Mar. Ecol. Prog. Ser.* **123**, 301–312 (1995).
14. Lehaitre, M., Delauney, L. & Compere, C. Biofouling and underwater measurements. *Real-time observation systems for ecosystem dynamics and harmful algal blooms. UNESCO, Paris* (2005).
15. Loeb, G. I. & Neihof, R. A. Marine conditioning films. *Adv Chem* **145**, 319–335 (1975).
16. Boks, N. P., Norde, W., Van Der Mei, H. C. & Busscher, H. J. Forces involved in bacterial adhesion to hydrophilic and hydrophobic surfaces. *Microbiology* **154**,

- 3122–3133 (2008).
17. Van Oss, C. J., Good, R. J. & Chaudhury, M. K. The role of van der Waals forces and hydrogen bonds in 'hydrophobic interactions' between biopolymers and low energy surfaces. *J Colloid Interf Sci* **111**, 378–390 (1986).
 18. Decho, A. In situ Imaging and Characterizing the Matrix of Extracellular Polymeric Substances (EPS) of Biofilms. *Microscopy and Microanalysis* **15**, 822–823 (2009).
 19. Dobretsov, S., Dahms, H.-U. & Qian, P.-Y. Inhibition of biofouling by marine microorganisms and their metabolites. *Biofouling* **22**, 43–54 (2006).
 20. U.S. Naval Institute. Marine Fouling and its Prevention. *Woods Hole Oceanographic Institute & United States Naval Academy* (1952).
 21. Omae, I. Organotin antifouling paints and their alternatives. *Appl. Organometal. Chem.* **17**, 81–105 (2003).
 22. Yebra, D., Kiil, S. & Dam-Johansen, K. Antifouling technology - past, present and future steps towards efficient and environmentally friendly antifouling coatings. *Prog Org Coat* **50**, 75–104 (2004).
 23. Evans, S. M., Leksono, T. & McKinnell, P. D. Tributyltin pollution: a diminishing problem following legislation limiting the use of TBT-based anti-fouling paints. *Marine Pollution Bulletin* **30**, 14–21 (1995).
 24. Krishnan, S., Weinman, C. J. & Ober, C. K. Advances in polymers for anti-biofouling surfaces. *J Mater Chem* **18**, 3405–3413 (2008).
 25. Bixler, G. D. & Bhushan, B. Biofouling: lessons from nature. *Philos Transact A Math Phys Eng Sci* **370**, 2381–2417 (2012).
 26. Tuson, H. H. & Weibel, D. B. Bacteria–surface interactions. *Soft Matter* **9**, 4368 (2013).
 27. Rechendorff, K. The influence of surface roughness on protein adsorption. *PhD thesis* 1–120 (2006).
 28. Graham, M. & Cady, N. Nano and Microscale Topographies for the Prevention of Bacterial Surface Fouling. *Coatings* **4**, 37–59 (2014).
 29. Genzer, J. & (null). Recent developments in superhydrophobic surfaces and their relevance to marine fouling: a review. *Biofouling* **22**, 339–360 (2006).
 30. Myan, F. W. Y., Walker, J. & Paramor, O. The interaction of marine fouling organisms with topography of varied scale and geometry: a review. *Biointerphases* **8**, 30 (2013).
 31. Marmur, A. Super-hydrophobicity fundamentals: implications to biofouling prevention. *Biofouling* **22**, 107–115 (2006).
 32. Kristensen, J. B. *et al.* Antifouling enzymes and the biochemistry of marine settlement. *Biotechnology Advances* **26**, 471–481 (2008).
 33. Olsen, S. M., Pedersen, L. T., Laursen, M. H., Kiil, S. & Dam-Johansen, K. Enzyme-based antifouling coatings: a review. *Biofouling* **23**, 369–383 (2007).

34. Zhang, M., Zhang, K., De Gusseme, B. & Verstraete, W. Biogenic silver nanoparticles (bio-Ag). *Water Res* **46**, 2077–2087 (2012).
35. Callow, J. A. & Callow, M. E. Trends in the development of environmentally friendly fouling-resistant marine coatings. *Nature Communications* **2**, 244 (2011).
36. Yasani, B. R. *et al.* A comparison between different fouling-release elastomer coatings containing surface-active polymers. *Biofouling* **30**, 387–399 (2014).
37. Molena, E. *et al.* Applied Surface Science. *Appl Surf Sci* **309**, 160–167 (2014).
38. Chapman, R. G. *et al.* Polymeric Thin Films That Resist the Adsorption of Proteins and the Adhesion of Bacteria. *Langmuir* **17**, 1225–1233 (2001).
39. Konradi, R., Acikgoz, C. & Textor, M. Polyoxazolines for Nonfouling Surface Coatings - A Direct Comparison to the Gold Standard PEG. *Macromol Rapid Comm* **33**, 1663–1676 (2012).
40. Chen, S., Zheng, J., Li, L. & Jiang, S. Strong resistance of phosphorylcholine self-assembled monolayers to protein adsorption: insights into nonfouling properties of zwitterionic materials. *J Am Chem Soc* **127**, 14473–14478 (2005).
41. Chen, S., Li, L., Zhao, C. & Zheng, J. Surface hydration: Principles and applications toward low-fouling/nonfouling biomaterials. *Polymer* **51**, 5283–5293 (2010).
42. Schilp, S. *et al.* Physicochemical Properties of (Ethylene Glycol)-Containing Self-Assembled Monolayers Relevant for Protein and Algal Cell Resistance. *Langmuir* **25**, 10077–10082 (2009).
43. Sofia, S., Premnath, V. & Merrill, E. Poly(ethylene oxide) grafted to silicon surfaces: Grafting density and protein adsorption. *Macromolecules* **31**, 5059–5070 (1998).
44. (null) *et al.* Poly(L-lysine)-g-poly(ethylene glycol) layers on metal oxide surfaces: Attachment mechanism and effects of polymer architecture on resistance to protein adsorption. *J Phys Chem B* **104**, 3298–3309 (2000).
45. Ostuni, E., Chapman, R. G., Holmlin, R. E., Takayama, S. & Whitesides, G. M. A Survey of Structure–Property Relationships of Surfaces that Resist the Adsorption of Protein. *Langmuir* **17**, 5605–5620 (2001).
46. Nagasaki, Y. Construction of a densely poly(ethylene glycol)-chain-tethered surface and its performance. *Polym J* **43**, 949–958 (2011).
47. Pasche, S., De Paul, S., Voros, J., Spencer, N. & Textor, M. Poly(L-lysine)-graft-poly(ethylene glycol) assembled monolayers on niobium oxide surfaces: A quantitative study of the influence of polymer interfacial architecture on resistance to protein adsorption by ToF-SIMS and in situ OWLS. *Langmuir* **19**, 9216–9225 (2003).
48. Ekblad, T. *et al.* Poly(ethylene glycol)-containing hydrogel surfaces for antifouling applications in marine and freshwater environments. *Biomacromolecules* **9**, 2775–2783 (2008).

49. Ogaki, R. *et al.* Temperature-Induced Ultradense PEG Polyelectrolyte Surface Grafting Provides Effective Long-Term Bioresistance against Mammalian Cells, Serum, and Whole Blood. *Biomacromolecules* **13**, 3668–3677 (2012).
50. Kingshott, P., Thissen, H. & Griesser, H. J. Effects of cloud-point grafting, chain length, and density of PEG layers on competitive adsorption of ocular proteins. *Biomaterials* **23**, 2043–2056 (2002).
51. Herrwerth, S., Eck, W., Reinhardt, S. & Grunze, M. Factors that Determine the Protein Resistance of Oligoether Self-Assembled Monolayers – Internal Hydrophilicity, Terminal Hydrophilicity, and Lateral Packing Density. *J Am Chem Soc* **125**, 9359–9366 (2003).
52. Jeon, S. I., Lee, J. H., Andrade, J. D. & De Gennes, P. Protein–surface interactions in the presence of polyethylene oxide: I. Simplified theory. *J Colloid Interf Sci* **142**, 149–158 (1991).
53. Szleifer, I. Protein adsorption on surfaces with grafted polymers: A theoretical approach. *Biophys J* **72**, 595–612 (1997).
54. Sharma, S., Johnson, R. W. & Desai, T. A. Evaluation of the Stability of Nonfouling Ultrathin Poly(ethylene glycol) Films for Silicon-Based Microdevices. *Langmuir* **20**, 348–356 (2004).
55. Zoulalian, V. *et al.* Self-Assembly of Poly(ethylene glycol)–Poly(alkyl phosphonate) Terpolymers on Titanium Oxide Surfaces: Synthesis, Interface Characterization, Investigation of Nonfouling Properties, and Long-Term Stability. *Langmuir* **26**, 74–82 (2010).
56. Michel, R., Pasche, S., Textor, M. & Castner, D. G. Influence of PEG architecture on protein adsorption and conformation. *Langmuir* **21**, 12327–12332 (2005).
57. Sundaram, H. S. *et al.* Fluorine-free mixed amphiphilic polymers based on PDMS and PEG side chains for fouling release applications. *Biofouling* **27**, 589–602 (2011).
58. Wang, Y. *et al.* Amphiphilic Co-networks with Moisture-Induced Surface Segregation for High-Performance Nonfouling Coatings. *Langmuir* **27**, 10365–10369 (2011).
59. Wang, Y. *et al.* Investigation of the role of hydrophilic chain length in amphiphilic perfluoropolyether/poly(ethylene glycol) networks: towards high-performance antifouling coatings. *Biofouling* **27**, 1139–1150 (2011).
60. Han, S., Kim, C. & Kwon, D. Thermal/oxidative degradation and stabilization of polyethylene glycol. *Polymer* **38**, 317–323 (1997).
61. Woodle, M., Engbers, C. & Zalipsky, S. New Amphipatic Polymer Lipid Conjugates Forming Long-Circulating Reticuloendothelial System-Evading Liposomes. *Bioconjugate Chem* **5**, 493–496 (1994).
62. Wang, H., Li, L., Tong, Q. & Yan, M. Evaluation of Photochemically Immobilized Poly(2-ethyl-2-oxazoline) Thin Films as Protein-Resistant Surfaces. *Acs Appl Mater Inter* **3**, 3463–3471 (2011).

63. Rovira-Bru, M., Giralt, F. & Cohen, Y. Protein adsorption onto zirconia modified with terminally grafted polyvinylpyrrolidone. *J Colloid Interf Sci* **235**, 70–79 (2001).
64. Robinson, S. & Williams, P. Inhibition of protein adsorption onto silica by polyvinylpyrrolidone. *Langmuir* **18**, 8743–8748 (2002).
65. Wu, Z. *et al.* Protein Adsorption on Poly(N-vinylpyrrolidone)-Modified Silicon Surfaces Prepared by Surface-Initiated Atom Transfer Radical Polymerization. *Langmuir* **25**, 2900–2906 (2009).
66. Rasmussen, K. & Ostgaard, K. Adhesion of the marine fouling diatom *Amphora coffeaeformis* to non-solid gel surfaces. *Biofouling* **17**, 103–115 (2001).
67. Murosaki, T. *et al.* Antifouling properties of tough gels against barnacles in a long-term marine environment experiment. *Biofouling* **25**, 657–666 (2009).
68. Rasmussen, K., Willemsen, P. & Ostgaard, K. Barnacle settlement on hydrogels. *Biofouling* **18**, 177–191 (2002).
69. Perrino, C., Lee, S., Choi, S. W., Maruyama, A. & Spencer, N. D. A biomimetic alternative to poly(ethylene glycol) as an antifouling coating: Resistance to nonspecific protein adsorption of poly(L-lysine)-graft-dextran. *Langmuir* **24**, 8850–8856 (2008).
70. Feng, W., Zhu, S., Ishihara, K. & Brash, J. L. Protein resistant surfaces: Comparison of acrylate graft polymers bearing oligo-ethylene oxide and phosphorylcholine side chains. *Biointerphases* **1**, 50 (2006).
71. Ladd, J., Zhang, Z., Chen, S., Hower, J. C. & Jiang, S. Zwitterionic Polymers Exhibiting High Resistance to Nonspecific Protein Adsorption from Human Serum and Plasma. *Biomacromolecules* **9**, 1357–1361 (2008).
72. (null), Chen, X., (null), (null) & Whitesides, G. Zwitterionic SAMs that resist nonspecific adsorption of protein from aqueous buffer. *Langmuir* **17**, 2841–2850 (2001).
73. Utrata-Wesołek, A. Antifouling surfaces in medical application. *Polimery* **58**, (2013).
74. Hayward, J. A. & Chapman, D. Biomembrane surfaces as models for polymer design: the potential for haemocompatibility. *Biomaterials* **5**, 135–142 (1984).
75. Chang, Y., Chen, S., Zhang, Z. & Jiang, S. Highly protein-resistant coatings from well-defined diblock copolymers containing sulfobetaines. *Langmuir* **22**, 2222–2226 (2006).
76. Quintana, R. *et al.* Colloids and Surfaces B: Biointerfaces. *Colloid Surface B* **120**, 118–124 (2014).
77. Kostina, N. Y., Rodriguez-Emmenegger, C., Houska, M., Brynda, E. & Michálek, J. Non-fouling Hydrogels of 2-Hydroxyethyl Methacrylate and Zwitterionic Carboxybetaine (Meth)acrylamides. *Biomacromolecules* 121116090145004 (2012). doi:10.1021/bm301441x
78. Zhang, Z., Chen, S. & Jiang, S. Dual-functional biomimetic materials: Nonfouling

- poly(carboxybetaine) with active functional groups for protein immobilization. *Biomacromolecules* **7**, 3311–3315 (2006).
79. Murphy, E. F. *et al.* Characterization of Protein Adsorption at the Phosphorylcholine Incorporated Polymer–Water Interface. *Macromolecules* **33**, 4545–4554 (2000).
 80. Watanabe, A., Kojima, M., Ishihara, K. & Nakabayashi, N. [Interaction of platelets and cultured cells with polymers containing phospholipid polar groups]. *Tokyo Ika Shika Daigaku Iyo Kizai Kenkyusho Hokoku* **23**, 31–39 (1989).
 81. West, S. L. *et al.* The biocompatibility of crosslinkable copolymer coatings containing sulfobetaines and phosphobetaines. *Biomaterials* **25**, 1195–1204 (2004).
 82. Galvin, C. J. & Genzer, J. Progress in Polymer Science. *Prog Polym Sci* **37**, 871–906 (2012).
 83. Goldman, A. S., Glassner, M., Inglis, A. J. & Barner-Kowollik, C. Post-Functionalization of Polymers via Orthogonal Ligation Chemistry. *Macromol Rapid Comm* **34**, 810–849 (2013).
 84. Wang, H., Ren, J., Hlaing, A. & Yan, M. Fabrication and anti-fouling properties of photochemically and thermally immobilized poly(ethylene oxide) and low molecular weight poly(ethylene glycol) thin films. *J Colloid Interf Sci* **354**, 160–167 (2011).
 85. Labbe, G. Decomposition And Addition Reactions Of Organic Azides. *Chem Rev* **69**, 345–& (1969).
 86. Scriven, E. Azides and nitrenes: reactivity and utility. (1984).
 87. Brase, S., Gil, C., Knepper, K. & Zimmermann, V. Organic azides: An exploding diversity of a unique class of compounds. *Angew Chem Int Edit* **44**, 5188–5240 (2005).
 88. Keana, J. F. & Xiong Cai, S. Functionalized perfluorophenyl azides: New reagents for photoaffinity labeling. *Journal of Fluorine Chemistry* **43**, 151–154 (1989).
 89. Keana, J. & Cai, S. X. New Reagents For Photoaffinity-Labeling - Synthesis And Photolysis Of Functionalized Perfluorophenyl Azides. *J Org Chem* **55**, 3640–3647 (1990).
 90. Baruah, H., Puthenveetil, S., Choi, Y.-A., Shah, S. & Ting, A. Y. An Engineered Aryl Azide Ligase for Site-Specific Mapping of Protein-Protein Interactions through Photo-Cross-Linking. *Angew Chem Int Edit* **47**, 7018–7021 (2008).
 91. Bräse, S. & Banert, K. Organic Azides: Syntheses and Applications. (2010).
 92. Callow, J. A. & Callow, M. E. The Ulva Spore Adhesive System. 1–16 (2006).
 93. Tian, W. J., Zhang, H. Y. & Shen, J. C. Some properties of interfaces between metals and polymers. *Surface Review and Letters* **4**, 703–708 (1997).
 94. Rodriguez Emmenegger, C. *et al.* Interaction of Blood Plasma with Antifouling Surfaces. *Langmuir* **25**, 6328–6333 (2009).

95. Murata, H., Chang, B. J., Prucker, O., Dahm, M. & Ruhe, J. Polymeric coatings for biomedical devices. *Surf Sci* **570**, 111–118 (2004).
96. Ozaydin-Ince, G., Coclite, A. M. & Gleason, K. K. CVD of polymeric thin films: applications in sensors, biotechnology, microelectronics/organic electronics, microfluidics, MEMS, composites and membranes. *Rep. Prog. Phys.* **75**, 016501 (2011).
97. Correa, D. S., Medeiros, E. S., Oliveira, J. E., Paterno, L. G. & Mattoso, L. H. C. Nanostructured Conjugated Polymers in Chemical Sensors: Synthesis, Properties and Applications. *J Nanosci Nanotechnol* **14**, 6509–6527 (2014).
98. Shao, Q. *et al.* High-Performance and Tailorable Pressure Sensor Based on Ultrathin Conductive Polymer Film. *Small* **10**, 1466–1472 (2014).
99. Focke, M. *et al.* Lab-on-a-Foil: microfluidics on thin and flexible films. *Lab Chip* **10**, 1365 (2010).
100. Heremans, P., Cheyns, D. & Rand, B. P. Strategies for Increasing the Efficiency of Heterojunction Organic Solar Cells: Material Selection and Device Architecture. *Accounts of chemical research* **42**, 1740–1747 (2009).
101. Rohwerder, M., Grundmeier, G. & Stratmann, M. Corrosion prevention by adsorbed organic monolayers and ultrathin plasma polymer films. *Corrosion Technology-New York And Basel-* **17**, 479–528 (2002).
102. Bielecki, R. M., Doll, P. & Spencer, N. D. Ultrathin, Oil-Compatible, Lubricious Polymer Coatings: A Comparison of Grafting-To and Grafting-From Strategies. *Tribol Lett* **49**, 273–280 (2012).
103. Yin, H. Thermal And Dynamic Glass Transition In Ultrathin Films Of Homopolymers And A Miscible Polymer Blend. *PhD thesis* (2014).
104. Mukherjee, M., Chebil, M. S., Delorme, N. & Gibaud, A. Power law in swelling of ultra-thin polymer. *Polymer* **54**, 4669–4674 (2013).
105. Kuhn, W. Über die gestalt fadenförmiger moleküle in lösungen. *Kolloid-Zeitschrift* **68**, 2–15 (1934).
106. Teraoka, I. Models of Polymer Chains. *Polymer Solutions: An Introduction to Physical ...*
107. Flory, P. J. Principles of polymer chemistry. (1953).
108. Huggins, M. L. Some Properties of Solutions of Long-chain Compounds. *The Journal of Physical Chemistry* **46**, 151–158 (1942).
109. Schmid, F. Theory and simulation of multiphase polymer systems. *Handbook of Multiphase Polymer Systems* 31–80 (2011).
110. Goodwin, J. Colloids and interfaces with surfactants and polymers. (2009).
111. Jenckel, E. & Rumbach, B. Über die Adsorption von hochmolekularen Stoffen aus der Lösung. *Zeitschrift für Elektrochemie und angewandte physikalische Chemie* **55**, 612–618 (1951).
112. Currie, E., Norde, W. & Stuart, M. Tethered polymer chains: surface chemistry

- and their impact on colloidal and surface properties. *Adv Colloid Interfac* **100**, 205–265 (2003).
113. Rhe, J. Polymer brushes: on the way to tailor-made surfaces. *Polymer Brushes* 1–31 (2004).
 114. Szleifer, I. Protein adsorption on tethered polymer layers: effect of polymer chain architecture and composition. *Physica A* **244**, 370–388 (1997).
 115. He, G.-L., Merlitz, H., Sommer, J.-U. & Wu, C.-X. Static and Dynamic Properties of Polymer Brushes at Moderate and High Grafting Densities: A Molecular Dynamics Study. *Macromolecules* **40**, 6721–6730 (2007).
 116. Tsujii, Y., Ohno, K., Yamamoto, S., Goto, A. & Fukuda, T. Structure and properties of high-density polymer brushes prepared by surface-initiated living radical polymerization. *Adv Polym Sci* **197**, 1–45 (2006).
 117. Jhaveri, S. B., Beinhoff, M., Hawker, C. J., Carter, K. R. & Sogah, D. Y. Chain-End Functionalized Nanopatterned Polymer Brushes Grown via Nitroxide Free Radical Exchange. *Acs Nano* **2**, 719–727 (2008).
 118. Elias, V. H. G. Konstitution und lsungeigenschaften von makromoleklen. I. ermittlung von Θ -lsungen. *Die Makromolekulare Chemie* **50**, 1–19 (1961).
 119. Minko, S. Responsive polymer brushes. *Polym Rev* **46**, 397–420 (2006).
 120. Nalam, P. C. *Polymer Brushes in Aqueous Solvent Mixtures: Impact of Polymer Conformation on Tribological Properties*. 1–188 (PhD Thesis, 2012).
 121. (null), (null) & Braun, P. V. Solvent Quality Effects on Scaling Behavior of Poly(methyl methacrylate) Brushes in the Moderate- and High-Density Regimes. *Langmuir* **27**, 3698–3702 (2011).
 122. Xue, C. *et al.* Protein Adsorption on Poly(N-isopropylacrylamide) Brushes: Dependence on Grafting Density and Chain Collapse. *Langmuir* **27**, 8810–8818 (2011).
 123. Cheesman, B. T. *et al.* Polyelectrolyte brush pH-response at the silica–aqueous solution interface: a kinetic and equilibrium investigation. *Phys. Chem. Chem. Phys.* **15**, 14502 (2013).
 124. Kobayashi, M., Terayama, Y., Kikuchi, M. & Takahara, A. Chain dimensions and surface characterization of superhydrophilic polymer brushes with zwitterion side groups. *Soft Matter* **9**, 5138 (2013).
 125. Huang, N.-P. *et al.* Poly(L-lysine)- g-poly(ethylene glycol) Layers on Metal Oxide Surfaces: Surface-Analytical Characterization and Resistance to Serum and Fibrinogen Adsorption. *Langmuir* **17**, 489–498 (2001).
 126. Pasche, S. Mechanisms of Protein Resistance of Adsorbed PEG-graft Copolymers. *PhD thesis* 1–243 (2008).
 127. Roosjen, A., Van Der Mei, H. C., Busscher, H. J. & Norde, W. Microbial Adhesion to Poly(ethylene oxide) Brushes: Influence of Polymer Chain Length and Temperature. *Langmuir* **20**, 10949–10955 (2004).
 128. Zhao, C., Li, L., Wang, Q., Yu, Q. & Zheng, J. Effect of Film Thickness on the

- Antifouling Performance of Poly(hydroxy-functional methacrylates) Grafted Surfaces. *Langmuir* **27**, 4906–4913 (2011).
129. Chen, C. S. Geometric Control of Cell Life and Death. *Science* **276**, 1425–1428 (1997).
 130. Otsuka, H. Nanofabrication of Nonfouling Surfaces for Micropatterning of Cell and Microtissue. *Molecules* **15**, 5525–5546 (2010).
 131. Orski, S. V., Fries, K. H., Sontag, S. K. & Locklin, J. Fabrication of nanostructures using polymer brushes. *J Mater Chem* **21**, 14135–14149 (2011).
 132. Xu, F. J., Kang, E. T. & Neoh, K. G. Resist-free micropatterning of binary polymer brushes on Si(100) via surface-initiated living radical polymerizations. *J Mater Chem* **16**, 2948 (2006).
 133. Xu, F. J. *et al.* Controlled Micropatterning of a Si(100) Surface by Combined Nitroxide-Mediated and Atom Transfer Radical Polymerizations. *Macromolecules* **38**, 6254–6258 (2005).
 134. Sterner, O. *et al.* Photochemically Prepared, Two-Component Polymer-Concentration Gradients. *Langmuir* **29**, 13031–13041 (2013).
 135. Wang, X., Tu, H., Braun, P. V. & Bohn, P. W. Length Scale Heterogeneity in Lateral Gradients of Poly(N-isopropylacrylamide) Polymer Brushes Prepared by Surface-Initiated Atom Transfer Radical Polymerization Coupled with In-Plane Electrochemical Potential Gradients. *Langmuir* **22**, 817–823 (2006).
 136. Hucknall, A. *et al.* Versatile synthesis and micropatterning of nonfouling polymer brushes on the wafer scale. *Biointerphases* **4**, FA50 (2009).
 137. Yang, W. J., Neoh, K.-G., Kang, E.-T., Teo, S. L.-M. & Rittschof, D. Progress in Polymer Science. *Prog Polym Sci* **39**, 1017–1042 (2014).
 138. O’Shaughnessy, B. & Vavylonis, D. Non-equilibrium in adsorbed polymer layers. *J. Phys.: Condens. Matter* **17**, R63–R99 (2005).
 139. Pavluchina, S. & Sukhishvili, S. Polymer Adsorption. *Encyclopedia Of Polymer Science and Technology* (2010).
 140. Van de Steeg, H. G., Cohen Stuart, M. A., De Keizer, A. & Bijsterbosch, B. H. Polyelectrolyte adsorption: a subtle balance of forces. *Langmuir* **8**, 2538–2546 (1992).
 141. Szilagyi, I., Trefalt, G., Tiraferri, A., Maroni, P. & Borkovec, M. Polyelectrolyte adsorption, interparticle forces, and colloidal aggregation. *Soft Matter* **10**, 2479 (2014).
 142. Tredgold, R. H. The physics of Langmuir-Blodgett films. *Rep. Prog. Phys.* **50**, 1609 (1987).
 143. Hagting, J. G., de Vos, R. E. T. P., Sinkovics, K., Vorenkamp, E. J. & Schouten, A. J. Langmuir–Blodgett Mono- and Multilayers of (Di)alkoxy-Substituted Poly(p-phenylenevinylene) Precursor Polymers. 1. Langmuir Monolayers of Homo- and Copolymers of (Di)alkoxy-Substituted Precursor PPVs. *Macromolecules* **32**, 3930–3938 (1999).

144. Hussain, S. A. Langmuir-Blodgett Films a unique tool for molecular electronics. *arXiv* (2009).
145. Delamarche, E. & Michel, B. Structure and stability of self-assembled monolayers. *Thin Solid Films* **273**, 54–60 (1996).
146. Raman, A. *et al.* Understanding Organic Film Behavior on Alloy and Metal Oxides. *Langmuir* **26**, 1747–1754 (2010).
147. Laibinis, P. E., Hickman, J. J., Wrighton, M. S. & Whitesides, G. M. Orthogonal self-assembled monolayers: alkanethiols on gold and alkane carboxylic acids on alumina. *Science* **245**, 845–847 (1989).
148. Schwartz, D. K. Mechanisms and kinetics of self-assembled monolayer formation. *Annu Rev Phys Chem* **52**, 107–137 (2001).
149. Newton, L., Slater, T., Clark, N. & Vijayaraghavan, A. Self assembled monolayers (SAMs) on metallic surfaces (gold and graphene) for electronic applications. *J. Mater. Chem. C* **1**, 376 (2012).
150. Gooding, J. J., Mearns, F., Yang, W. & Liu, J. Self-assembled monolayers into the 21st century: recent advances and applications. *Electroanalysis* **15**, 81–96 (2003).
151. Yan, X. *et al.* Reduction of friction at oxide interfaces upon polymer adsorption from aqueous solutions. *Langmuir* **20**, 423–428 (2004).
152. Senaratne, W., Andruzzi, L. & Ober, C. Self-assembled monolayers and polymer brushes in biotechnology: Current applications and future perspectives. *Biomacromolecules* **6**, 2427–2448 (2005).
153. Ulman, A. Formation and Structure of Self-Assembled Monolayers. *Chem Rev* **96**, 1533–1554 (1996).
154. Advincula, R. C. & Knoll, W. A Perspective and Introduction to Organic and Polymer Ultrathin Films: Deposition, Nanostructuring, Biological Function, and Surface Analytical Methods. *Functional Polymer Films* (2012).
155. Decher, G. Fuzzy Nanoassemblies: Toward Layered Polymeric Multicomposites. *Science* **277**, 1232–1237 (1997).
156. Kumara, M. T., Tripp, B. C. & Muralidharan, S. Layer-by-Layer Assembly of Bioengineered Flagella Protein Nanotubes. *Biomacromolecules* **8**, 3718–3722 (2007).
157. Berndt, P., Kurihara, K. & Kunitake, T. Adsorption of poly (styrenesulfonate) onto an ammonium monolayer on mica: a surface forces study. *Langmuir* **8**, 2486–2490 (1992).
158. Ariga, K., Hill, J. P. & Ji, Q. Layer-by-layer assembly as a versatile bottom-up nanofabrication technique for exploratory research and realistic application. *Phys. Chem. Chem. Phys.* **9**, 2319 (2007).
159. Ariga, K., Nakanishi, T. & Michinobu, T. Immobilization of Biomaterials to Nano-Assembled Films (Self-Assembled Monolayers, Langmuir-Blodgett Films, and Layer-by-Layer Assemblies) and Their Related Functions. *J Nanosci*

- Nanotechno* **6**, 2278–2301 (2006).
160. Bel-Hassen, R., Boufi, S., Salon, M.-C. B., Abdelmouleh, M. & Belgacem, M. N. Adsorption of silane onto cellulose fibers. II. The effect of pH on silane hydrolysis, condensation, and adsorption behavior. *J Appl Polym Sci* **108**, 1958–1968 (2008).
 161. Yang, Y., Bittner, A. M., Baldelli, S. & Kern, K. Study of self-assembled triethoxysilane thin films made by casting neat reagents in ambient atmosphere. *Thin Solid Films* **516**, 3948–3956 (2008).
 162. Arkles, B., Steinmetz, J. R. & Zazyczny, J. *Factors Contributing to the stability of alkoxysilanes in aqueous solution*. 91–104 (Silanes and Other Coupling Agents, 1992).
 163. Waite, J. H., Andersen, N. H., Jewhurst, S. & Sun, C. Mussel adhesion: finding the tricks worth mimicking. *The journal of adhesion* **81**, 297–317 (2005).
 164. Fan, X., Lin, L., Dalsin, J. L. & Messersmith, P. B. Biomimetic anchor for surface-initiated polymerization from metal substrates. *J Am Chem Soc* **127**, 15843–15847 (2005).
 165. Raymond, K. N., Dertz, E. A. & Kim, S. S. Enterobactin: an archetype for microbial iron transport. *P Natl Acad Sci Usa* **100**, 3584–3588 (2003).
 166. Zürcher, S. *et al.* Biomimetic Surface Modifications Based on the Cyanobacterial Iron Chelator Anachelin. *J Am Chem Soc* **128**, 1064–1065 (2006).
 167. Mosca, P. J., Lin, H. B. & Hamlin, J. L. Mimosine, a novel inhibitor of DNA replication, binds to a 50 kDa protein in Chinese hamster cells. *Nucleic Acids Res.* **23**, 261–268 (1995).
 168. Connor, P. A., Dobson, K. D. & McQuillan, A. J. New sol-gel attenuated total reflection infrared spectroscopic method for analysis of adsorption at metal oxide surfaces in aqueous solutions. Chelation of TiO₂, ZrO₂, and Al₂O₃ surfaces by catechol, 8-quinolinol, and acetylacetone. *Langmuir* **11**, 4193–4195 (1995).
 169. Gulley-Stahl, H. *et al.* Surface Complexation of Catechol to Metal Oxides: An ATR-FTIR, Adsorption, and Dissolution Study. *Environ Sci Technol* **44**, 4116–4121 (2010).
 170. Sever, M. J., Weisser, J. T., Monahan, J., Srinivasan, S. & Wilker, J. J. Metal-Mediated Cross-Linking in the Generation of a Marine-Mussel Adhesive. *Angew Chem Int Edit* **43**, 448–450 (2004).
 171. Malisova, B., Tosatti, S., Textor, M., Gademann, K. & Zuercher, S. Poly(ethylene glycol) Adlayers Immobilized to Metal Oxide Substrates Through Catechol Derivatives: Influence of Assembly Conditions on Formation and Stability. *Langmuir* **26**, 4018–4026 (2010).
 172. Cropek, D., Kemme, P. A., Makarova, O. V., Chen, L. X. & Rajh, T. Selective Photocatalytic Decomposition of Nitrobenzene Using Surface Modified TiO₂ Nanoparticles. *J. Phys. Chem. C* **112**, 8311–8318 (2008).
 173. Wehlauch, R., Hoecker, J. & Gademann, K. Nitrocatechols as Tractable Surface Release Systems. *ChemPlusChem* **77**, 1071–1074 (2012).

174. Gillich, T. Self-Organization of Catechol -Functionalized Dendrons for the Creation of Non-Interactive, Antifouling Bointerfaces in 2D and 3D. *PhD thesis* 1–289 (2012).
175. Malisova, B. Polymer Immobilization to Metal Oxide Substrates through Catechol Derivatives as Surface Anchors. *PhD thesis* 1–147 (2010).
176. Rodenstein, M., Zuercher, S., Tosatti, S. G. P. & Spencer, N. D. Fabricating Chemical Gradients on Oxide Surfaces by Means of Fluorinated, Catechol-Based, Self-Assembled Monolayers. *Langmuir* **26**, 16211–16220 (2010).
177. Li, S.-C. & Diebold, U. Direction-dependent intermolecular interactions: catechol on TiO₂ (110)-1×1. 73960P–73960P–7 (2009).
178. Martin, S. T., Kesselman, J. M., Park, D. S., Lewis, N. S. & Hoffmann, M. R. Surface structures of 4-chlorocatechol adsorbed on titanium dioxide. *Environ Sci Technol* **30**, 2535–2542 (1996).
179. Li, S.-C. *et al.* Correlation between Bonding Geometry and Band Gap States at Organic–Inorganic Interfaces: Catechol on Rutile TiO₂(110). *J Am Chem Soc* **131**, 980–984 (2009).
180. (null) *et al.* Influence of alkyl chain length on phosphate self-assembled monolayers. *Langmuir* **23**, 8053–8060 (2007).
181. Gao, W., Dickinson, L., Grozinger, C., Morin, F. G. & Reven, L. Self-assembled monolayers of alkylphosphonic acids on metal oxides. *Langmuir* **12**, 6429–6435 (1996).
182. Michel, R. *et al.* Selective Molecular Assembly Patterning: A New Approach to Micro- and Nanochemical Patterning of Surfaces for Biological Applications. *Langmuir* **18**, 3281–3287 (2002).
183. Yoo, M. *et al.* Facile Synthesis of Thermally Stable Core–Shell Gold Nanoparticles via Photo-Cross-Linkable Polymeric Ligands. *Macromolecules* **43**, 3570–3575 (2010).
184. Pöttsch, R. & Voit, B. Thermal and Photochemical Crosslinking of Hyperbranched Polyphenylene With Organic Azides. *Macromol Rapid Comm* **33**, 635–639 (2012).
185. Yan, M. & Ren, J. Covalent Immobilization of Ultrathin Polymer Films by Thermal Activation of Perfluorophenyl Azide. *Chem. Mater.* **16**, 1627–1632 (2004).
186. Yang, H., Lazos, D. & Ulbricht, M. Thin, highly crosslinked polymer layer synthesized via photoinitiated graft copolymerization on a self-assembled-monolayer-coated gold surface. *J Appl Polym Sci* **97**, 158–164 (2005).
187. Chen, Y. L. & Rånby, B. Photocrosslinking of polyethylene. I. Photoinitiators, crosslinking agent, and reaction kinetics. *J Polym Sci Pol Chem* **27**, 4051–4075 (1989).
188. Yoon, U. C. *et al.* Applications of Phthalimide Photochemistry to Macrocyclic Polyether, Polythioether, and Polyamide Synthesis. *J Org Chem* **66**, 939–943 (2001).

189. Chae, K. H., Cho, H. I., Kim, Y. H. & Yang, U. C. *European Polymer Journal. Eur Polym J* **48**, 1186–1194 (2012).
190. Lancaster, J. A. *A 'Toolkit' of Small Molecules for Polymer Assembly and Post-Synthetic Modification Using "Click" and Photoactive Chemistries*. 1–237 (PhD Thesis, 2011).
191. Claude, R. T. A. Rapid crystal growth of benzophenone by low temperature solution growth and its characterization. *Archives of Applied Science Research* **4**, 898–905 (2012).
192. Kestur, U. S. *et al.* Effects of the Molecular Weight and Concentration of Polymer Additives, and Temperature on the Melt Crystallization Kinetics of a Small Drug Molecule. *Crystal Growth & Design* **10**, 3585–3595 (2010).
193. Horspool, W. M. & Lenci, F. *CRC Handbook of Organic Photochemistry and Photobiology, Volumes 1 & 2*. (2010).
194. Hermanson, G. T. *Bioconjugate techniques*. (2013).
195. Park, H., Park, K. & Shalaby, W. S. *Biodegradable hydrogels for drug delivery*. (2011).
196. Ismaili, H., Lee, S. & Workentin, M. S. Diazirine-Modified Gold Nanoparticle: Template for Efficient Photoinduced Interfacial Carbene Insertion Reactions. *Langmuir* **26**, 14958–14964 (2010).
197. Platz, M. S. Comparison of phenylcarbene and phenylnitrene. *Accounts of chemical research* **28**, 487–492 (1995).
198. Saxer, S. *Ultrathin, Non-fouling Coatings Exploiting Biomimetic Surface Anchorage Concepts - A Combination of Electrostatic & Coordinative Binding Mechanisms. PhD thesis* 1–150 (2011).
199. Zoulalian, V. *Functionalization of Titanium Oxide Surfaces By means of Poly(Alkyl-Phosphonate) Polymers. PhD thesis* 1–309 (2008).
200. Mayer, C. *Poly(alkyl-phosphonates), a modular approach to functionalization of surfaces. PhD thesis* 1–330 (2012).
201. Serrano, Â. *et al.* Nonfouling Response of Hydrophilic Uncharged Polymers. *Adv. Funct. Mater.* **23**, 5706–5718 (2013).
202. Cordeiro, A. L. *et al.* Temperature dependent physicochemical properties of poly(N-isopropylacrylamide-co-N-(1-phenylethyl) acrylamide) thin films. *Soft Matter* **5**, 1367–1377 (2009).
203. Zürcher, S., Tosatti, S., Dorcier, A., Fusco, S. & Lopez, I. Adhesion promoter based on a functionalized macromolecule comprising photoreactive groups. *Patent EP2236524, October* **6**, (2010).
204. Pranzetti, A. *et al.* Model organic surfaces to probe marine bacterial adhesion kinetics by surface plasmon resonance. *Adv. Funct. Mater.* **22**, 3672–3681 (2012).
205. Thome, I. *et al.* Conditioning of surfaces by macromolecules and its implication for the settlement of zoospores of the green alga *Ulva linza*. *Biofouling* **28**, 501–

- 510 (2012).
206. Ramos, J. J. I. & Moya, S. E. Water content of hydrated polymer brushes measured by an in situ combination of a quartz crystal microbalance with dissipation monitoring and spectroscopic ellipsometry. *Macromol Rapid Comm* **32**, 1972–1978 (2011).
 207. Höök, F. *et al.* Variations in Coupled Water, Viscoelastic Properties, and Film Thickness of a Mefp-1 Protein Film during Adsorption and Cross-Linking: A Quartz Crystal Microbalance with Dissipation Monitoring, Ellipsometry, and Surface Plasmon Resonance Study. *Anal Chem* **73**, 5796–5804 (2001).
 208. Hartung, W., Drobek, T., Lee, S., Zuercher, S. & Spencer, N. D. The influence of anchoring-group structure on the lubricating properties of brush-forming graft copolymers in an aqueous medium. *Tribol Lett* **31**, 119–128 (2008).
 209. Pincus, P. Colloid stabilization with grafted polyelectrolytes. *Macromolecules* **24**, 2912–2919 (1991).
 210. Greene, G., Yao, G. & Tannenbaum, R. Deposition and Wetting Characteristics of Polyelectrolyte Multilayers on Plasma-Modified Porous Polyethylene. *Langmuir* **20**, 2739–2745 (2004).
 211. Feuz, L., Leermakers, F. A. M., Textor, M. & Borisov, O. Adsorption of Molecular Brushes with Polyelectrolyte Backbones onto Oppositely Charged Surfaces: A Self-Consistent Field Theory. *Langmuir* **24**, 7232–7244 (2008).
 212. Matsuda, T., Smith, G., Winkler, R. & Yoon, D. Stochastic Dynamics Simulations Of N-Alkane Melts Confined Between Solid-Surfaces - Influence Of Surface-Properties And Comparison With Scheutjens-Fleer Theory. *Macromolecules* **28**, 165–173 (1995).
 213. Iyer, K. & Luzinov, I. Effect of macromolecular anchoring layer thickness and molecular weight on polymer grafting. *Macromolecules* **37**, 9538–9545 (2004).
 214. Jones, R. L., Spontak, R. J., (null) & (null). Effect Of Chain-Length And Surface-Density On Looped Polymers Grafted To An Impenetrable Surface. *J Chem Phys* **103**, 5137–5143 (1995).
 215. Fritsche, M., Heermann, D. W., Dutra, M. & Cordeiro, C. E. Conformational and Dynamical Properties of the Isolated, Three-Dimensional Single- and Double-Tethered Polymer Chain on an Infinite Surface. *Macromol. Theory Simul.* **19**, 440–448 (2010).
 216. McMahan, S. A. & Burgess, R. R. Use of Aryl Azide Cross-Linkers To Investigate Protein-Protein Interactions: An Optimization of Important Conditions as Applied to Escherichia coli RNA Polymerase and Localization of a. sigma. 70-. alpha. Cross-Link to the C-Terminal Region of. alpha. *Biochemistry* **33**, 12092–12099 (1994).
 217. Griffin, R. J. 3 The Medicinal Chemistry of the Azido Group. *Progress in medicinal chemistry* **31**, 121 (1994).
 218. Schilp, S. *et al.* Settlement and adhesion of algal cells to hexa(ethylene glycol)-containing self-assembled monolayers with systematically changed wetting

- properties. *Biointerphases* **2**, 143 (2007).
219. Samuelsson, M. O. & Kirchman, D. L. Degradation of adsorbed protein by attached bacteria in relationship to surface hydrophobicity. *Appl Environ Microbiol* **56**, 3643–3648 (1990).
220. Wiencek, K. M. & Fletcher, M. Bacterial Adhesion To Hydroxyl-Terminated And Methyl-Terminated Alkanethiol Self-Assembled Monolayers. *J Bacteriol* **177**, 1959–1966 (1995).
221. Ederth, T. *et al.* Resistance of galactoside-terminated alkanethiol self-assembled monolayers to marine fouling organisms. *Acs Appl Mater Inter* **3**, 3890–3901 (2011).
222. Liu, C. & Zhao, Q. The CQ ratio of surface energy components influences adhesion and removal of fouling bacteria. *Biofouling* **27**, 275–285 (2011).
223. Argibay, N., Perrino, C., Rimann, M., Lee, S. & Spencer, N. D. Bacterially induced degradation of aqueous solutions of poly(l-lysine)- graft-poly(ethylene glycol) and poly(l-lysine)- graft-dextran: consequences for their lubrication properties. *Lubrication Science* **21**, 415–425 (2009).
224. Eberhardt, M. & Theato, P. RAFT polymerization of pentafluorophenyl methacrylate: preparation of reactive linear diblock copolymers. *Macromol Rapid Comm* **26**, 1488–1493 (2005).
225. Durmaz, F. A Modular Approach to Functional Self-Assembled Monolayers. *PhD thesis* 1–140 (2010).
226. Fournier, D., Hoogenboom, R. & Schubert, U. S. Clicking polymers: a straightforward approach to novel macromolecular architectures. *Chem Soc Rev* **36**, 1369–1380 (2007).
227. Lowe, A. B. Thiol-ene ‘click’ reactions and recent applications in polymer and materials synthesis. *Polym. Chem.* **1**, 17–36 (2010).
228. Kakuchi, R. & Theato, P. Post-polymerization Modifications via Active Esters. *Functional Polymers by Post-Polymerization Modification: Concepts, Guidelines and Applications* (2013).
229. Eberhardt, M., Mruk, R., Zentel, R. & Theato, P. Synthesis of pentafluorophenyl(meth)acrylate polymers: New precursor polymers for the synthesis of multifunctional materials. *Eur Polym J* **41**, 1569–1575 (2005).
230. Moad, G., Rizzardo, E. & Thang, S. Living radical polymerization by the RAFT process. *Aust J Chem* **58**, 379–410 (2005).
231. Moad, G., Rizzardo, E. & Thang, S. H. Living Radical Polymerization by the RAFT Process - A Second Update. *Aust J Chem* **62**, 1402–1472 (2009).
232. Rizzardo, E. *et al.* RAFT Polymerization: Adding to the Picture. *Macromol. Symp.* **248**, 104–116 (2007).
233. Walker, L. C. P. RAFT – choosing the right agent. *CSIRO Materials Science and Engineering* 1–19 (2012).
234. Perrier, S. & Haddleton, D. M. In Situ NMR Monitoring of Living Radical

- Polymerization. 125–146 (2003).
235. Quek, J. Y., Roth, P. J., Evans, R. A., Davis, T. P. & Lowe, A. B. Reversible addition–fragmentation chain transfer synthesis of amidine-based, CO₂-responsive homo and AB diblock (Co) polymers comprised of histamine and their gas-triggered self-assembly in water. *J Polym Sci Pol Chem* **51**, 394–404 (2013).
 236. Tonelli, A. E. & White, J. L. NMR spectroscopy of Polymers. 359–383 (2007).
 237. Choi, J. *et al.* Functionalization and patterning of reactive polymer brushes based on surface reversible addition and fragmentation chain transfer polymerization. *J Polym Sci Pol Chem* **50**, 4010–4018 (2012).
 238. Nanci, A. *et al.* Chemical modification of titanium surfaces for covalent attachment of biological molecules. *J Biomed Mater Res* **40**, 324–335 (1998).
 239. Willcock, H. & O'Reilly, R. K. End group removal and modification of RAFT polymers. *Polym. Chem.* **1**, 149 (2010).
 240. Saxer, S. *et al.* Surface Assembly of Catechol-Functionalized Poly(L-lysine)-graft-poly(ethylene glycol) Copolymer on Titanium Exploiting Combined Electrostatically Driven Self-Organization and Biomimetic Strong Adhesion. *Macromolecules* **43**, 1050–1060 (2010).
 241. Neogi, P. Diffusion in polymers. **32**, (1996).
 242. George, S. C. & Thomas, S. Transport phenomena through polymeric systems. *Prog Polym Sci* **26**, 985–1017 (2001).
 243. Lienkamp, K., Kins, C. F., Alfred, S. F., Madkour, A. E. & Tew, G. N. Water-soluble polymers from acid-functionalized norbornenes. *J Polym Sci Pol Chem* **47**, 1266–1273 (2009).
 244. Sterner, O. *et al.* Delineating Fibronectin Bioadhesive Micropatterns by Photochemical Immobilization of PS and PVP. *Submitted* 1–39 (2014).
 245. Goren, T., Spencer, N. D. & Crockett, R. Impact of chain morphology on the lubricity of surface-grafted polysaccharides. *RSC Adv.* **4**, 21497 (2014).
 246. Nagaiyanallur, V. V., Kumar, D., Rossi, A., Zürcher, S. & Spencer, N. D. Tailoring SU-8 Surfaces: Covalent Attachment of Polymers by Means of Nitrene Insertion. *Langmuir* **30**, 10107–10111 (2014).
 247. Soshee, A., Zürcher, S., Spencer, N. D., Halperin, A. & Nizak, C. General In Vitro Method to Analyze the Interactions of Synthetic Polymers with Human Antibody Repertoires. *Biomacromolecules* **15**, 113–121 (2014).
 248. Vicente, J., Chicote, M. T., Abrisqueta, M. D., González-Herrero, P. & Guerrero, R. Recent advances in the chemistry of gold (I) complexes with C-, N- and S-donor ligands part I: alkynyl, amino, imino and nitrido derivatives. *Gold Bulletin* **31**, 83–87 (1998).
 249. Hofer, R., Textor, M. & Spencer, N. Alkyl phosphate monolayers, self-assembled from aqueous solution onto metal oxide surfaces. *Langmuir* **17**, 4014–4020 (2001).

250. Edwards, J. C. Principles of NMR. *Process NMR Associates LLC, 87A Sand Pit Rd, Danbury CT 6810*, (2009).
251. Macomber, R. S. A complete introduction to modern NMR spectroscopy. *Nova York* (1998).
252. Ernst, R. R., Bodenhausen, G. & Wokaun, A. Principles of nuclear magnetic resonance in one and two dimensions. (1991).
253. Mori, S. & Barth, H. G. Size exclusion chromatography. (1999).
254. Kirmse, W. Organic elemental analysis: Ultramicro, micro, and trace methods. (1983).
255. Smith, B. C. Fundamentals of Fourier transform infrared spectroscopy. (2011).
256. Woollam, J. A. *et al.* Overview of variable angle spectroscopic ellipsometry (VASE), part I: basic theory and typical applications. *SPIE, CR72* 3–28 (1999).
257. Johs, B. D. *et al.* Overview of variable-angle spectroscopic ellipsometry (VASE): II. Advanced applications. **1**, 29–58 (1999).
258. Fowkes, F. M. & Zisman, W. A. Contact angle, wettability, and adhesion. (1964).
259. Spori, D. M. Structural Influences on Self-cleaning Surfaces. *PhD thesis* 1–201 (2010).
260. Reilman, R. F., Msezane, A. & Manson, S. T. Relative intensities in photoelectron spectroscopy of atoms and molecules. *Journal of Electron Spectroscopy and Related Phenomena* **8**, 389–394 (1976).
261. Scofield, J. H. Hartree-Slater subshell photoionization cross-sections at 1254 and 1487 eV. *Journal of Electron Spectroscopy and Related Phenomena* **8**, 129–137 (1976).
262. Crobu, M., Rossi, A., Mangolini, F. & Spencer, N. D. Chain-length-identification strategy in zinc polyphosphate glasses by means of XPS and ToF-SIMS. *Anal Bioanal Chem* **403**, 1415–1432 (2012).
263. Briggs, D. & Grant, J. T. Surface analysis by Auger and X-ray photoelectron spectroscopy. (2003).
264. Vickerman, J. C. & Gilmore, I. S. Surface analysis: the principal techniques. **2**, (2009).
265. Watts, J. F. & Wolstenholme, J. An introduction to surface analysis by XPS and AES. *An Introduction to Surface Analysis by XPS and AES, by John F. Watts, John Wolstenholme, pp. 224. ISBN 0-470-84713-1. Wiley-VCH, May 2003.* **1**, (2003).
266. Rodahl, M. *et al.* Simultaneous frequency and dissipation factor QCM measurements of biomolecular adsorption and cell adhesion. *Faraday Disc.* **107**, 229–246 (1997).
267. Dixon, M. C. Quartz crystal microbalance with dissipation monitoring: enabling real-time characterization of biological materials and their interactions. *J Biomol Tech* **19**, 151–158 (2008).

268. Marx, K. A. Quartz Crystal Microbalance: A Useful Tool for Studying Thin Polymer Films and Complex Biomolecular Systems at the Solution–Surface Interface. *Biomacromolecules* **4**, 1099–1120 (2003).
269. Haensch, C., Hoepfener, S. & Schubert, U. S. Chemical modification of self-assembled silane based monolayers by surface reactions. *Chem Soc Rev* **39**, 2323 (2010).
270. Mashl, R. J., Grønbech-Jensen, N., Fitzsimmons, M. R., Lütt, M. & Li, D. Theoretical and experimental adsorption studies of polyelectrolytes on an oppositely charged surface. *J Chem Phys* **110**, 2219 (1999).
271. Gnauck, M. *et al.* Carboxy-Terminated Oligo(ethylene glycol)–Alkane Phosphate: Synthesis and Self-Assembly on Titanium Oxide Surfaces. *Langmuir* **23**, 377–381 (2007).
272. Li, S. C., Chu, L. N., Gong, X. Q. & Diebold, U. Hydrogen Bonding Controls the Dynamics of Catechol Adsorbed on a TiO₂(110) Surface. *Science* **328**, 882–884 (2010).
273. Roncaroli, F. & Blesa, M. A. Kinetics of adsorption of carboxylic acids onto titanium dioxide. *Phys. Chem. Chem. Phys.* **12**, 9938 (2010).
274. Dettin, M. *et al.* Covalent surface modification of titanium oxide with different adhesive peptides: Surface characterization and osteoblast-like cell adhesion. *J Biomed Mater Res* **90A**, 35–45 (2009).
275. Choi, C. H. J., Zuckerman, J. E., Webster, P. & Davis, M. E. Targeting kidney mesangium by nanoparticles of defined size. *P Natl Acad Sci Usa* **108**, 6656–6661 (2011).
276. Papadakis, C. M. *et al.* Micellar structure of amphiphilic poly(2-oxazoline) diblock copolymers. *J Appl Crystallogr* **40**, S361–S362 (2007).
277. (null), (null), (null) & (null). Protein interactions in covalently attached dextran layers. *Colloid Surface B* **13**, 325–336 (1999).
278. Lommerts, B. J. & Sikkema, D. J. Synthesis and Structure of a New Polyalcohol. *Macromolecules* **33**, 7950–7954 (2000).
279. Pei, J., Hall, H. & Spencer, N. D. Biomaterials. *Biomaterials* **32**, 8968–8978 (2011).
280. Vlugt-Wensink, K. D. F. *et al.* Modeling the release of proteins from degrading crosslinked dextran microspheres using kinetic Monte Carlo simulations. *J Control Release* **111**, 117–127 (2006).
281. Tillman, E. S., Contrella, N. D. & Leasure, J. G. Monitoring the nitroxide-mediated polymerization of styrene using gel permeation chromatography and proton NMR. *Journal of Chemical Education* **86**, 1424 (2009).
282. Schu, F. Controlled/living radical polymerization: progress in ATRP, NMP and RAFT: ACS symposium series no 768 Edited by: Krzysztof Matyjaszewski American Chemical Society, Washington, DC, September 2000 pp 484, price \$150.00 ISBN 0-8412-3707-7. *Polym. Int.* **51**, 370–370 (2002).

-
283. Craver, C. & Carraher, C. Applied polymer science: 21st century: 21st century. (2000).
 284. Barner-Kowollik, C. Handbook of RAFT polymerization. (2008).
 285. Krstina, J. *et al.* Narrow polydispersity block copolymers by free-radical polymerization in the presence of macromonomers. *Macromolecules* **28**, 5381–5385 (1995).
 286. Chiefari, J. *et al.* Living free-radical polymerization by reversible addition-fragmentation chain transfer: the RAFT process. *Macromolecules* **31**, 5559–5562 (1998).
 287. Zetterlund, P. B. Nitroxide-Mediated Radical Polymerization of Butyl Acrylate Using TEMPO: Improvement of Control Exploiting Nanoreactors? *Macromolecular Reaction Engineering* **4**, 663–671 (2010).
 288. Moad, G. *et al.* Living free radical polymerization with reversible addition-fragmentation chain transfer (the life of RAFT). *Polym. Int.* **49**, 993–1001 (2000).
 289. Qiu, J., Charleux, B. & Matyjaszewski, K. Controlled/living radical polymerization in aqueous media: homogeneous and heterogeneous systems. *Prog Polym Sci* **26**, 2083–2134 (2001).

List of Abbreviations

AIBN	Azobisisobutyronitrile
Al ₂ O ₃	Aluminium oxide
ASW	Artificial seawater
At.%	Atomic percent
ATRP	Atom transfer radical polymerization
BE	Binding energy
BSA	Bovine serum albumin
°C	Celsius degrees
CaCl ₂ ·2H ₂ O	Calcium chloride dihydrate
CDCl ₃	Deuterated chloroform
CH ₂ Cl ₂	Dichloromethane
⟨CL⟩	Average chain length
cm	Centimeter
COSY	Correlation Spectroscopy
CTA	Chain transfer agent
CTAB	Cetyl trimethylammonium bromide
<i>d</i>	Grafting density
D ₂ O	Deuterated water
dCA	Dynamic contact angle
DCM	Dichloromethane
DGTS	Deuterated triglycine sulfate
DHPAA	3,4-dihydroxyphenyl acetic acid

DMF	N,N-Dimethylformamide
DNA	Deoxyribonucleic acid
DOPA	3,4-dihydroxyphenylalanine
<i>DP</i>	Degree of polymerization
EA	Elemental analysis
<i>Eff</i>	Efficiency factor
EG	Ethylene glycol
EPS	Extracellular polymeric substances
eV	Electron volt
FRP	Free radical polymerization
FT-IR	Fourier transform infrared spectroscopy
FWHM	Full width at half maximum
<i>g</i>	Graft
g	Gram
GL	Gaussian line
GPC	Gel permeation chromatography
<i>h</i>	Dry thickness
HCl	Hydrochloride
HEPES	4-(2-hydroxyethyl)-1-piperazineethanesulfonic acid
ICP-AES	Inductively coupled plasma atomic emission spectroscopy
IEP	Isoelectric point
K ₂ CO ₃	Potassium carbonate
KBr	Potassium bromide
KCl	Potassium chloride
kDa	Kilo Dalton
<i>L</i>	Distance between anchoring sites

LB	Langmuir-Blodgett films
LbL	Layer-by-layer
L_{id}	Average distance between attachment points
LL	Average loop length
M	Molar
m	Mass
mbar	Millibar
mg	Miligram
$MgCl_2 \cdot 6H_2O$	Magnesium chloride hexahydrate
MHz	Megahertz (10^6 s^{-1})
min	Minute
mL	Milliliter
mm	Millimeter
mM	Millimolar
mmol	Millimole
M_n	Number average molecular weight
mPEG	Methoxy terminated poly(ethylene glycol)
M_r	Relative molecular weight
M_w	Absolute molecular weight (g mol^{-1})
MWCO	Molecular weight cut-off
N	Number of segments along a polymer chain
Na_2SO_4	Sodium sulphate
NaCl	Sodium chloride
NaOH	Sodium hydroxide
N_{Av}	Avogadro number
Nb_2O_5	Niobium oxide (niobia)

List of Abbreviations

ng	Nanogram
NHS	<i>N</i> -Hydroxysuccinimide
nm	Nanometer
NMP	Nitroxide-mediated polymerization
NMR	Nuclear magnetic resonance
OD	Optical density
OEG	Oligo(ethylene glycol)
p	p-value
Pa	Pascal (1 kg/(m·s ²))
PAA	Poly(acrylic acid)
PAAm	Polyallylamine
PDI	Polydispersity Index
PEG	Poly(ethylene glycol)
PEOXA	Poly(2-ethyl-2-oxazoline)
PFPA	Perfluorophenyl azide
PFPAc	Pentafluorophenyl acrylate
pKa	Acid dissociation constant
PLL	Poly-L-lysine
ppb	Parts per billion
PPFPAc	Poly(pentafluorophenyl acrylate)
ppm	Parts per million
PVA	Poly(vinyl alcohol)
PVP	Poly(vinylpyrrolidone)
QCM-D	Quartz crystal microbalance with dissipation
RAFT	Reversible addition–fragmentation transfer

R_c	Coiled radius
R_g	Radius of gyration
rpm	Rotations per minute
RSF	Relative sensitivity factor
s	Second
SAM	Self-assembled monolayer
SDS	Sodium dodecyl sulphate
SiO_2	Silicon oxide
Ta_2O_5	Tantalum oxide
THF	Tetrahydrofuran
TiO_2	Titanium oxide (titania)
UV	Ultraviolet
UV-C	Ultraviolet C (100 – 280 nm)
v	Volume
VASE	Variable-angle spectroscopic ellipsometry
V_{sphere}	Volume of a sphere
W	Watt ($1 \text{ kg}\cdot\text{m}^2 \text{ s}^{-3}$)
w	Weight
XPS	X-ray photoelectron spectroscopy
ZrO_2	Zirconium oxide (zirconia)
ΔD	Dissipation change (QCM-D)
Δf	Frequency change (QCM-D)
μL	Microliter
μm	Micrometer
μM	Micromolar

Acknowledgements

This manuscript, but most importantly all that it entails, could not have been written without the crucial help and support of so many people that never, for one moment, hesitated in sharing their wisdom with me. Being it scientific, worldly or just miscellaneous.

Firstly I would like to thank the Holy Trinity of bosses I had throughout almost four and a half years: Nic, Samuele and Stefan. Besides the obvious and unquestionable scientific knowledge you all taught me there was always more than that. Nic for giving me the chance to learn under his wing and work with so many fantastic people, for his constant interest and for those amazing speed reading skills. I'm still fascinated. To Samuele for helping me thickening my skin, for teaching me to always look for the bigger picture, for pushing further my *story telling* skills and for Miglio. To Stefan whom I annoyed constantly and with no boundaries with (ir)relevant questions, who witnessed every embarrassing lab incident I committed and still could keep looking me in the eye afterwards. Thank you all for keeping the faith.

To the Seacoat network and all the fantastic interdisciplinary brainstorming that kept happening. Special thanks to the fellows Alice, Alessio, Stéphanie and Luigi for making me looking forward to our gatherings. Our late night socializing and insane conversations were nothing less than a true pleasure.

To Olof. You need a whole damn paragraph. I am not overemphasizing the importance you had in all of this when I say I would not be here if it wasn't for you. You were there throughout almost every low point I had inside and outside the lab and although I could've never asked this much, you were just simply there. You were a perfect project partner that easily became a good friend. I deeply thank you for everything. I still remember that first knock in those outstanding Kinderspital facilities: *Misery will always love company.*

To the astonishing multicultural platform that is LSST. Special mentions go to

Cathrein who never hesitated in giving me her friendship, Josephine for constantly applying her life saving techniques on my personal issues, Vikrant for always turning every conversation into a novelty (high expectations for the next one), Mirren and Nick whose unbeatable good mood I miss every single day, to Clément for always helping me out and greeting me with a smile, to Shiva for those incredible Bollywood moves, to Andrea for teaching me the importance of Mexican cats in my life, to Sara and her constantly available help (thank you for the abstract and do expect a couple of magic bottles towards your way), to Prathima for letting me annoy her so much with QCM related questions, to the older crowd Robert, Whitney, Maura, Chris, Bara and Christoph for being excellent companies in every possible social scenario. Thank you all that were and are now at LSST.

To the SuSoS crew Marcella, Rūdi, Mine, Sabine, Liz and Max for always bringing excellent mood (and dogs) to the work place.

To my portuguese *family* a heartfelt bow is mandatory. Making the decision of leaving all of Lisbon behind for so long was never an easy one. You made it a home I still count the hours to go back to. Now more than ever. To the incredible strength of amiga Ana, to the always inspirational Nixa, to the insanity of Mike, to the constant life improvements of Terra, to the shared nostalgia of Guedes, to the constant musical updates and *too honest* photographic skills of Bruno, to the timeless Joanhina, to everyone everyone every single one. Carlos, Ruiva, Gonçalo, Ana Neves, Marta, Rosa, Diana, Galvão, Paulinha, Ana Tomás, Ana Filipa, Metelo, Joana, Hugo, Duarte, Ritates, Ana Marta, Raquel, Aida and so many more. I will thank you soon and live.

To the *hard core* of this *family*: Maria, Trezinha, Loira e Vera, I can never explain, nor retribute, the importance you have had in my life for over 10 years. The blindly committed friendship, the unquestionable support, the mutual admiration, love and respect are above anything I have ever known. Thank you is not sufficient for consistently showing me that time and geography are irrelevant in a friendship. You are bigger than life and I can only hope this paragraph remains as actual in another 10 years time as it is now.

To Dani, Palma, Mário and Márcia for bringing me a little bit of home almost on a daily basis. Life is a whole lot better with you here.

Last but not least to my dear and gorgeous family: Lu, Toni and Bro. For always being there no matter what, for making me laugh even in the most difficult periods, for the 'initial' complaining but always accepting and supporting my choices. I do feel more is yet to come but maybe the worse is over. I can only say that right now all of this is yours.

Curriculum Vitae

Personal Information

Name	Ângela Serrano
Date of Birth	February 25, 1983
Nationality	Portuguese
Current Address	Zentralstrasse 153 CH-8003 Zürich Switzerland

Education

2010 - 2014	Doctoral student at SuSoS AG, Dübendorf, Switzerland and Laboratory for Surface Science and Technology, Materials Department, ETH Zürich, Zürich, Switzerland.
2007 - 2009	Master degree in Chemistry by Instituto Superior Técnico, University of Lisbon, Lisbon, Portugal.
2008 - 2009	Internship for the Master dissertation under Erasmus/Socrates Programme at Göteborgs Universitet, Göteborg, Sweden.
2001 - 2007	Bachelor degree in Chemistry by Instituto Superior Técnico, University of Lisbon, Lisbon, Portugal.

Working Experience

2014 - current	Researcher at SuSoS AG, Dübendorf, Switzerland.
2009 - 2010	Researcher at YDreams, Caparica, Portugal in the field of

electrochromic cells, nanomaterials and electronic devices.

Publications

2013 Photochemically Prepared, Two-Component Polymer-Concentration Gradients

Olof Sterner, Ângela Serrano, Sophie Mieszkin, Stefan Zürcher, Samuele Tosatti, Maureen E. Callow, James A. Callow, Nicholas D. Spencer, *Langmuir*; 2013; 29(42) pp 13031-13041.

2013 Nonfouling response of hydrophilic uncharged polymers

Ângela Serrano, Olof Sterner, Sophie Mieszkin, Stefan Zürcher, Samuele Tosatti, Maureen E. Callow, James A. Callow and Nicholas D. Spencer, *Advanced Functional Materials*; 2013; 23(46) pp 5706 – 5718.

2014 Functional Polymer

Ângela Serrano, Stefan Zürcher and Samuele Tosatti, patent PCT/EP2014/002453, submitted on 11/09/2014.

2014 Multimodal Binding of a Nonfouling Polymer

Ângela Serrano, Stefan Zürcher, Samuele Tosatti and Nicholas D. Spencer, *manuscript in preparation*.

Oral Presentations

2011 Development of a Comparative Protocol for Anti-Fouling Surfaces Based on Polymer Brushes

Ângela Serrano, Olof Sterner, Stefan Zürcher, Samuele Tosatti and Nicholas D. Spencer, AVS 58th International Symposium & Exhibition, Nashville, USA.

2012 Nonfouling response of hydrophilic uncharged polymers

Ângela Serrano, Olof Sterner, Sophie Mieszkin, Stefan Zürcher, Samuele Tosatti, Maureen E. Callow, James A. Callow and Nicholas D. Spencer, 16th ICMCF, Seattle, USA.

Poster Presentations

2011 Development of a Comparative Protocol for Nonfouling Surfaces Based on Polymer Brushes

Ângela Serrano, Olof Sterner, Stefan Zürcher, Samuele Tosatti and Nicholas D. Spencer, International Workshop ONR/SEACOAT, Las Vegas, USA.

Workshops/Advanced Training Courses (ATC)

2010	ATC1 Surface Engineering at University of Heidelberg, Germany.
2010	ATC2 Developments in Surface Analysis: <i>in situ</i> to <i>in vácuo</i> at ETH Zürich, Switzerland.
2010	ATC3 Biofouling & Bioadhesion Processes at University of Birmingham, United Kingdom..
2011	ATC4 Biofouling In The Industrial Environment at Akzo Nobel, Newcastle, United Kingdom
2011	Workshop in Intellectual Property as a Business Tool at Linköping University, Sweden.
2011	International Workshop ONR/SEACOAT, Las Vegas, USA;
2011	Workshop on Supervising Students – dealing with roles and relationships at ETH Zürich, Switzerland.
2012	Workshop in Paper Writing and Planning Sessions in Pisa, Italy.
2012	Workshop in Grant Proposal Writing in Heidelberg, Germany.
2012	8 th European Workshop on Secondary Ion Mass Spectrometry, SIMS Europe 2012, Münster, Germany
2013	Workshop in Career Development at ETH Zürich, Switzerland.